IAEA TECDOC SERIES

IAEA-TECDOC-2058

IAEA-TECDOC-2058

Advancing the State of the Practice in Uncertainty and Sensitivity Methodologies for Severe Accident Analysis in Water Cooled Reactors of CANDU Types

Final Report of a Coordinated Research Project

IAEA
International Atomic Energy Agency

ADVANCING THE STATE OF THE PRACTICE IN UNCERTAINTY AND SENSITIVITY METHODOLOGIES FOR SEVERE ACCIDENT ANALYSIS IN WATER COOLED REACTORS OF CANDU TYPES

The following States are Members of the International Atomic Energy Agency:

AFGHANISTAN
ALBANIA
ALGERIA
ANGOLA
ANTIGUA AND BARBUDA
ARGENTINA
ARMENIA
AUSTRALIA
AUSTRIA
AZERBAIJAN
BAHAMAS
BAHRAIN
BANGLADESH
BARBADOS
BELARUS
BELGIUM
BELIZE
BENIN
BOLIVIA, PLURINATIONAL STATE OF
BOSNIA AND HERZEGOVINA
BOTSWANA
BRAZIL
BRUNEI DARUSSALAM
BULGARIA
BURKINA FASO
BURUNDI
CABO VERDE
CAMBODIA
CAMEROON
CANADA
CENTRAL AFRICAN REPUBLIC
CHAD
CHILE
CHINA
COLOMBIA
COMOROS
CONGO
COSTA RICA
CÔTE D'IVOIRE
CROATIA
CUBA
CYPRUS
CZECH REPUBLIC
DEMOCRATIC REPUBLIC OF THE CONGO
DENMARK
DJIBOUTI
DOMINICA
DOMINICAN REPUBLIC
ECUADOR
EGYPT
EL SALVADOR
ERITREA
ESTONIA
ESWATINI
ETHIOPIA
FIJI
FINLAND
FRANCE
GABON
GAMBIA
GEORGIA
GERMANY
GHANA
GREECE
GRENADA
GUATEMALA
GUINEA
GUYANA
HAITI
HOLY SEE
HONDURAS
HUNGARY
ICELAND
INDIA
INDONESIA
IRAN, ISLAMIC REPUBLIC OF
IRAQ
IRELAND
ISRAEL
ITALY
JAMAICA
JAPAN
JORDAN
KAZAKHSTAN
KENYA
KOREA, REPUBLIC OF
KUWAIT
KYRGYZSTAN
LAO PEOPLE'S DEMOCRATIC REPUBLIC
LATVIA
LEBANON
LESOTHO
LIBERIA
LIBYA
LIECHTENSTEIN
LITHUANIA
LUXEMBOURG
MADAGASCAR
MALAWI
MALAYSIA
MALI
MALTA
MARSHALL ISLANDS
MAURITANIA
MAURITIUS
MEXICO
MONACO
MONGOLIA
MONTENEGRO
MOROCCO
MOZAMBIQUE
MYANMAR
NAMIBIA
NEPAL
NETHERLANDS, KINGDOM OF THE
NEW ZEALAND
NICARAGUA
NIGER
NIGERIA
NORTH MACEDONIA
NORWAY
OMAN
PAKISTAN
PALAU
PANAMA
PAPUA NEW GUINEA
PARAGUAY
PERU
PHILIPPINES
POLAND
PORTUGAL
QATAR
REPUBLIC OF MOLDOVA
ROMANIA
RUSSIAN FEDERATION
RWANDA
SAINT KITTS AND NEVIS
SAINT LUCIA
SAINT VINCENT AND THE GRENADINES
SAMOA
SAN MARINO
SAUDI ARABIA
SENEGAL
SERBIA
SEYCHELLES
SIERRA LEONE
SINGAPORE
SLOVAKIA
SLOVENIA
SOUTH AFRICA
SPAIN
SRI LANKA
SUDAN
SWEDEN
SWITZERLAND
SYRIAN ARAB REPUBLIC
TAJIKISTAN
THAILAND
TOGO
TONGA
TRINIDAD AND TOBAGO
TUNISIA
TÜRKİYE
TURKMENISTAN
UGANDA
UKRAINE
UNITED ARAB EMIRATES
UNITED KINGDOM OF GREAT BRITAIN AND NORTHERN IRELAND
UNITED REPUBLIC OF TANZANIA
UNITED STATES OF AMERICA
URUGUAY
UZBEKISTAN
VANUATU
VENEZUELA, BOLIVARIAN REPUBLIC OF
VIET NAM
YEMEN
ZAMBIA
ZIMBABWE

The Agency's Statute was approved on 23 October 1956 by the Conference on the Statute of the IAEA held at United Nations Headquarters, New York; it entered into force on 29 July 1957. The Headquarters of the Agency are situated in Vienna. Its principal objective is "to accelerate and enlarge the contribution of atomic energy to peace, health and prosperity throughout the world''.

IAEA-TECDOC-2058

ADVANCING THE STATE OF THE PRACTICE IN UNCERTAINTY AND SENSITIVITY METHODOLOGIES FOR SEVERE ACCIDENT ANALYSIS IN WATER COOLED REACTORS OF CANDU TYPES

FINAL REPORT OF A COORDINATED RESEARCH PROJECT

INTERNATIONAL ATOMIC ENERGY AGENCY
VIENNA, 2024

COPYRIGHT NOTICE

For further information on this publication, please contact:

Nuclear Power Technology Development Section
International Atomic Energy Agency
Vienna International Centre
PO Box 100
1400 Vienna, Austria
Email: Official.Mail@iaea.org

Printed by the IAEA in Austria
June 2024
https://doi.org/10.61092/iaea.wy1x-075c

IAEA Library Cataloguing in Publication Data

Names: International Atomic Energy Agency.
Title: Advancing the state of the practice in uncertainty and sensitivity methodologies for severe accident analysis in water cooled reactors of CANDU types / International Atomic Energy Agency.
Description: Vienna : International Atomic Energy Agency, 2024. | Series: IAEA TECDOC series, ISSN 1011-4289 ; no. 2058 | Includes bibliographical references.
Identifiers: IAEAL 24-01689 | ISBN 978-92-0-122024-0 (paperback : alk. paper) | ISBN 978-92-0-122124-7 (pdf)
Subjects: LCSH: CANDU reactors — Safety measures. | Water cooled reactors — Safety measures. | Nuclear reactor accidents.

FOREWORD

In 2019 the IAEA initiated a coordinated research project entitled Advancing the State of Practice in Uncertainty and Sensitivity Methodologies for Severe Accident Analysis in Water Cooled Reactors. This project aimed to enhance the understanding and characterization of uncertainties affecting key figure of merit predictions in severe accident codes for water cooled reactors. By bringing together experts from Member States with relevant technologies, the primary objectives of the coordinated research project were to improve capabilities and expertise in performing state of the art uncertainty and sensitivity analysis with severe accident codes and to support relevant research by graduate students.

Participating Member State organizations contributed to two major exercises within the project: the Quench-06 test application uncertainty exercise and the plant application uncertainty exercise. The latter was divided into five subtasks addressing various existing reactor lines including boiling water reactors, pressurized water reactors (including small modular reactor designs), pressurized heavy water reactors and water cooled, water moderated power reactors.

This publication presents the contributions from three individual organizations from three Member States describing their employed uncertainty and sensitivity assessment methods for severe accident analysis in CANDU pressurized heavy water reactors.

The IAEA acknowledges the efforts and assistance provided by the contributors listed at the end of this publication. The IAEA officer responsible for this publication was T. Jevremovic of the Division of Nuclear Power.

EDITORIAL NOTE

This publication has been prepared from the original material as submitted by the contributors and has not been edited by the editorial staff of the IAEA. The views expressed remain the responsibility of the contributors and do not necessarily represent the views of the IAEA or its Member States.

Guidance and recommendations provided here in relation to identified good practices represent expert opinion but are not made on the basis of a consensus of all Member States.

Neither the IAEA nor its Member States assume any responsibility for consequences which may arise from the use of this publication. This publication does not address questions of responsibility, legal or otherwise, for acts or omissions on the part of any person.

The use of particular designations of countries or territories does not imply any judgement by the publisher, the IAEA, as to the legal status of such countries or territories, of their authorities and institutions or of the delimitation of their boundaries.

The mention of names of specific companies or products (whether or not indicated as registered) does not imply any intention to infringe proprietary rights, nor should it be construed as an endorsement or recommendation on the part of the IAEA.

The authors are responsible for having obtained the necessary permission for the IAEA to reproduce, translate or use material from sources already protected by copyrights.

The IAEA has no responsibility for the persistence or accuracy of URLs for external or third party Internet web sites referred to in this publication and does not guarantee that any content on such web sites is, or will remain, accurate or appropriate.

Contents

1. INTRODUCTION

1.1. BACKGROUND

Since the Three Mile Island Unit 2 (TMI-2) accident, significant efforts have been made to develop severe accident codes to address the lack of understanding of what occurred during that incident. The TMI-2 degraded core accident, which surpassed design basis accidents, prompted new initiatives and a revaluation of regulatory processes. The Fukushima accident in 2011 further highlighted the need to expand international research and development efforts to encompass containment phenomena affecting the environment, including aerosol and core melt behaviour, risks of combustible gas mixtures, and related phenomena. In the decades following the TMI-2 accident, the codes were predominantly based on deterministic models, where single representative accidents were modelled to represent classes of accidents, such as large and small break loss of coolant accidents (LOCAs) or station blackout (SBO). These analyses were computationally intensive being conducted on slower computers with limited memory compared to modern platforms. Uncertainties in the operative physics and stochastic aspects of these analyses were acknowledged but challenging to quantify, leading to conservative biases in the deterministic results, aiming to meet requirements such as public exposure limits.

Over time, as severe accident codes improved in robustness and computational platforms became significantly faster, sampling-based uncertainty studies emerged using statistical tools. These methodologies allowed uncertainties in the analysis to be expressed in terms of variability in the code input and boundary conditions, producing an ensemble of answers and probability distributions instead of single realization point values. This approach enabled obtaining likelihood distributions of accident figures of merit (FOM), providing insights into mean values, central tendencies, and dispersion in the answers. Presently, the codes have significantly enhanced robustness, and computational platforms offer much faster execution, including massively parallel computational resources with thousands of individually addressable processors. As a result, sampling-based uncertainty methods have become more accessible and applicable to severe accident analysis for selected accident sequences.

The International Atomic Energy Agency (IAEA) Coordinated Research Project (CRP) on Advancing the State-Of-Practice in Uncertainty and Sensitivity Methodologies for Severe Accident Analysis in Water Cooled Reactors (WCRs) in 2019. The primary objective of this CRP was to improve the understanding and characterization of sources of uncertainty and study their effects on the FOMs of severe accident code predictions in water cooled reactors. Within the five year duration of the CRP, 22 organizations representing 18 Member States have been developing and evaluating calculation platforms based on severe accident codes and relevant uncertainty tools or uncertainty and sensitivity analyses of severe accident scenarios in different water cooled reactors, the Pressurized Water Reactor (PWR), Boiling Water Reactor (BWR), CANada Deuterium Uranium reactor (CANDU), Water-Water Energetic Reactor (VVER), and Small Modular Reactors (SMRs, PWR-like, CAREM-25 design (Central Argentina de Elementos Modulares (Argentina Modular Power Plant). In the CRP framework, the uncertainty and sensitivity analysis of the QUENCH-06 experiment has also been undertaken to provide relevant insights. Thus, this CRP was specifically aimed at improving the state of practice in severe accident analyses by examining and characterizing the impact of uncertainty and variability on severe accident simulation and modelling. Various widely used severe accident codes such as MELCOR (Methods of Estimation of Leakages and Consequences of Releases), MAAP (Modular Accident Analysis Program), ASTEC (Accident Source Term

Evaluation Code) to mention just a few, are used to evaluate model form uncertainty by benchmarking them against each other. In particular, the objectives of this CRP were to bring together the current state-of-knowledge on uncertainty propagation in severe accident analyses that has been accumulated by experienced analysts with the aim of increasing the sophistication and competency of the practitioners in this field as follows:

- Achieve significant improvement in sophistication and quality of severe accident analyses performed by the participants from Member States with well-developed knowledge, adequate simulation capabilities (both software and hardware) and long years of relevant practice;
- Enable objective peer review of the benchmark studies with various codes by the participating Member States and thus lead to new knowledge and sharing of research results relevant to evaluation of uncertainties in severe accident analyses;
- Foster national excellence and international cooperation through an exercise to elevate the capability and sophistication of global severe accident code users;
- Promote sharing of newly developed knowledge and contribute to capacity building in developing countries.

The participating Member State organizations contributed to two major exercises named: QUENCH-06 test application uncertainty exercise and plant application uncertainty exercise that was divided into five subtasks addressing the existing reactor lines: BWRs, PWRs inclusive of SMRs designs, pressurized heavy water reactors (PHWRs), and VVERs.

1.2. OBJECTIVE

The objective of this publication is to provide description of the uncertainty and sensitivity analysis performed by three individual institutions from three Member States describing their methods for severe accident evaluation of a generic CANDU 6 (single unit) NPP. The results of the developed analysis consolidate the existing experience in the development of a strong technical basis for establishing uncertainty and sensitivity methodologies in severe accident analyses that has been accumulated by experienced analysts with the aim to increase sophistication and competency of the practitioners in this field. The insights gained from this exercise feeds new knowledge to be implemented in the uncertainty and sensitivity studies and methods for severe accident analysis codes with the intent of implementing the best practices and lessons learned.

1.3. SCOPE

The scope of this publication is the PHWR (CANDU 6, a generic single unit station) plant application exercise performed by the CRP participants in support of addressing improvement in sophistication and quality of severe accident analyses with various codes that generated new knowledge relevant to evaluation of uncertainties and sensitivity analysis of severe accident simulation and modelling. The CRP exercises were structured according to the depicted flow diagram in Fig. 1, encompassing five distinct TECDOC publications. Each of these publications pertains to a specific plant application exercise presenting pertinent technical findings with lessons learned and best practices.

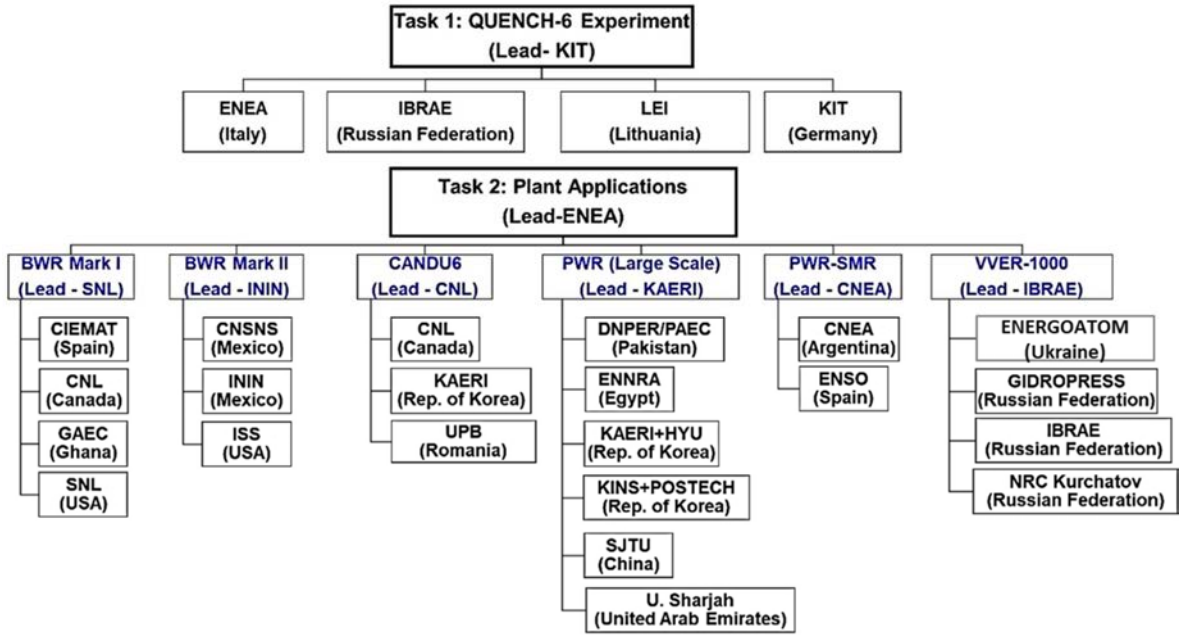

FIG. 1. CRP tasks and participants (refer to Abbreviations for the organizations full names).

Participating organizations in this exercise and contributors to this publication were:

- Canadian Nuclear Laboratories (CNL, Canada);
- Polytechnic University of Bucharest (UPB, Romania);
- Korea Atomic Energy Research Institute (KAERI, Republic of Korea).

The overall focus of the presented analysis is to assess the uncertainty and sensitivity involved in severe accident calculations concerning the progression and consequences of accidents. The primary FOMs chosen for the severe accident modelling of a CANDU 6 plant include, but are not limited to, hydrogen generation, event timings, and fission product release to the environment. Various participating organizations conducted uncertainty and sensitivity assessments on these major FOMs using their respective analysis tools, and the outcomes are compared. This publication also delves into the analysis and description of the relative contributions of individual uncertain input parameters to the FOMs through sensitivity studies. The tools and approaches employed are thoroughly detailed in the relevant sections.

This publication specifically focuses on a generic CANDU 6 plant undergoing a postulated SBO accident. The implemented accident scenario, major analysis assumptions, normal operating conditions of the CANDU 6 plant, and failure criteria align closely with those outlined in [1]. It is important to note that the benchmarking study discussed in [1] aimed to investigate major accident event timings and reference numbers of FOMs, such as hydrogen produced inside the reactor vessel, without explicitly focusing on systematic uncertainty and sensitivity assessment.

1.4. STRUCTURE

This publication is structured such to provide a logical analysis sequence starting from the general technical background/work scope (Section 1), analysis framework, CANDU 6 nuclear power plant and a station blackout accident descriptions, description of the codes used by every participant (Section 2), uncertainty and sensitivity analysis methodologies (Section 3), detailed information regarding calculations and benchmark results and comparisons among all participants (Section 4), discussion and lessons learned (Section 5), and finally, main conclusions (Section 6).

2. ANALYSIS SCOPE AND FRAMEWORK

This chapter presents description of the scope of performed analysis and framework developed for the uncertainty and sensitivity analysis. The methods applied, the main FOMs and the codes used are discussed. The summary information on the scope and reference plant data are provided.

2.1. OVERVIEW

Main frameworks for the uncertainty and sensitivity analysis, analysis methods as well as main FOMs, which were employed by the participating organizations are summarized in Tables 1–3. As indicated in Table 1, all three participating organizations selected un-mitigated SBO scenario for the reference CANDU 6 plant.

The MAAP-CANDU (Modular Accident Analysis Program for CANDU), RELAP/SCDAPSIM (Reactor Excursion and Leak Analysis Program / Severe Core Damage Analysis Package SIMulation), and CAISER (Candu Advanced Integrated SevERe accident analysis) codes are used in simulation and analysis. The framework was focused on either supporting the regulatory review or severe accident management (SAM) and Level 2 probabilistic safety assessment (PSA).

TABLE 1. SCOPE AND REFERENCE PLANT WITH MODELED SCENARIOS

Participating Organization	Reference Plant	Reference Scenario (Scope)	Severe Accident Code	Framework of Analysis
CNL (Canada)	CANDU 6	Un-mitigated SBO (in-/ex-vessel)	MAAP-CANDU v5.00A	Regulatory review support
UPB (Romania)	CANDU 6	Un-mitigated SBO (in-vessel)	RELAP/SCDAPSIM/ MOD3.6	Regulatory review support
KAERI (Republic of Korea)	CANDU 6	Un-mitigated SBO (in-vessel)	CAISER	SAM & Level 2 PSA support

Table 2 summarizes the analysis methods per participating organization. The uncertainty quantification methods include GRS (Gesellschaft fur Anlagenund Reaktor Sieherheit) method, the Monte Carlo method and the Wilk's formula, while the sensitivity methods are based on the Pearson and Spearman correlation coefficients.

The uncertainty quantification tools applied are either based on SUSA (Software for Uncertainty and Sensitivity Analyses) or RELAP/SCDAPSIM MOSAIQUE (Module for SAmpling Input and QUantifying Estimator) module.

TABLE 2. ANALYSIS METHODS

Participating Organization	Uncertainty Quantification Method	Sensitivity Analysis Method	Uncertainty Quantification Tool
CNL (Canada)	GRS method, Wilk's formula	Pearson, Spearman, correlation coefficients	SUSA
UPB (Romania)	GRS method, Wilk's formula	Pearson, Spearman, correlation coefficients	Integrated uncertainty analysis package in RELAP/SCDAPSIM
KAERI (Republic of Korea)	Wilk's formula, Monte Carlo simulation with the response surface	Pearson, Spearman, correlation coefficients	MOSAIQUE (

Relevant FOMs are defined in Table 3. Each participating organization selected the FOMs based on the selected scenario. Further details are provided in the following sections.

TABLE 3. PROPOSED MAIN FOMs

Participating organization	Main FOMs
CNL (Canada)	In-/ex-vessel hydrogen generation; Fission product mass released to the environment.
UPB (Romania)	Hydrogen mass generation (in-vessel); Time to the fuel channel failure (first fuel channel failure); Time to the calandria vessel failure.
KAERI (Republic of Korea)	Hydrogen mass generation; Time to the fuel channel failure; Time to the calandria vessel failure.

2.2. DESCRIPTION OF CODES

This section provides description of the codes used in simulations of selected accident scenarios and tools for uncertainty and sensitivity analysis. The descriptions include: MAAP-CANDU, SUSA, RELAP/SCDAPSIM and CAISER codes.

2.2.1. MAAP-CANDU Code

Under the management of the Electric Power Research Institute (EPRI), MAAP is an industry standard comprehensive systems code, designated for the thorough analysis of severe accidents at the plant level, encompassing the behaviour of fission products. In the mid-1990s, the emergence of MAAP4 was followed by substantial expansion, aimed at enabling a more versatile assessment of advanced Light Water Reactors (LWRs). This extension also accounted for mitigation strategies incorporated within SAM protocols. Key enhancements encompass the refinement of models for the reactor core and the lower plenum of the reactor pressure vessel, the introduction of a versatile node and junction containment model, and the incorporation of models representing features specific to advanced LWR designs, inclusive of passive safety mechanisms. The code is based on the algorithms and parametric models, particularly relevant for Level 2 PSA analyses. However, the use of a fixed nodalization for the reactor coolant system in LWRs imposes limitations on its applicability to experiments with varying geometries.

The development of the CANDU variant of the code (MAAP-CANDU) spanned from the mid of 1988 to the 1990. This endeavour was prompted by a recommendation from the Ontario Nuclear Safety Review calling for the thorough analysis of severe accidents concerning Ontario Hydro plants. MAAP-CANDU

draws upon the foundation of MAAP for LWRs. A collaborative effort between a team from Ontario Hydro, Atomic Energy Canada Limited, and international specialists culminated in the development of CANDU specific models, adhering to stringent quality assurance protocols to uphold the integrity of both generic and phenomenological models and to affirm the accuracy of novel CANDU specific models [1].

MAAP-CANDU quantitatively predicts the evolution of a severe core damage accident in a CANDU pressurized heavy water reactor, for both single unit and multi unit plants. The simulations start from initial conditions (including steady state) given a set of system faults and initiating events including (but not limited to) SBO, large and small LOCA, and steam generator tube rupture. The simulations progress through events such as: primary heat transport system (PHTS) failure, core disassembly and melt, calandria vessel failure, shield tank/reactor vault failure, and containment failure, and molten core concrete interaction. Engineered safety systems, such as emergency core cooling, containment dousing, and filtered containment venting can be made available to halt or slow down the accident progression. Various models can be included (automatic, manual, full/partial/non availability) to represent operator or external actions that could stop, delay or mitigate the accident by cooling the debris in the calandria vessel or containment, and could prevent or delay containment failure. The flexible structure of the input allows for many features of the reactor and associated systems to be changed and supports easy modifications for different CANDU reactor designs. However, the nodalization of the reactor coolant system is not flexible, nor the safety systems that to be modelled; this is because most of these features are hard coded. However, with the introduction of MAAP5-CANDU the core can be nodalized with much-higher degree, enabling a more realistic core disassembly. Experimental work is underway to support or modify newly implemented theoretical models of core disassembly, and to improve/verify other user-input values.

The MAAP-CANDU code can be broadly divided into three parts:

- Part I: generic MAAP components, which model systems and processes common to multiple reactor types, using several generalized models (e.g., containment, fission product releases, transport and deposition);
- Part II: CANDU-specific models (e.g., fuel channel/core and reactor (calandria vessel), reactor (calandria) vault and associated end shields, emergency core cooling, etc.) developed/adapted from MAAP for Light Water Reactors (LWRs) models;
- Part III: the Channel System, which models the CANDU core, was developed by Ontario Hydro (now Ontario Power Generation Inc. (OPG)). The intellectual property of this portion of MAAP-CANDU remains with OPG but is maintained by the CANDU Owners Group (COG).

The MAAP-CANDU code possesses the capability to effectively simulate the response of a CANDU power plant throughout severe accident sequences, incorporating both the actions taken as part of accident management procedures. These predictions encompass the complete evolution of a severe accident, commencing from normal full power operating conditions. When provided with a comprehensive set of system faults and initiating events, the code tracks the progression of events through various critical phases. These phases encompass scenarios such as core meltdown, potential failures within the PHTS, calandria vessel and shield tank failures, as well as possible containment breaches. Furthermore, the code includes intricate models to represent the potential actions that could intervene and mitigate the unfolding accident. Specifically, these models simulate the cooling of debris within the calandria vessel or containment structure, potentially halting the progression of the severe accident.

MAAP-CANDU is equipped to model various aspects of the plant's behaviour, including thermal hydraulics interactions and the behaviour of fission products. This encompasses the PHTS system, steam generators, and pressurizers within loops 1 and 2. Moreover, the code also accounts for the behaviour of the calandria vessel, shield tank, containment structure, and vacuum building. Notably, the code features models that represent the logical operations and performance of engineered safeguard systems. This ensures that safety systems are accurately integrated into the simulations. Additionally, the code allows for the simulation of operator actions. By specifying intervention conditions and corresponding responses, the code can replicate the actions taken by operators in response to the evolving severe accident scenario.

The MAAP-CANDU Channels System is a specialized component within the MAAP-CANDU code, tailored to model the behaviour of individual channels or fuel channels in CANDU type nuclear reactors during severe accident scenarios. This system focuses on analysing the response and potential consequences of the individual fuel channels within the reactor core. The primary purpose of the MAAP-CANDU Channels System is to simulate the thermal hydraulic behaviour, heat transfer, and potential failure modes of the individual fuel channels within the core of a CANDU reactor during a severe accident. It provides insights into the progression of events that may occur in each fuel channel, helping to understand the consequences and informing safety assessments. The Channels System employs detailed modelling of individual fuel channels, capturing factors such as heat generation, heat transfer, coolant flow, and possible degradation mechanisms. It considers both normal operating conditions and extreme scenarios that lead to severe accidents. Within the Channels System, each fuel channel is treated as an independent entity with its own characteristics. The system models the behaviour of the fuel, cladding, coolant, and any potential interactions between them. It considers parameters such as pressure, temperature, heat flux, and chemical reactions that may occur within each channel. The Channels System simulates a range of phenomena that may occur in individual fuel channels during a severe accident. This includes heat-up, oxidation of fuel cladding, fuel degradation, and the potential for cladding breach due to high temperatures or other factors. The Channels System analyses potential failure modes of fuel channels, such as ballooning or rupture of fuel cladding, leading to the release of radioactive materials from the fuel. It also accounts for potential interactions between failed fuel channels and other reactor components. The system generates detailed output data for each modelled fuel channel, including information about temperature profiles, cladding integrity, and potential release of fission products. These outputs help analyse the behaviour of individual channels during a severe accident, understand potential consequences, and inform strategies for mitigating the effects.

The CANDU core is different from that of PWRs and BWRs. The disassembly of the horizontal channels and core relocation during a severe accident is very different from LWRs. Several phenomenological models specific to the CANDU core have been developed and implemented allowing to perform best estimate calculations [2, 3].

2.2.2. SUSA Code

GRS developed SUSA (Software for Uncertainty and Sensitivity Analyses) with the aim of simplifying the execution of uncertainty and sensitivity analyses utilizing the Monte Carlo simulation approach. It integrates well known methods such as probability calculus and mathematical statistics with graphical user interface. The concept of SUSA enables the user to focus analysis on identifying input parameters that predominantly contribute to the uncertainty in the output of the employed computer code and articulating the uncertainties

associated with these identified parameters. Based on this, SUSA facilitates the probabilistic quantification of parameter uncertainties and subsequently guides users through the entire analysis process. This encompasses everything from sampling parameter values, initiating corresponding computer code runs, to computing statistical metrics that explain both the uncertainty and sensitivity of the computational outcome.

2.2.3. RELAP/SCDAPSIM Code

RELAP (Reactor Excursion and Leak Analysis Program) developed at the Idaho National Laboratory, is a best estimate simulation code for analysing both transients and loss of coolant accidents (LOCAs) [4–7]. Designed to solve the thermal hydraulics in real time scenarios and efficiently compute system transients, the code employs rapid and partially implicit numerical schemes to solve nonhomogeneous and non-equilibrium models for two phase systems. The software integrates several component models to replicate general systems, validate experimental findings, and accurately model the flow of multi phase fluids within piping networks. Offering the flexibility of accommodating time varying conditions, RELAP computes reactor thermal hydraulics in steady state and transient scenarios, encompassing accidents. The containment and related components are not incorporated within the code. As a result, the code is widely employed and benchmarked by various entities, including utility companies and regulatory bodies. The most recent version, as of June 2019, is RELAP 7.

RELAP/SCDAPSIM developed by the Innovative Systems Software as part of the international SCDAP Development and Training Program, integrates different versions of RELAP code, such as SCDAP/RELAP5/MOD3.2 models developed for severe accident analysis and RELAP/MOD3. models for best estimate system analysis. The last version MOD3.5 is currently in use for the validation of experimental facilities such as PHEBUS and QUENCH alongside its application for user training purposes.

The primary purpose of the SCDAP code is to simulate and analyse the behaviour of nuclear reactor cores during severe accidents. It provides insights into the progression of events that occur following a loss of core cooling, potential core meltdown, and release of radioactive materials. SCDAP employs a multi-dimensional approach to model the complex phenomena that take place during a severe accident. The code uses mathematical and physical models to represent various physical and chemical processes occurring in the core, such as heat transfer, thermal hydraulics, fission product release, and material degradation. The code models the progression of core degradation, including fuel rod overheating, fuel melting, fuel rod cladding failure, and relocation of molten fuel considering interactions between different materials in the core and their impact on the overall behaviour of the reactor core. Modelling of the release, transport, and behaviour of radioactive fission products within the reactor core includes their release into the coolant, transport through the reactor systems, and potential containment breach. The modelling of behaviour of containment structures during a severe accident includes the pressure and temperature conditions within the containment and assessing potential containment failure modes. A two dimensional finite element model, based on the COUPLE (COde for a Unified multi-Physics simuLation Environment) code, is utilized to calculate the heat-up of debris and surrounding structures. This model considers factors such as decay heat and initial internal energy of slumped debris, and it computes the conduction based transport of heat radially and axially to the adjacent wall structures and surrounding water. This model is especially crucial in determining the time at which the reactor vessel may rupture due to heat effects [6, 7]. Improvements have been made in COUPLE subroutines to enable accurate modelling of a horizontal cylinder, such as the

calandria vessel commonly found in certain reactor designs. This enhancement ensures a more precise representation of the vessel's behaviour and response during severe accidents.

2.2.4. CAISER Code

CAISER (Candu Advanced Integrated SevERe accident analysis code) was developed by KAERI [8]. The CAISER code consists of several codes, which are separately developed and incorporated into the CAISER code system:

- CAISER-C code simulating a core degradation phenomena in a calandria vessel;
- MARS-KS code simulating a thermal hydraulics in PHTS;
- CONTAIN code simulating a severe accident phenomena in containment;
- SIRIUS (SImulation of Radioactive nuclide Interaction Under Severe accident) code simulating a fission product behavior.

The CAISER-C code simulates various aspects of severe accidents, including LOCA, core meltdown, fuel degradation, fission product behaviour, heat-up of structures, potential containment failure, and other phenomena. Similar to other severe accident analysis codes, CAISER integrates a series of physical models that describe the complex thermal-hydraulic, chemical, and mechanical processes occurring within the reactor during a severe accident. These models include the behaviour of the reactor core, reactor coolant system, and containment structures.

The CAISER code consists of two interconnected modules, the fuel rod degradation module and the fuel channel degradation module, which collectively simulate severe accident phenomena in a CANDU type nuclear reactor. These modules are designed to model the complex processes occurring within a fuel channel and a calandria vessel during a severe accident. The fuel rod degradation module simulates a series of severe accident phenomena within a fuel channel such as: core uncover, fuel rod heat-up, hydrogen generation, fuel rod slumping, fuel rod melting and relocation, and thermal interactions between the relocated molten material and the pressure tube or calandria tube. The fuel channel degradation module simulates phenomena at the broader scale of the calandria vessel: sagging of fuel channel, debris bed formation, molten pool formation and calandria vessel failure due to ablation and creep rupture of its walls. Both the fuel rod degradation module and the fuel channel degradation module track changes in mass and energy for various components, such as fuel, cladding, pressure tube, calandria tube, debris bed, and molten corium pools. The two modules are closely interconnected to simulate phenomena occurring simultaneously within a fuel channel and a calandria vessel. Additionally, the coolant behaviour within a fuel channel is simulated using the MARS-KS thermal hydraulics system code. The communication between the fuel rod degradation module (CAISER-C) and MARS-KS involves the exchange of relevant variables at each time step. This communication allows CAISER to send convective heat transfer rates to MARS-KS while receiving coolant temperature and convective heat transfer coefficients in return.

The fission product inventory for CANDU 6 plant has been calculated by using ORIGEN code, and it is implemented in SIRIUS code [9], which simulates the fission product release from fuel pellet, transport in thermal hydraulic system, and deposit on the circuit solid wall. The fission products in a primary circuit become to transport to the containment through degasser condenser relief valve or through a corium discharge when a calandria vessel is failed. The severe accident phenomena in a containment is simulated

by utilizing CONTAIN code [10], which deals with a thermal-hydraulics behaviour including hydrogen combustion, the fission product behaviour in a containment, the molten corium concrete interaction, direct containment heating, and engineered safety features such as spray. In the CAISER code system, CONTAIN code has been coupled with MARS-KS, CAISER-C, and SIRIUS code, to provide the information of the liquid and vapour discharge from safety valve, and the corium discharge from calandria vessel, together with a fission product transport from a PHTS.

The detailed modelling for CAISER code has been described in reference [11] with the simulation of CS28-1 experiment.

2.3. DESCRIPTION OF THE CANDU 6 STATION BLACKOUT ACCIDENT

An SBO accident is defined as an event initiated by a complete loss of off-site alternating class IV power and unavailability of the Class III power as well as all back up power including loss of all on-site standby and emergency electric power supplies, i.e., the diesel generators etc. This results in the loss of decay heat removal capability, causing the nuclear core heat-up and substantial significant damage. This section outlines the main sequence of a severe accident scenario that is foreseen during an SBO event. The progression of processes and phenomena described in this section is simulated by the MAAP-CANDU code, with varying degrees of complexity depending on the specific phenomenon. It is important to note that certain severe core damage processes, such as the interaction between core debris and the calandria vessel, involve intricate dynamics and are modelled based on engineering judgment due to the absence of experimental data. Given the complexity and lack of empirical data for certain phenomena, the MAAP-CANDU code employs a combination of theoretical models and expert engineering insight. These assumptions and models are described within the code to transparently account for their potential influence on the overall accident progression and consequences. The description provided highlights the challenges of simulating severe accident sequences, particularly during SBO scenarios, where power loss can trigger a chain of events leading to core damage. While some processes are modelled with greater fidelity due to available data, others are handled using engineering judgment to account for the lack of experimental information. The use of assumptions and models, along with a transparent description of their impact, allows MAAP-CANDU to provide insights into the potential consequences of severe accidents during SBO events in CANDU type reactors. The accident progresses to core damage because of the loss of:

- PHTS inventory;
- ECC;
- Moderator cooling;
- Shield (and calandria vault) cooling.

The basic (un-mitigated) SBO accident sequence is described in Section 2.3.3.

2.3.1. Plant description and input data

The heavy water reactor plant considered for the benchmarking analysis is a generic 2,064 MWth CANDU 6 power plant [12]. The CANDU reactor design encompasses several distinctive features:

- Pressure boundary is established using numerous small diameter fuel channels;

— Moderator and cooling medium: heavy water (D_2O) is used as low pressure moderator and high pressure fuel cooling systems;
— On-power refueling: allowing fuel to be replaced without shutting down the reactor;
— Reactivity devices: located in the cool, low pressure moderator region safeguarded from high temperatures and pressures;
— Fuel: natural uranium;
— Safety shutdown systems: two fully independent safety shutdown systems, providing redundancy and autonomy.

The CANDU 6 plant consists of several key structures, including the containment (reactor) building, service building, turbine building, and auxiliary structures. The reactor building as shown in Fig. 2 contains all the equipment directly associated with steam generation, including PHTS, steam generators, reactor assembly and associated components.

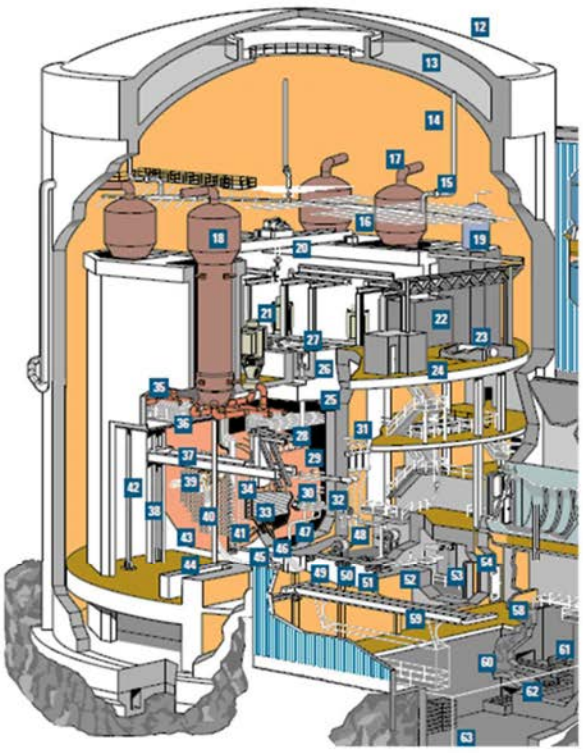

FIG. 2. Cutaway view of CANDU 6 reactor building [reproduced from [12] with permission courtesy of Atomic Energy of Canada Ltd].

Design features of the CANDU 6 plant are summarized in Table 4 [2]. The calandria vessel is a cylindrical structure that houses the fuel channels; it is constructed typically from stainless steel and serves as a barrier that contains the nuclear reactions. It is penetrated by 380 horizontal fuel channels and is filled with heavy water that acts as moderator (Fig. 3). Each fuel channel consists of a pressure tube, a calandria tube and 12

fuel bundles containing 37 fuel elements each. The calandria vessel is located inside a steel lined concrete reactor vault. The reactor vault, filled with water acts as a shielding medium and the presence of a coolant helps maintain a consistent thermal equilibrium, thereby contributing to stabilizing the calandria vessel's temperature during regular operational conditions.

TABLE 4. DESIGN CHARACTERISTICS OF CANDU 6

Parameter	**Value**
Reactor power	2155.9 MWth
PHTS pump power	17 MWth
Heat loss to containment	3 MW
Heat load to moderator	105.9 MW
Reactor inlet header (RIH) temperature	266 °C
Reactor outlet header (ROH) temperature	310 °C
RIH pressure	11.85 MPa
ROH pressure	10.1 MPa
Pressurizer pressure	9.99 MPa
PHTS loop flow	1935 kg/s
PHTS Loop coolant inventory	47,545 kg
Pressurizer coolant inventory	30,555 kg
Total primary inventory	125,704 kg
Steam generator secondary side pressure	4.7 MPa
Steam generator secondary side temperature	260 °C
Steam generator secondary side coolant inventory	38,000 kg
Moderator temperature	69 °C
Moderator inventory	227,000 kg
End shield coolant inventory	14,508 kg
End shield coolant pressure	101 kPa
End shield coolant temperature	63 °C
Reactor vault coolant pressure	101 kPa
Reactor vault coolant temperature	51.5 °C
Reactor vault coolant inventory	499,687 kg

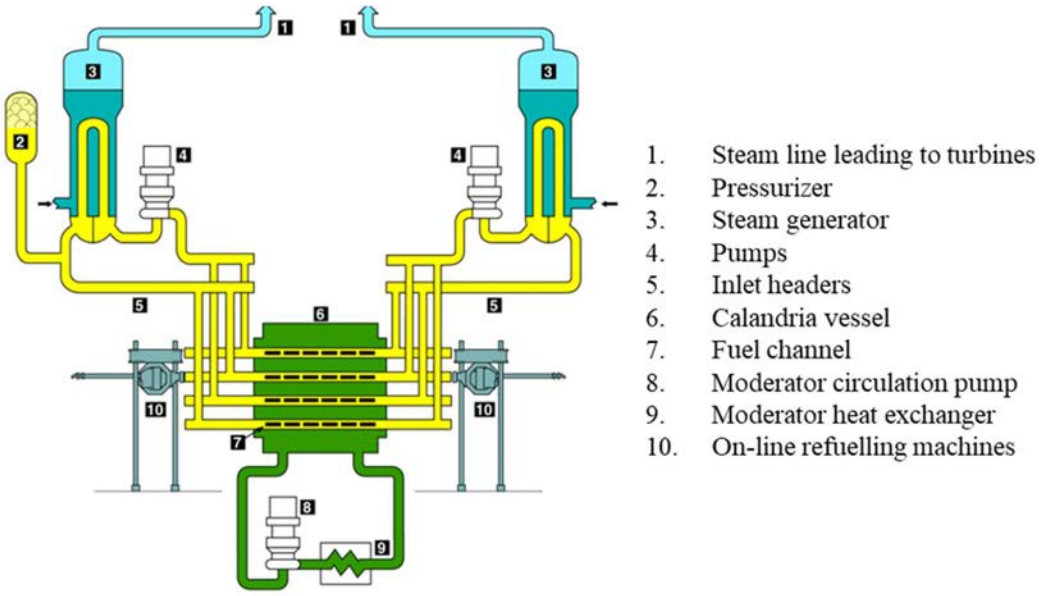

FIG. 3. Schematics of a CANDU PHTS [2].

The PHTS is designed to facilitate the controlled circulation of pressurized heavy water through the fuel channels. This circulation serves the crucial function of extracting the heat generated within the fuel. The extracted heat is subsequently carried by the reactor coolant—a component of the PHTS—towards the steam generators. Within these steam generators, the heat is transferred to light water, inducing the steam generation that drives the turbine generator, effectively converting thermal energy into mechanical energy. The coolant leaving the steam generators returns to the fuel channels, ultimately re-entering the reactor's core to repeat the heat removal cycle again. This cyclic circulation of the coolant ensures the continuous removal of heat from the fuel, maintaining operational stability.

The low pressure steam discharged from the low pressure turbine is condensed in the condensers. This condensation is facilitated by a flow of condenser cooling water. The feed water system processes the condensed steam from the condensers. This processed feed water is then returned to the steam generators through a system comprising pumps and a series of heaters. This cyclic process enables the regeneration of steam, which is utilized for further power generation. Besides that, the on-power refuelling maintains the reactor's fuel inventory without the need for reactor shutdown, the system is also used to remove a defective fuel bundle in the unlikely event that a fuel defect develops. The CANDU 6 pressure and inventory control system consist mainly of a pressurizer (ensures the control of reactor pressure through the careful management of steam and water volumes), degasser condenser (removes non-condensable gases from the primary coolant system, contributing to operational efficiency and maintaining desired pressure and inventory levels), D_2O storage tank (acts as a reservoir, ensuring a consistent supply for circulation within the reactor core), D_2O feed pumps (maintain the necessary flow rates and pressure levels), bleed cooler (manages heat transfer processes contributing to the overall thermal balance and maintaining controlled conditions), pressurizer relief valves (designed to release excess pressure from the system in the event of pressure buildup, preventing any potential overpressurization scenario) and heat transport system liquid relief valves (essential safety measure to release excess liquid from the heat transport system, ensuring controlled fluid levels and preventing potential operational transients). Pressurizer relief valves, steam bleed valves and PHTS liquid relief valves (LRV) discharge into the degasser condenser contributing to overall system stability and pressure management. The degasser condenser has spring-loaded relief valves that in the event of excess pressure release the accumulated pressure to a containment compartment. The LRVs are air operated, with back-up instrument air, and are designed to fail open. The back-up air supply should maintain the valves in operation for two hours following power loss (as in SBO) and loss of normal instrument air. Pressurizer relief valves are designed to fail open. Further details of CANDU 6 power plant configuration can be found in [12].

2.3.2. Assumptions

A severe accident at a nuclear power plant involves numerous physical and chemical processes and phenomena, which are very complex to capture in computer models. Therefore, several assumptions were required for the analyses undertaken in this study for various plant systems, components and phenomena. Where possible, best estimate assumptions were used, including some conservative or bounding assumptions, when available information was limited (Table 5).

TABLE 5. SBO ANALYSIS ASSUMPTIONS FOR SYSTEMS AND COMPONENTS

System	Assumption	
	Available	**Not available**
Class IV power		√
Class III power		√
Reactor shutdown	√	
PHTS loop isolation		√
Emergency power supply		√
D_2O supply system		√
D_2O recovery system		√
D_2O make up system		√
Turbine main stop valve closure	√	
Main feed-water system		√
Auxiliary feed-water system		√
Emergency water supply system		√
Main steam safety valves	√ (Use lowest set-point of 5.11 MPa(a) only)	
Main steam isolation valves		√
Air operated atmospheric steam discharge valves		√ (Fail-closed)
Condenser steam discharge valves		√
Steam generator crash cool-down		√
Moderator cooling system		√
Shield cooling system		√
Shutdown cooling system		√
High pressure ECCS		√
Medium pressure ECCS		√
Low pressure ECCS		√
Dousing spray		√
Local air coolers in containment		√
Moderator rupture disk rupture	√	
Calandria bleed valve	√	
Passive autocatalytic recombiners (PAR)	CNL	√
Hydrogen igniters		√
Containment isolation system		√
Containment ventilation system		√
Calandria (or Reactor) vault rupture disk rupture	√	
PHTS LRV fail open	√ (Degasser condenser relief valve at LRV location)	
Degasser condenser tank and related pressure & inventory control components	KAERI	√
Operator interventions		√

For comparing analysis results produced by various codes all participating organizations applied the same assumptions and initial conditions:

1) Class IV and Class III electrical power supplies were lost at time 0 s, and not recovered.
2) Emergency power supply system: unavailable.
3) Reactor shutdown occurred at time 0 s (reactor tripped on loss of Class IV).
4) Primary pumps ran down and the moderator cooling, shield cooling and shutdown cooling systems became unavailable at time 0 s (no power for pumps).
5) Steam generator main steam safety valves are available, they open and close at set point to relieve pressure.
6) Moderator drain: not assumed (a pressure tube + calandria tube rupture can also rupture the fuel channel bellows, causing the moderator to drain through the ruptured channel).

2.3.3. Description of the station blackout accident progression

This section describes the basic severe accident sequences as anticipated for the SBO scenario. Various processes leading to severe core damage, such as the formation and movement of core debris, as well as the interaction of debris with the calandria vessel, are intricate in nature. Consequently, these processes are modelled based on engineering judgement due to a lack of experimental data.

The progression of the SBO accident sequence is instigated by a power loss, triggering a reactor trip and resulting in the shutdown of pumps (PHTS, moderator cooling, shield cooling, steam generator feed water, and recirculating cooling water). Subsequently, the accident advances towards core damage due to the loss of PHTS inventory, extended emergency core cooling, loss of moderator cooling, as well as the absence of shield and calandria vault cooling.

Certain sensitivity scenarios attribute safety related functions (such as emergency core cooling and rapid cooldown mechanisms). These systems appear to delay the progression of the accident and modify the release of fission products. However, it is important to note that these interventions do not completely arrest the accident sequence unless a regime of long term cooling is either maintained or reinstated (such as low pressure emergency core cooling with a heat exchanger or calandria vault cooling).

The basic SBO accident sequence (no mitigating systems), as modelled by MAAP-CANDU are:

1) Loss of power sources: accident begins with the loss of both off-site and on-site power sources. This loss of power disables the systems that are integral to maintaining reactor operations, including cooling mechanisms and other safety systems.
2) Reactor shutdown: initially at full power and pressure; at time 0 s, with power sources unavailable, the reactor's control systems trip, initiating a shutdown of nuclear reactions. However, residual heat from the recent operation continues to be produced.
3) Cooling degradation and heat accumulation: without active cooling mechanisms, the reactor core's temperature increases; PHTS temperature and pressure stay high.
4) Fuel element degradation: loss of primary coolant elevated uncovers fuel and the temperatures cause the degradation of fuel elements, including potential damage to the fuel rods.
5) Fuel rod failure: with sustained heat accumulation, fuel rods may experience failure, leading to the release of fission products into the reactor coolant.
6) Fuel channel degradation: degradation of fuel elements contributes to the degradation of fuel channels, potentially compromising structural integrity.

7) Calandria vessel pressurization: ruptured fuel channels within the reactor result in the release of high pressure coolant and steam. This abrupt release of pressure pressurizes the calandria vessel.
8) Calandria vessel rupture disk activation: increased pressure within the calandria vessel surpasses the designed limits, leading to the activation of rupture disks installed as safety measures. These rupture disks are intended to relieve excessive pressure to prevent structural damage. Consequently, the rupture disks burst open, providing a pathway for the release of pressurized material.
9) Release of a moderator into containment: as the rupture disks burst, a portion of the moderator is expelled from the calandria vessel. This expulsion occurs through designated calandria vessel relief ducts, leading to the containment structure.
10) Moderator boil-off: simultaneously, within the remaining fuel channels, the cooling mechanisms continue to degrade due to the absence of active cooling systems. As a result, the fuel channels start to dry out on the inside, causing the coolant to boil off. This vaporization of the moderator contributes to an increase in heat generation within the reactor core.
11) Hydrogen generation: high temperatures may trigger chemical reactions between fuel cladding and coolant, potentially leading to the generation of hydrogen gas.
12) Core degradation: cumulative effects of heat accumulation, fuel element degradation, and potential reactivity changes contribute to core degradation.
13) Core debris relocation: degradation of cooling mechanisms and structural integrity within the reactor core leads to a significant change in the disposition of core materials. Because of the core's deterioration, a portion of the core debris, comprising damaged fuel elements and structural materials, relocates onto the floor of the calandria vault. This relocation is driven by factors such as gravity and the loss of structural support.
14) Calandria vault water loss: simultaneously, the water present within the calandria vault, serving as a coolant and moderator is further depleted. As the reactor's operational conditions deteriorate, and the cooling mechanisms continue to degrade, the remaining water within the calandria vault begins to boil off.
15) Debris heating and core concrete interactions: as the core materials continue to deteriorate and accumulate on the calandria vault floor, the intense heat generated by the degraded fuel elements and structural materials heats up the debris. This elevated temperature initiates molten core concrete interaction. As the heated debris comes into contact with the concrete structures of the calandria vault floor, chemical and thermal interaction takes place that can lead to the erosion and melting of the concrete materials.

The potential for airlock seal failures within the containment structure becomes particularly pronounced in the course of various events, notably during phases marked by rapid steam generation. These instances include occurrences like core collapse, calandria vessel failure, and calandria vault failure, which lead to abrupt pressure surges. Amid multiple stages of the accident scenario, the emission of fission products from the fuel becomes plausible due to the presence of intensely heated core debris. The extent of this release can be noteworthy, especially when hot core debris is suspended within the calandria vessel or during the interaction of the molten core with concrete.

This is where user input and code assumptions can significantly influence the accident sequence / timing. An earlier occurrence of core collapse, for instance, reduces the duration during which debris remains suspended within the calandria vessel. This, in turn, mitigates the production of hydrogen and the release of fission products. Furthermore, an early core collapse also has the potential to diminish the pressure spike

triggered by the quenching of debris, thus avoiding the risk of containment failure during that specific timeframe.

2.3.4. Plant initial conditions

Although consistent initial conditions in the codes were used, some variations were unavoidable, and they are factored into the inter-comparisons. The major initial conditions of CANDU 6 for normal operating conditions are shown in Table 6.

TABLE 6. INITIAL CANDU 6 NORMAL OPERATING CONDITIONS

Parameters	Unit	Target value	CNL	KAERI	UPB
Core thermal power	MWth	2,155.9	2,155.9	2155.9	2,072
PHTS pump power	MW	17.0		17.0	
Heat loss to containment	MW	3		3	
Heat load to moderator	MW	105.9		105.9	
Thermal power to steam generators		2,064	2,082	2,064	2,071.8
RIH temperature	°C	266	289	268	267
ROH temperature	°C	310	289	311	311
RIH pressure	MPa(a)	11.85	10.69	11.83	11.23
ROH pressure	MPa(a)	10.1	10.69	9.81	10.02
Pressurizer pressure	MPa(a)	9.99	10.69	9.9	9.85
PHTS loop flow	kg/s	1925	1925	1899.6	1,917.78
Loop inventory (one loop)	kg	47,545	47,545	40,919	45,935.6
Pressurizer inventory	kg	30,555	30,614	31,143	25,803.1
Total primary inventory including pressurizer	kg	125,704	125,704	112,982	117,635.2
Steam generator pressure	MPa(a)	4.7	4.7	4.7	4.7
Steam generator temperature	°C	260	260.2	261	260
Steam generator inventory (per steam generator)	kg	38,000	38,000	38,000	38,003.4
Moderator cover gas pressure	kPa(a)	123	97	123	121.675
Moderator temperature	°C	69	69	68.9	69.8
Moderator inventory	kg	227,000	227,000	214,800	235,578
End shield pressure	kPa(a)	101	101	111.6	101.3
End shield temperature	°C	63	63	63.4	53.9
End shield inventory	kg	14,508	14,508	14,272	14,647.0
Reactor vault pressure	kPa(a)	101	101	111.6	101
Reactor vault temperature	°C	51.5	51.5	51.8	53.9
Reactor vault inventory	kg	499,687	499,687	512,300	534,975
Reactor vault pressure relieve valves opening pressure	kPa(d)	70	70		
Reactor vault pressure relieve valves flow area	m^2	0.016206	0.016206		
Containment pressure	kPa(a)	101	101	100.8	101
Containment temperature	°C	31.85	31.85	32	34
Total containment free volume	m^3	51,325	51,325	51,325	51,325

2.4. CANDU 6 PLANT NODALIZATION

Nodalization for severe accident analysis in a CANDU 6 nuclear power plant involves the development of a detailed computational model that divides the plant into discrete nodes or regions to simulate the behaviour of the reactor system during severe accident scenarios. Nodalization is a crucial step in conducting safety assessments and understanding the consequences of such accidents. In general, the nodalization for severe accident analysis is a complex and resource intensive task that requires expertise in thermal hydraulics modelling, nuclear engineering, and severe accident analysis. This section describes approaches taken by every of three participants.

2.4.1. Canadian Nuclear Laboratories

In this section the system idealization, the major initial and boundary conditions used in the benchmark analysis are described. The CANDU 6 plant nodalization is nearly identical to the nodalization described in [2]. The CANDU 6 plant is described in Section 2.3.1.

2.4.1.1. Containment model

The CANDU 6 containment is a very complex engineered enclosure as described in [2] serves as a robust and multi-layered protective barrier against the release of radioactive materials in the event of an accident or operational anomalies. The containment's design and structure are engineered to withstand various scenarios, ensuring the safety of personnel, the public, and the environment. In instances where multiple rooms are interconnected by sizable openings, the gas pressure within those rooms tends to equalize, resulting in a coherent pressure environment. Consequently, these rooms can be effectively combined for analysis purposes. The containment structure is divided into 13 nodes and 31 flow junctions, as illustrated in Fig. 4. Details of the containment compartments implemented in MAAP-CANDU nodalization used in this benchmark, were obtained from the CANDU 6 containment design drawings. In the representation depicted in Fig. 4, solid lines represent open junctions between nodes enabling fluid flow between them, while dotted lines represent failure junctions that activate in response to pressure differentials or, in the case of junction J29, due to interactions between molten corium and concrete. J30 is containment failure junction that leads to the environment, J26 corresponds to the rupture disk positioned between the reactor vault and the containment structure while J32 represents the containment leakage and J17 represents a hatchway, yet it is kept sealed by imposing a very large pressure differential.

The containment nodalization includes reactor vault and end shields as containment designated as Containment Nodes 10 and 11 in Fig. 4. Additionally, the nodalization includes the segmentation of the steam generator rooms into two distinct nodes, Nodes 8 and 13. The nodalization configuration aligns with the principles explained in [2]; the total of 90 wall heat sinks (walls and floors) in containment are included in the model. Structural steel in the containment (steel beams, columns, gratings, etc.) with a total mass of 820,000 kg is represented as a two-sided steel plate with a thickness of 2.54 cm and a total surface area of 8,200 m^2. The structural steel mass is distributed within the containment compartments.

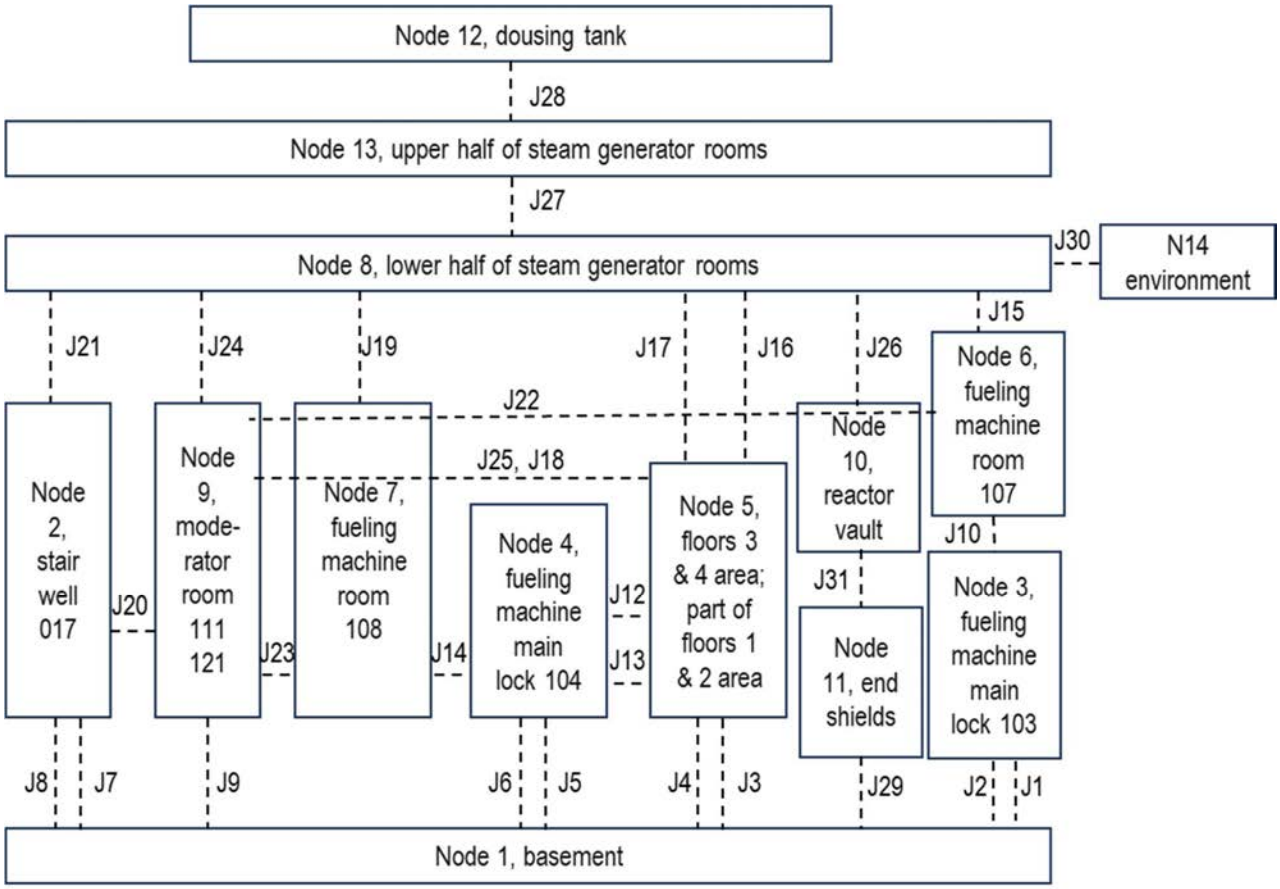

FIG. 4. Nodalization scheme for CANDU 6 containment.

2.4.1.2. Primary heat transport system nodalization

The CANDU 6 PHTS nodalization is nearly identical to the nodalization described in [2]. The CANDU 6 PHTS is comprised of two loops, each serving a specific subset of 190 out of the total 380 fuel channels. Each of these loops is supplied with a suite of components to facilitate efficient heat transfer and circulation of coolant. The individual components within each loop include two steam generators, two pumps, two heat headers and two outlet headers. The integration of these components facilitates the controlled flow of coolant throughout the system. The coolant flow is directed through feeders that link the inlet and outlet ends of the fuel channels to their corresponding reactor inlet and outlet headers. This arrangement ensures the effective exchange of heat between the reactor core and the coolant.

The PHTS configuration in the CANDU 6 reactor system is particularly notable for its distinctive “figure of eight” flow pattern. In this configuration, the flow direction within the fuel channels of one loop follows a pattern resembling a “figure of eight.” This design approach introduces a level of intricacy where certain channels carry coolant flow inward toward the reactor core, while others channel the flow outward from each reactor face. This flow arrangement contributes to efficient heat transfer and temperature moderation within the core. Figure 5 provides a visual representation of this configuration as modelled in MAAP-CANDU, illustrating the arrangement of coolant flow within the PHTS loops.

The following PHTS components are modelled as 14 nodes in MAAP-CANDU as per Fig. 5:

1. Pump discharge line before inlet header 1
2. Reactor inlet header 1
3. Reactor outlet header 2
4. Inlet piping of steam generator 2
5. Hot leg tubes of steam generator 2
6. Cold leg tubes of steam generator 2
7. Pump suction line after cold leg tubes of steam generator 2
8. Pump discharge line before inlet header 2
9. Reactor inlet header 2
10. Reactor outlet header 1
11. Inlet piping of steam generator 1
12. Hot leg tubes of steam generator 1
13. Cold leg tubes of steam generator 1
14. Pump suction line after cold leg tubes of steam generator 1

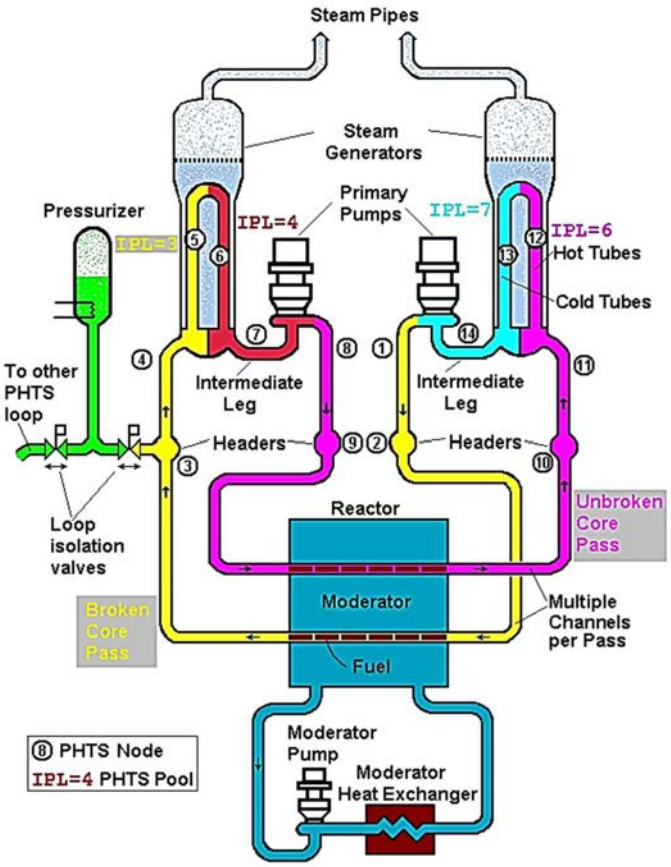

FIG. 5. MAAP-CANDU simplified PHTS nodalization (showing both core passes of one PHTS loop).

The feeder pipes, which serve to connect the headers and fuel channels within the PHTS are incorporated into the fuel channel nodalization. The 380 inlet feeder pipes, responsible for transporting coolant from the

headers to the fuel channels, are modelled with 18 distinct nodes allocated to capture their behaviour and interactions. Each node captures specific characteristics and dynamics associated with the inlet feeder pipes. Similarly, the 380 outlet feeder pipes, responsible for transferring coolant from the fuel channels to the headers, are allocated an additional 18 nodes in the nodalization scheme.

2.4.1.3. Core and fuel channel nodalization

The CANDU 6 core and fuel channel nodalizations are nearly identical to the nodalizations described in [2].

The CANDU 6 core's 380 fuel channels are arranged in a grid pattern of 22 rows and 22 columns as illustrated in Fig. 6. However, not every fuel channel is modelled in MAAP-CANDU. A simplified core model includes dividing the 22 rows into six vertical nodes, with the allocation of rows as follows: 4, 4, 3, 3, 4, and 4 rows in each respective node.

Within each of these vertical nodes, a further division is made into three distinct fuel power groups: high power channels representing the highest power group within the given vertical node, medium power channels corresponding to the medium power group within the vertical node, and low power channels corresponding to the lowest power group within the vertical node, completing the segmentation. This arrangement is depicted in Fig. 7.

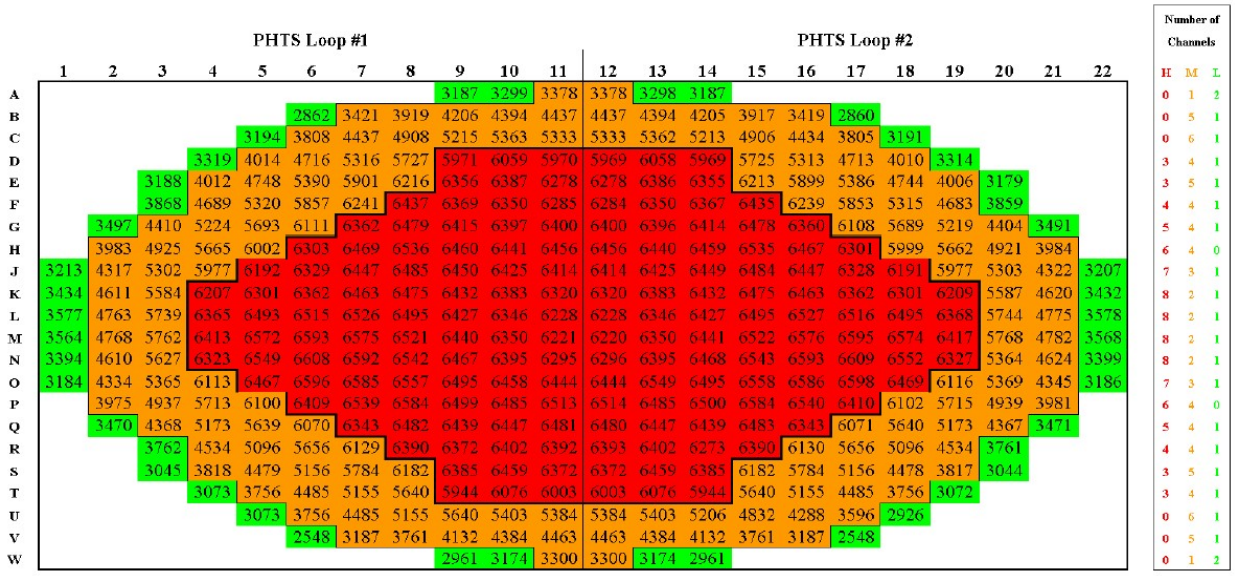

FIG. 6. Nodalization Scheme for CANDU 6 core: time averaged power for each channel is shown with four digits in [kW]; the notations H, M and L refer to high, medium and low power groupings per loop [2].

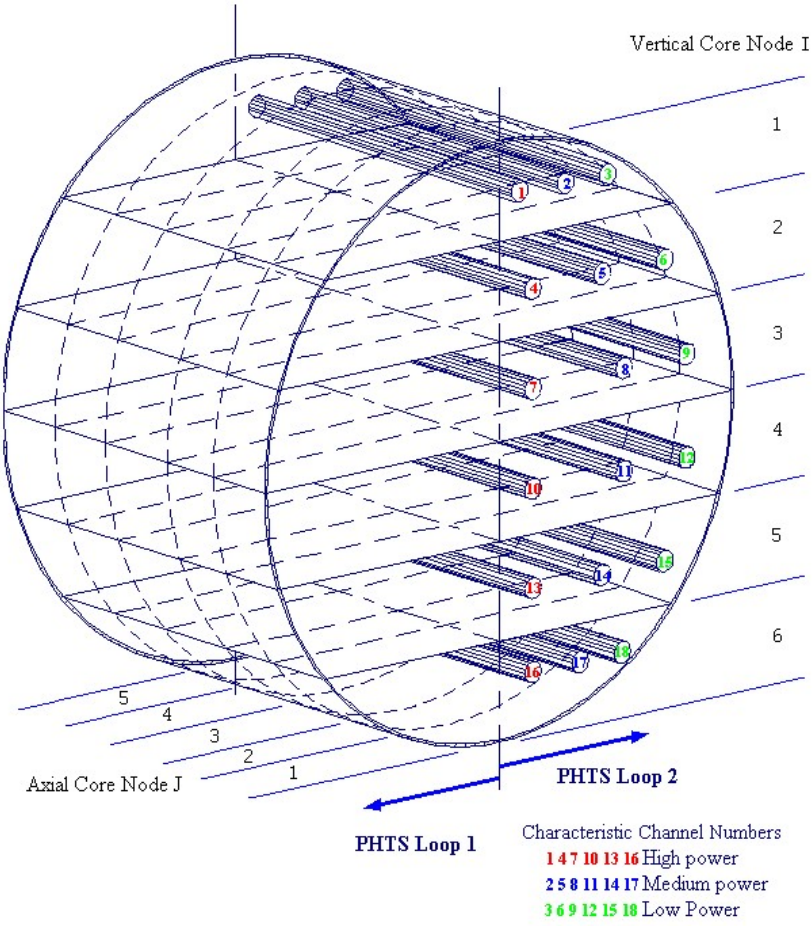

FIG. 7. Nodalization scheme for CANDU 6 core [2].

The 22 columns of fuel channels are symmetrically divided into two loops around the vertical axis. This division reduces the total number of fuel channels to two loops, each consisting of 18 (= 6×3) representative channel groups. Each fuel channel in CANDU 6 accommodates 12 individual fuel bundles. For the purpose of this study, each of these fuel bundles is treated as an individual axial node, as illustrated in Fig. 7. Consequently, the total of 380 fuel channels, each comprising 12 fuel bundles, translates to a total of 432 nodes (2×6×3×12) in the MAAP-CANDU model, as depicted in Fig. 7.

Each CANDU 6 fuel channel consists of a calandria tube, a pressure tube, and 37 fuel elements organized into four distinct rings: central, inner, intermediate, and outer rings, as shown in Fig. 8. In the modelling approach, each of the inner, intermediate, and outer fuel rings is equivalently treated as two separate rings, leading to a total representation of nine rings for a CANDU 6 fuel channel configuration, as illustrated in Fig. 9.

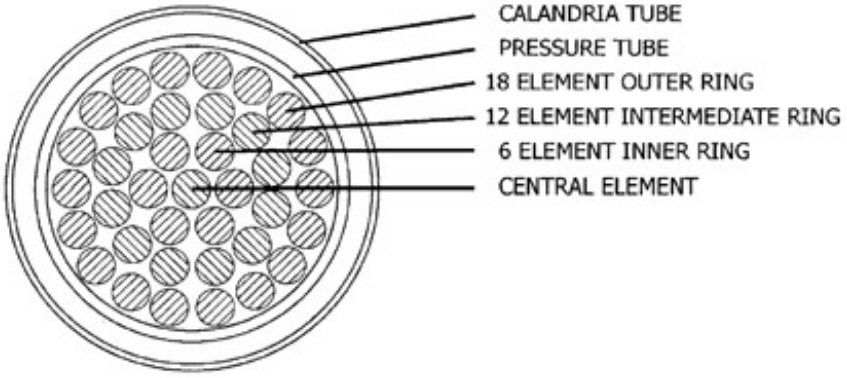

FIG. 8. CANDU 6 Fuel bundle consisting of a calandria tube, a pressure tube and 37 fuel elements [2].

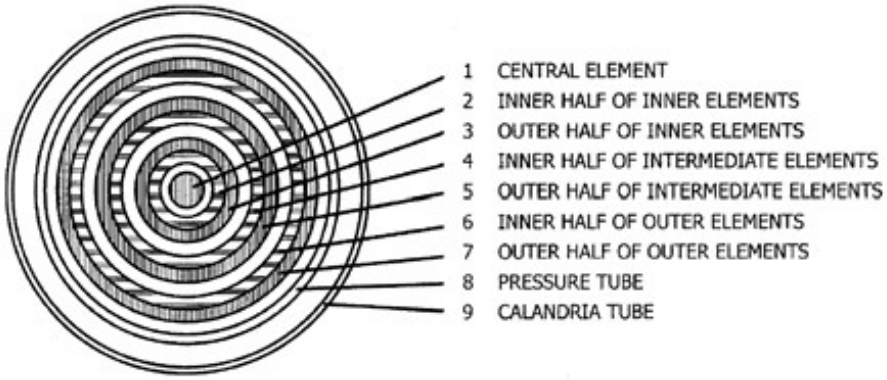

FIG. 9. CANDU 6 Fuel channel nodalization scheme used in MAAP4-CANDU [2].

2.4.1.4. Calandria vessel wall nodalization

The CANDU 6 calandria vessel nodalization is nearly identical to the nodalization described in [2].

MAAP-CANDU model of temperature distribution in the calandria vessel walls is based on two dimensional approach. Two types of the calandria vessel walls are considered: front and back face of the calandria vessel are seen as flat surfaces (wall-type), and the cylindrical shell wall representing the cylindrical surface of the calandria vessel. Each of these wall types is discretized into 15 horizontal nodes that span from the base of the vessel to the ceiling, following the elevation levels, as visually illustrated in Fig. 10. Additionally, the thickness of the calandria vessel walls is divided into radial nodes, a division that plays a critical role in facilitating internal heat conduction calculations within the walls. The thickness of each radial node is determined by the MAAP-CANDU code, which ensures a rigorous treatment of heat conduction mechanisms within the walls. The modelling approach within MAAP-CANDU involves certain simplifications for computational efficiency: for the circumferential wall slice of the calandria vessel, it is assumed that the temperature is uniform along the surface at any given time, streamlining the analysis by considering circumferential uniformity, and for each slice of the front and back face of the calandria vessel, uniformity in temperature is assumed along the vertical direction.

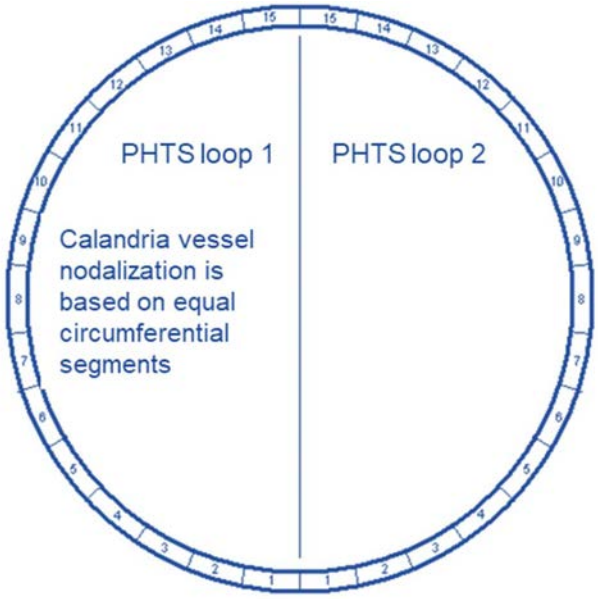

FIG. 10. Nodalization for CANDU 6 calandria vessel wall [according to 2].

2.4.1.5. Steam generator model

The CANDU 6 steam generator model and nodalization are nearly identical to the nodalization and model described in [2].

In the MAAP-CANDU simulation, the steam generator system is characterized by its nodal representation, wherein each component's behaviour is modelled within specific nodes. The configuration comprises distinct nodes to account for both the primary and secondary sides of the steam generator as follows:

- Primary side of the steam generator is divided into two separate nodes: the cold legs and the hot legs. These nodes include the essential features of the primary system, allowing for the thorough simulation of heat exchange and fluid flow within the steam generator;
- Secondary side of the steam generator is represented as a unified node that addresses the behavior and characteristics of the secondary coolant system, reflecting its interactions and thermal exchanges during operational and transient scenarios.

The MAAP-CANDU input deck includes a range of parameters to accurately describe the design and functioning of both the primary and secondary sides of the steam generator. These parameters include the pressure set point for safety relief valves, the total volume of the primary side, the count of U shaped tubes, the internal diameter of the U shaped tubes, the diameter of the tube sheet, the vertical distance between the shell and the tube sheet, and a tabulated dataset illustrating the correlation between volume and height on the secondary side.

2.4.1.6. Pressure and inventory control system modelling

The CANDU 6 pressure and inventory control system modelling features are nearly identical to the modelling approach as described in [2].

The pressure and inventory control system within the CANDU 6 plant comprises several key components that facilitate safe operation and respond to varying conditions: pressurizer, degasser condenser, D_2O storage tank, D_2O feed pumps, bleed cooler, pressurizer relief valves and PHTS liquid relief valves. The pressurizer relief valves, steam bleed valves, and PHTS liquid relief valves discharge their contents into the degasser condenser, which features spring loaded relief valves that discharge into a designated containment compartment. It is important to note that the backup air operated PHTS LRVs are designed to fail open, ensuring continued system operation under critical scenarios such as power loss.

The pressurizer, which is connected to the reactor outlet header, is included in the MAAP-CANDU model. Furthermore, a motor operated pressurizer isolation valve is integrated into the line connecting the pressurizer and the reactor outlet header. This valve is designed to automatically close in the event of a LOCA, and its closure parameters can be user specified.

The analysis considers various thermal hydraulic processes, including boiling, condensation, flashing, and rain out. The behaviour of fission products and pressurizer heaters is also modelled in MAAP-CANDU. However, the degasser condenser is not included in the analysis. Pressurizer steam bleed valves and pressurizer relief valves are assumed to be closed due to the absence of electrical power. The opening and closing set points for the LRVs are artificially set to values corresponding to degasser condenser spring loaded relief valves. It is assumed that no backup instrument air is available to maintain LRV operation after the SBO event initiation.

The analysis considers various failure criteria for different components of the CANDU 6 reactor, such as containment, calandria vessel, fuel channel, and reactor vault. Some criteria require user input values, while others are calculated by the MAAP-CANDU code based on experimental data or engineering judgment when experimental data are not available. To model the pressure and inventory control system configuration for SBO event, the following assumptions are applied:

- Pressurizer steam bleed valves (PCV5 and PCV6): these valves are not spring-loaded and are assumed to remain closed throughout the analysis due to the absence of electrical power;
- Pressurizer relief valves (PV47 and PV48): these valves have higher set points than the LRVs are also assumed to be closed all the time;
- LRVs set points: are artificially set to match the set points of the degasser condenser spring loaded relief valves (RV-11 and RV-21) in the parameter file. It is assumed that there is no backup instrument air available to maintain LRV operation after the SBO event begins;
- Failure criteria: the analysis outcome depends on the failure criteria applied to various components of the CANDU 6 reactor, including containment, calandria vessel, fuel channels, and reactor vault. Some criteria require input from the user, while others are computed and applied by the MAAP-CANDU code. These criteria are established based on experimental data when available, and engineering judgment is used when experimental data is lacking. A description of the failure criteria used in the present analysis is given in Section 2.5.1.

2.4.2. Polytechnic University of Bucharest

This section describes the nodalization approach applied in the modelling of the SBO event in CANDU 6 plant.

2.4.2.1. Primary heat transport system modelling

The nodalization scheme used for the PHTS is shown in Fig. 11; four (4) hydrodynamic characteristic channels per pass, 16 in total, are considered. Each representative channel is subdivided into 12 control volumes. The heat losses from the PHTS to the containment environment are modelled with RELAP heat structures with convective heat transfer as a boundary condition. The nodalization scheme for the steam generator and main steam lines is depicted in Fig. 11. The U tubes are discretized in eight (8) nodes. Separate nodes are allocated for the inlet and outlet plenum of the U tubes. The secondary side of the steam generator consists of several components: preheater, riser, separator, drum, and downcomer. Each of these components is discretized into a different number of nodes.

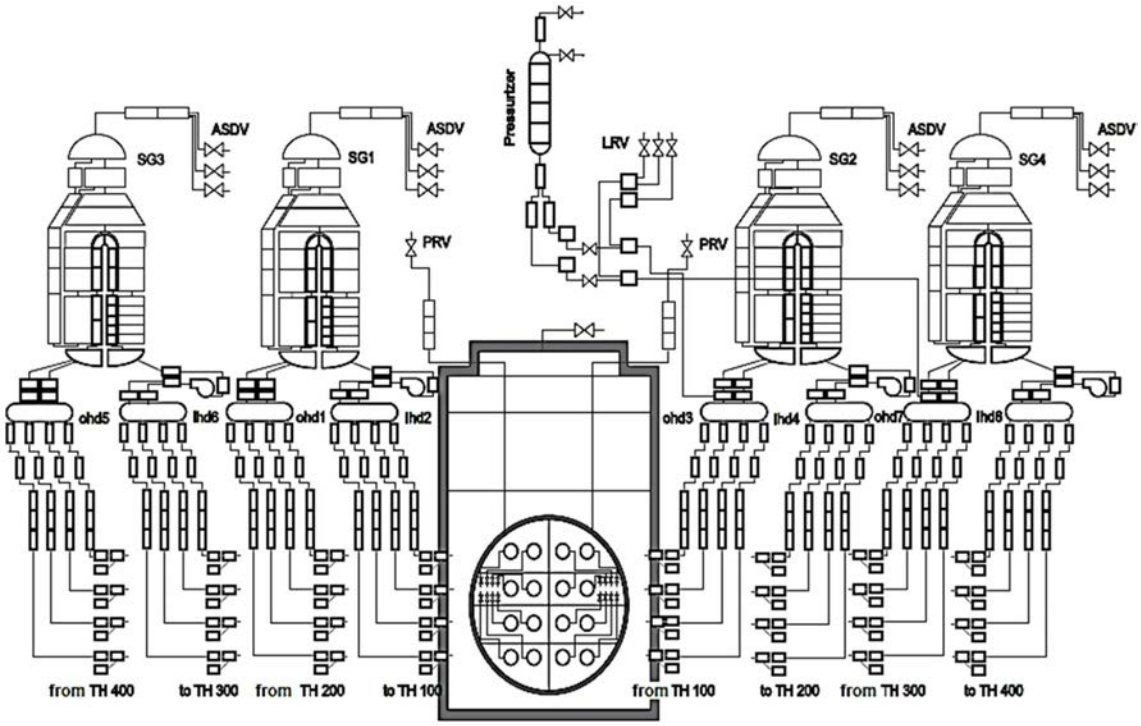

FIG. 11. PHTS nodalization.

2.4.2.2. Fuel channel modelling

In a fuel channel, the 37 fuel elements of the fuel bundle, the pressure tube and the calandria tube are modelled using SCDAP; the visual representation is shown in Fig. 12. All fuel elements which belong to the same fuel bundle are considered to have the same power. The pressure tube, the CO_2 filling the annular space between pressure tube and calandria tube, and the calandria tube are modelled using shroud components. The 12 bundles in a CANDU fuel channel were modelled as 12 axial nodes.

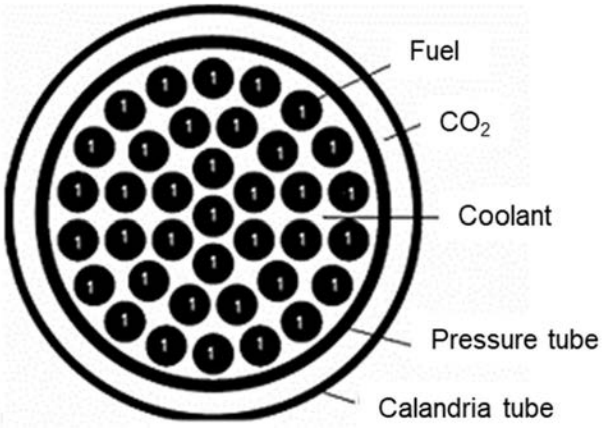

FIG. 12. SCDAP model for the fuel channel.

Four representative channels per core pass were considered to simulate the thermal response of fuel channels. Figure 13 depicts the reactor core with a visual representation of the core power map and an indication of how the channels are divided into the selected representative channels.

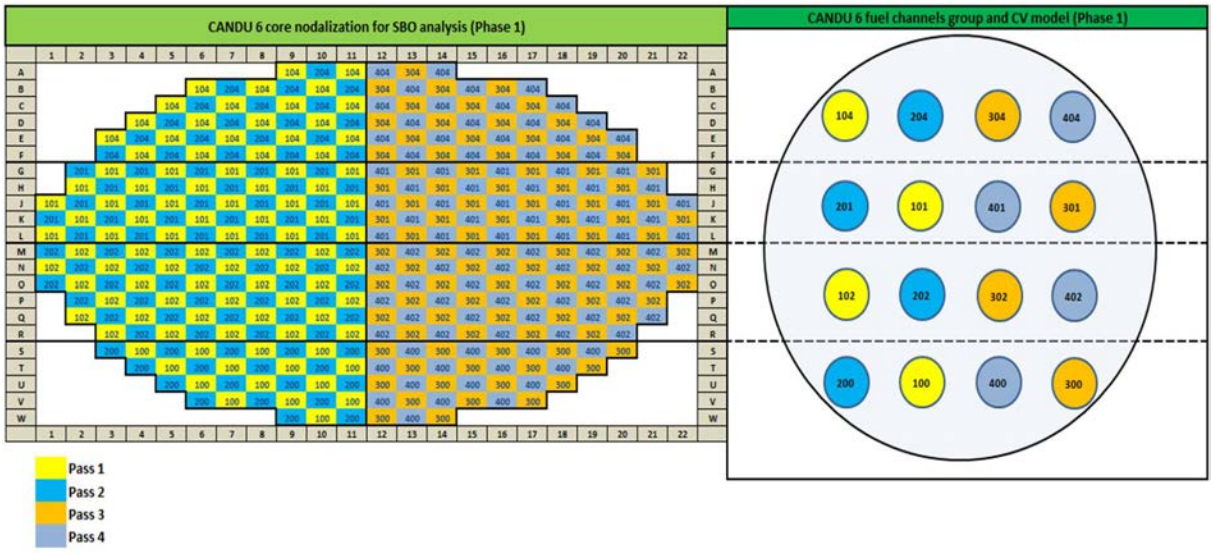

FIG. 13. Core power map and the division into representative channels.

2.4.2.3. Calandria vessel modelling

Calandria vessel is modelled as a pipe component. is divided into four sub-volumes with a vertical orientation. These sub-volumes represent the sections of the calandria vessel that are adjacent to the fuel channels. The analysis includes the modelling of four calandria pressure relief ducts. These are represented as pipe components with three sub-volumes each, oriented vertically. These ducts serve as pathways for pressure relief in case of overpressure conditions within the calandria vessel. The calandria overpressure rupture disk is modelled as a trip valve. This component connects the calandria vessel to the containment system. In the event of an overpressure situation within the calandria vessel, the rupture disk is designed to

release pressure by allowing gases to escape into the containment. Figure 14 shows the calandria vessel model.

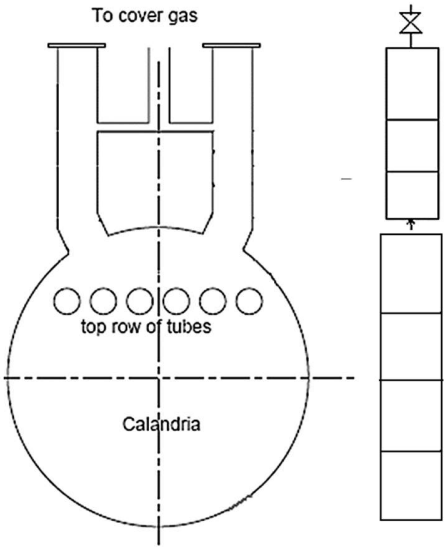

FIG. 14. Calandria vessel nodalization.

2.4.2.4. System modelling after calandria vessel dry-out

The SBO analysis involves two steps: the initial modelling of the plant's behaviour until core collapse and a subsequent step where the COUPLE module is used to model the behaviour of debris and structures post core collapse. Therefore, the first step involves analysing the reactor response during the initial stages of the SBO event, leading to the conditions that trigger the core collapse. After the fuel channels collapse onto the bottom of the calandria vessel (because of the core collapse), the analysis enters the second step. In this step, the focus shifts to modelling the debris and the calandria wall using the COUPLE module. The COUPLE module simulates the behaviour of debris and surrounding structures during severe accidents. This step involves calculating the heat up of the debris and the structural components that come into contact with the debris. A two dimensional finite element mesh is generated by the COUPLE module. This mesh helps discretize the modelling space into smaller elements, allowing for a detailed representation of the behaviour of the debris and structures. The COUPLE model for the bottom of the calandria vessel is shown in Fig. 15.

At the beginning of the COUPLE module phase, user defined slumping of debris is imposed within the mesh. This means that the arrangement and distribution of the debris are defined according to the input data. Parameters such as mass, composition, porosity, and particle diameter are defined for the debris. These characteristics impact how the debris interacts with its surroundings and how heat is generated. The rate of heat generation per unit volume is defined for the debris material. This heat generation contributes to the heat load applied to the calandria vessel wall. Convection and radiation heat transfer occur from the upper boundary of the debris bed to connected volumes within the simulation space. This reflects the heat transfer processes taking place within the debris. Convection heat transfer occurs between the calandria vessel wall and surrounding RELAP5 hydrodynamic volumes. This accounts for the heat exchange between the vessel wall and the fluid in its vicinity. A detailed mesh is created to represent the calandria vessel filled with

debris. The mesh structure allows for a granular representation of the spatial distribution of debris and its interactions. Volumes inside the mesh represent calandria vessel internals, while volumes outside the mesh represent the contents of the reactor vault. Both the calandria vessel and the reactor vault are connected to the containment, allowing for the modelling of heat transfer and mass flow interactions between these interconnected systems.

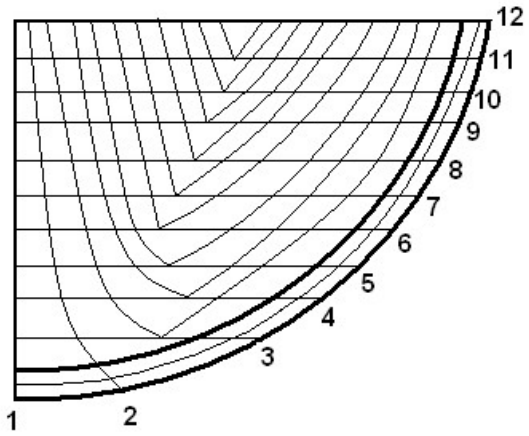

FIG. 15. COUPLE meshes (numbers refer to calandria vessel outside the wall nodes).

The heat generated in the corium located on to the bottom of calandria vessel is transferred to the water surrounding the calandria vessel through the calandria vessel wall and by radiation from the top surface of corium. This heat transfer by radiation is modelled by a fictitious heat slab placed on the top of the debris-bed and having the same temperature as the temperature of the top debris bed nodes. The model used for late phase of the severe accident calculation is shown in Fig. 16.

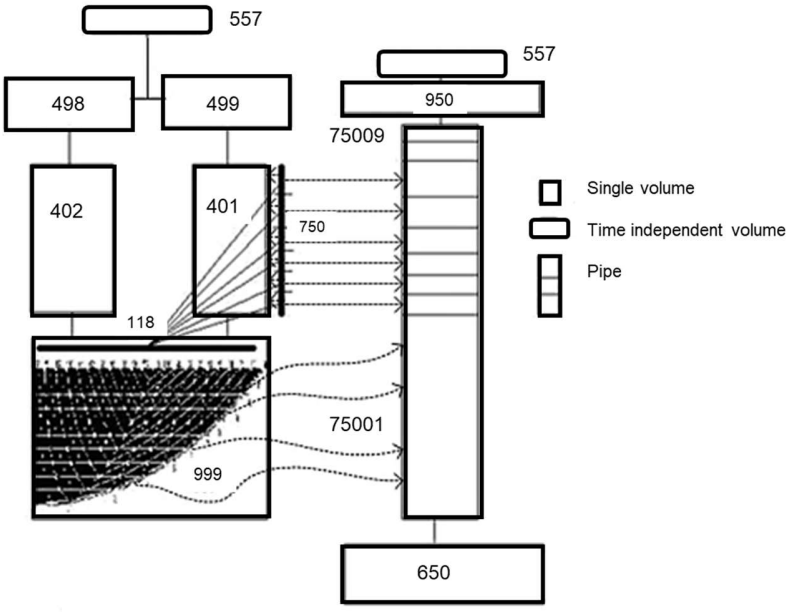

FIG. 16. Late phase of the severe accident calculation model.

2.4.3. Korea Atomic Energy Research Institute

CAISER core analysis code simulates the accident progression inside a fuel channel by utilizing the fuel rod degradation module and the global accident progression in a calandria vessel by utilizing the fuel channel degradation module. Since the CANDU 6 reactor core has 380 fuel channels, in order to simulate the global accident progression in a calandria vessel, the detailed information for the accident progression in each fuel channel is deemed necessary. Likewise, since the accident progression in a fuel channel is also affected by the thermal-hydraulic condition in a calandria vessel, the information for accident progression in a calandria vessel is necessary to analyse the severe accident phenomena in each fuel channel.

The CAISER-C code employs a structured approach to simulate the degradation phenomena in both fuel channels and fuel rods within a calandria vessel. The interaction between the fuel channel and fuel rod degradation modules involves repeated calculations, information exchange, and synchronization to accurately capture the complex behaviour of the system. This iterative approach allows for a comprehensive understanding of the core degradation process during an accident scenario. Thus, the simulation involves modelling both fuel channel and fuel rod degradation phenomena. The fuel channel refers to the larger structure that contains multiple fuel rods. Each fuel channel degradation module is designed to communicate with its corresponding fuel rod degradation modules. This suggests that the behaviour of the entire fuel channel is influenced by the individual behaviour of its constituent fuel rods. To accurately capture the interactions and conditions, the fuel rod degradation module's calculation is repeated for each node in the calandria vessel. Each node in the fuel channel degradation module represents an independent part of the calandria vessel, each with its own power and thermal hydraulics boundary conditions. This implies that for each time step, the fuel rod degradation module calculations are performed multiple times, equal to the number of nodes in the calandria vessel. The fuel channel degradation module is computed once all nodes of the corresponding fuel rod degradation modules have received information. After the fuel channel degradation module computation, each node of the fuel channel degradation module sends information back to the corresponding fuel rod degradation modules. This communication loop helps ensure that the interactions and effects between the fuel channel and individual fuel rods are captured accurately. Once this communication and computation cycle is completed for a time step, the simulation proceeds to the next time step.

2.4.3.1. Primary heat transport system modelling

In the CAISER code, the coolant in a fuel channel has been simulated by utilizing the existing thermal hydraulic system code (MARS-KS), which has 1-dimensional representation for a fuel channel in a flow direction. Fig. 17 shows the PHTS nodalization CANDU 6 of MARS-KS. It consists of 420 nodes and 455 junctions. The core consists of 16 flow channels having 12 nodes in a flow direction and each flow channel is coupled with that of CAISER-C code, which simulates core degradation in a fuel channel. Over pressure protection (safety valves) is modelled, including a pressurizer safety valve, liquid relief valve, degasser condenser tank, degasser condenser relief valve. The degasser condenser relief valve is connected to the volume of containment analysis code, CONTAIN. Additionally, when a calandria vessel is failed, corium from calandria vessel is discharged in containment compartment through a control functional valve, which is designed to open under a calandria vessel failure condition.

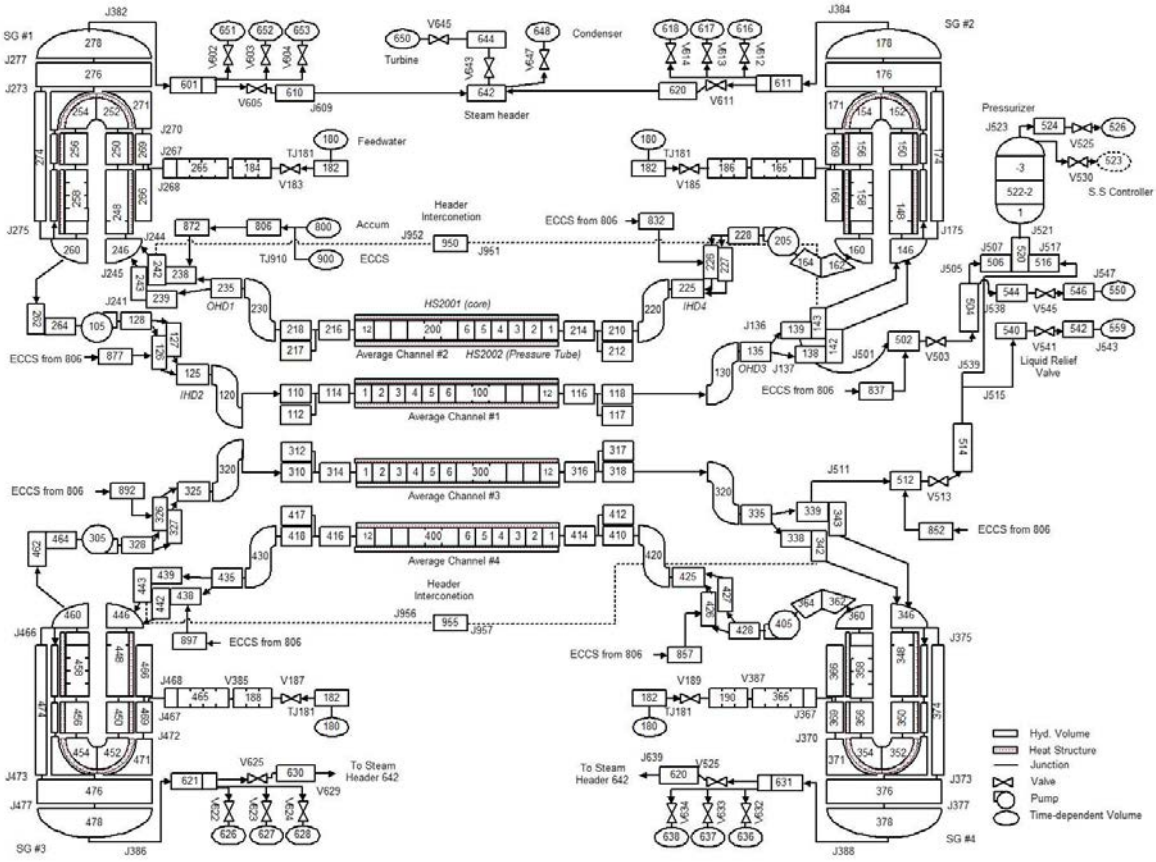

FIG. 17. Nodalization of CANDU 6 reactor used in the CAISER code.

2.4.3.2. Fuel channel modelling

Figures 18 and 19 illustrate the nodalization for the CAISER-C code, which consists of the fuel rod degradation module and the fuel channel degradation module. In a fuel rod degradation module, since a fuel rod bundle has a bilateral symmetry, the half of a fuel bundle is analysed, and modelled with the node number [*M*, *N*]. The fuel channel has an additional one dimensional node in a flow direction with the node number [*K*]. Hence, the fuel rods become to have three dimensional node system under the node number [*M*, *N*, *K*]. Similarly, to the node system in a fuel channel, CAISER-C supports the three dimensional node system in a Cartesian coordinate for 380 fuel channels in a calandria vessel, which has the node number of [*I*, *J*, *K*]. The number [*M*, *N*, *K*] and [*I*, *J*, *K*] are provided by the user in input data. The CAISER-C code has a generalized three dimensional Cartesian coordinates for the severe accident analysis in a fuel channel and in calandria vessel, which provides a proper nodalization approach.

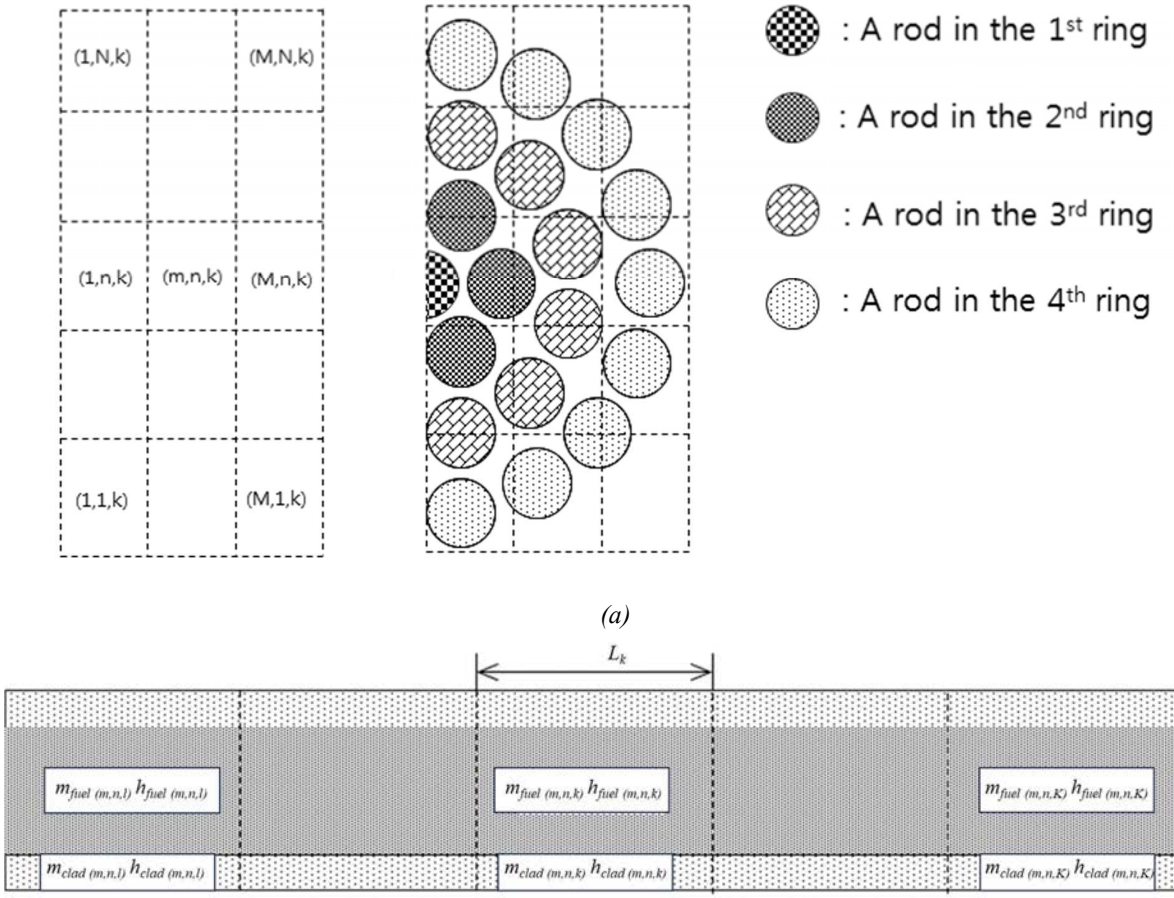

FIG. 18. CAISER nodalization for the fuel rod degradation module: (a) cross-sectional plain of a fuel channel; (b) flow directional plane of a fuel channel.

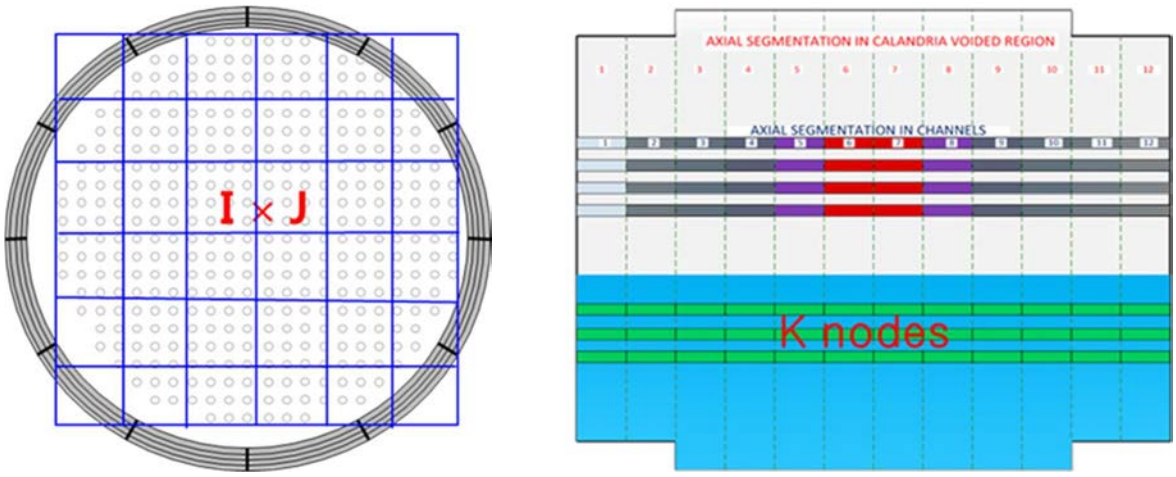

FIG. 19. CAISER nodalization for the fuel channel degradation module.

As shown in Fig. 19, i n the fuel channel degradation module, each node represents a portion of the calandria vessel. The number of fuel channels within each node is geometrically determined by the total node number, represented as [*I*, *J*] in the calandria vessel. This arrangement allows multiple fuel channels to be included in each node, capturing the distribution of fuel channels within the calandria vessel. Each node contains multiple fuel channels, but the governing equations are established for a representative fuel channel. This representative fuel channel is defined by having the average power of fuel channels and is located at the center of the node. The behaviour of the multiple fuel channels within each node is modelled by incorporating the number of fuel channels into the mass and energy equations of the representative fuel channel.

The progression of a severe accident within a representative fuel channel is simulated using the fuel rod degradation module. The outer conditions of a fuel channel, such as moderator water level and radiation heat transfer with the calandria vessel structure, significantly influence this progression. The overall severe accident progression within the calandria vessel is determined by the progression inside individual fuel channels, including factors like calandria tube temperature and fuel channel failure. To ensure accurate modelling, the fuel channel degradation module communicates relevant information with the fuel rod degradation module. This includes sharing information about fuel channel failure status, calandria tube temperature, moderator water level, and outer heat transfer rate.

The fuel rod degradation module provides information about the progression inside a fuel channel, while the fuel channel degradation module provides information related to the overall severe accident progression in the calandria vessel. The interaction and communication between the fuel channel degradation module and the fuel rod degradation module are crucial for accurately capturing the complex interplay between fuel channels and their impact on the overall behaviour of the calandria vessel during severe accidents.

2.4.3.3. Containment modelling

The containment is modelled using CONTAIN code developed for the simulation of severe accident phenomena in a containment building including general containment thermal hydraulics, transport of aerosol or fission product, hydrogen combustion, and molten-corium concrete interaction [10]. It is coupled with MARS-KS and CAISER-C which model in-vessel phenomena. CONTAIN receives from CAISER-C an information related to corium properties, fission product after a calandria vessel failure, while it receives from MARS-KS an information of fluid properties and its thermal hydraulic boundary conditions for the predefined coupled nodes. Pressure operated relief valve flow is connected to cell 33 (steam generator room), while a corium discharge is connected to cell 40 (reactor vault). In the present work, the containment has 41 cells, 72 links and 222 heat structures (Fig. 20).

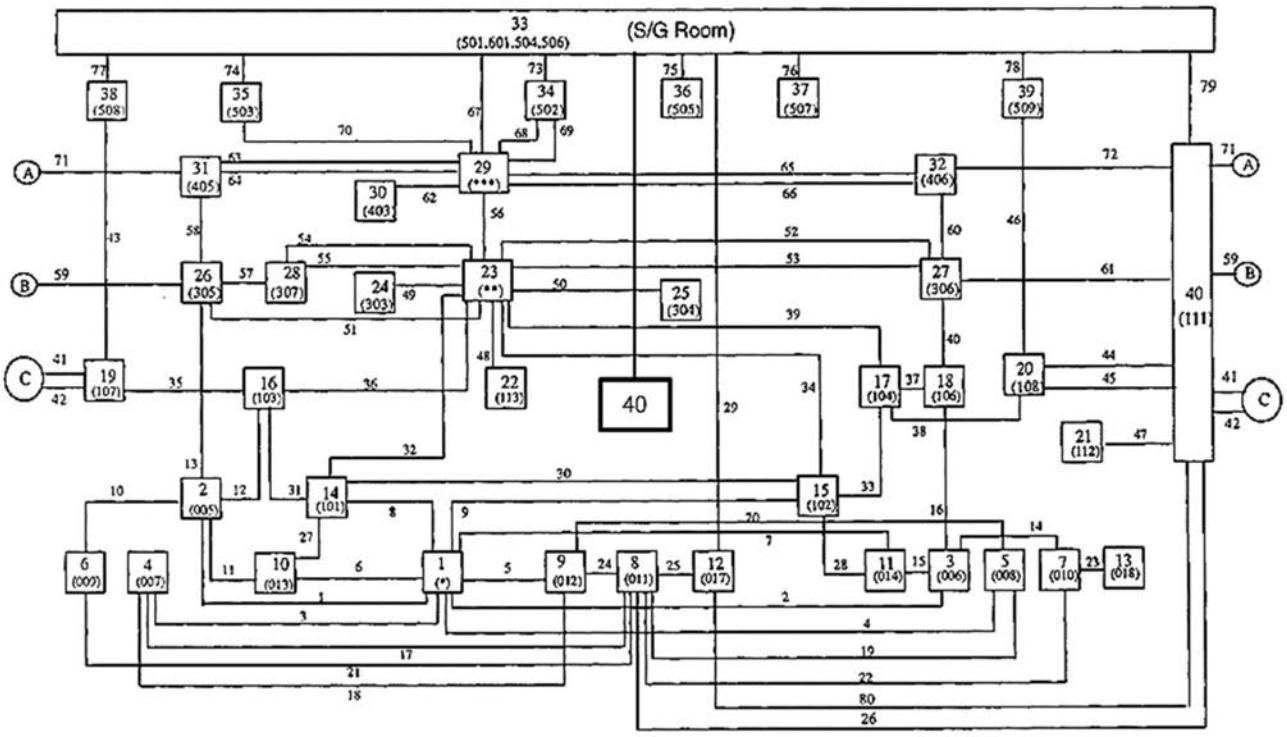

FIG. 20. Containment node system in CAISER code.

2.4.3.4. Calandria vessel wall nodalization

When fuel channel fails, it is transformed to a debris bed, which is ultimately relocated to the bottom of a calandria vessel. As times go on, the temperature of debris bed increases due to a decay heat, and it reaches the melting temperature of metallic and oxidic components. The energy from corium pool is transferred to the coolant in reactor vault. This causes increase in temperature of the calandria vessel wall, which would result in the calandria vessel failure. CAISER-C code simulates a debris bed layer, a metallic layer and an oxidic layer by solving mass and energy equations for each component. The CAISER-C code also considers the crust layer which is formed inside the calandria vessel wall and the inter-region between metallic and oxidic pools.

To predict calandria vessel failure time, the ablated wall thickness is calculated. In CAISER-C model, the vessel wall has a radial and azimuthal node, as shown in Fig. 19. In SBO simulation it is recognized that the calandria vessel wall ablation near a metallic pool is significant, and that it causes the calandria vessel failure (so-called focussing effect).

2.4.3.5. Fission products modeling

For the simulation of fission product behaviour, SIRIUS code is coupled with the CAISER code system. SIRIUS code is developed in KAERI; it is used for an analysis of fission product transport in a core, reactor coolant system, steam generator secondary side, and containment [9]. SIRIUS models behaviour of fission products and actinides in the form of gas and aerosol. The radionuclides are classified into eight (8) groups as shown in Table 7.

TABLE 7. RADIONUCLIDE GROUPS IN SIRIUS CODE

Group	Species
1. Noble gases	Xe, Kr
2. Alkali metal iodides	I
3. Alkali metal hydroxides	Cs
4. Chalcogens	Te, Sb, Se
5. Alkaline earths	Ba, Sr
6. Platinoids	Ru, Mo
7. Rare earths	La, Zr (fission)
8. Structural materials	Zr, Fe, Cr, Ni, Mn,

SIRIUS simulates the release and transfer of gas-phase and aerosol-phase fission products and it also models phenomena such as condensation, evaporation, adsorption, impaction, gravitational precipitation, dispersion, and elimination by deposition on the wall due to temperature. Transport of fluids carrying the gas phase and aerosol phase fission products are calculated by MARS-KS for the PHTS. The fission product behaviour in a containment is analysed using the fission product analysis module in CONTAIN code.Thus, the SIRIUS code is a tool applicable to modelling fission products behaviour during severe accidents, capturing gas phase and aerosol phase interactions and transport. It collaborates with other codes, the MARS-KS and CONTAIN code, to provide the analysis of the behaviour of fission products within the PHTS and containment structure, respectively. This integrated approach allows for a detailed understanding of fission product behaviour across different reactor system components and containment under severe accident conditions.

2.5. FAILURE CRITERIA (FUEL, CHANNEL, CALANDRIA VESSEL, CONTAINMENT)

A summary of the failure criteria used by various analysis codes in the benchmarking study are described in the following Sections, and they are summarised in Table 8.

TABLE 8. A SUMMARY OF ADOPTED FAILURE CRITERIA

Phenomena	Participating Organization		
	CNL	UPB	KAERI
Fuel sheath failure	Fuel element temperature 1,273 K (1000°C)	Mechanistic model to calculate the elastic-plastic deformation using the theory of Hill and	Sheath temperature 1,073°K (800°C)
Fuel bundle slumping	Fuel element temperature of 2,123 K (1,850°C)	Not modelled	Fuel cladding temperature exceeds 1,173 K (900°C)
Fuel channel failure	High PHTS pressure: the ballooning criterion (calculated internally by the MAAP-CANDU code) is satisfied.	The channel is assumed to have failed when a user input pressure tube failure strain (typically 22%) is reached, according to [13].	- Larson-Miller creep-rupture model[1] - Local thermal failure of pressure tube and calandria tube, when the

[1] The model is used to predict when a material will experience rupture under specific temperature and stress conditions; it is empirical model and it thus requires material specific constants that are determined from experimental data.

TABLE 8. A SUMMARY OF ADOPTED FAILURE CRITERIA (Cont.)

Phenomena	Participating Organization		
	CNL	UPB	KAERI
	Low PHTS pressure (< 1.0 MPa(a)), fuel channels may fail because of: - Local melt-through or sagging of pressure and calandria tubes. if the local volume-weighted-average of the pressure-tube and the calandria-tube temperature is greater than the melting point of oxygenated zirconium, or if either tube is hotter than user input temperature currently used as 2,125 K (1,852°C). - Fuel channel is assumed to fail by sagging, when the fuel channel temperature exceeds 1,473 K (1,200°C).		
Fuel channel sagging to below channel	Fuel channel is assumed to fail by sagging, when the fuel channel temperature exceeds 1,473 K (1,200°C), and when there is less than 100 kg of water remaining in the calandria vessel (any remaining fuel channel nodes will disassemble to debris).	Fuel channel is modelled as one beam with two fixed ends before the channel contacts the lower assembly and after channel-to-channel contact, the interaction	Beam theory using the bending momentum with one-side sliding end supports. Sagging is governed by a weight of fuel channel itself and a load increase by a sagging of fuel channel above, together with
Fuel channel disassembly	- Fuel channel disassembles (i.e., separates from the remaining channel nodes to form debris) when the average pressure tube and calandria tube temperature reaches the oxygenated Zr melting point (currently set to 2,125 K (1,850°C)). - When the fuel channel temperature exceeds 1,473 K (1,200°C), and when there is less than 100 kg of water remaining in the calandria vessel, any remaining fuel channel nodes will disassemble to debris.	- Axial node disassembles when the calandria tube temperature exceeds the Zircaloy melting temperature (2,033 K). - Axial node disassembles when the longitudinal strain exceeds 20%. - Channel sagging exceeds two lattice pitches	Fuel channel disassembly is assumed to occur at the same time with a fuel channel failure

TABLE 8. A SUMMARY OF ADOPTED FAILURE CRITERIA (Cont.)

Phenomena	Participating Organization		
	CNL	UPB	KAERI
Core collapse	If the suspended debris bed mass exceeds 25,000 kg per one PHTS loop, the core material in the suspended bed, plus some of the intact channels covered by the moderator (for the same PHTS loop) relocate into the bottom of the calandria vessel.	Beam theory using the bending moment by considering an increase of load due to an accumulated debris mass, which is generated from a fuel channel sagging/disassembly in a core node above.	Since the fuel channel degradation in calandria vessel is step by step progressed by the fuel channel failure mechanisms, the assumption of core collapse is not used in CAISER simulation Elastic beam theory
Containment failure	Containment equipment airlock seal failure at 334 kPa(a).	Not modelled in this study	Containment airlock seal failure at 334 kPa(a). Gross failure at 500kPa(a)

2.5.1. Canadian Nuclear Laboratories

The following sections describe the failure criteria that were used in the CNL analysis. In the most part, the failure criteria for various plant components, are nearly identical to those described in [2].

2.5.1.1. Fuel sheath failure

Fuel cladding is assumed to fail if the average fuel element temperature is higher than a specified value of 1,273K (1,000°C); it is used as the fuel sheath failure criterion in MAAP-CANDU input parameter TCLRUP. Bundle slumping is defined when the fuel element temperature reaches 2,123K (1,850°C), the Zircaloy melting temperature; it is used as the bundle slumping criteria in MAAP-CANDU input parameter TRELOC.

2.5.1.2. Fuel channel failure

Fuel channel failure is defined as a perforation in both the pressure tube and calandria tube, allowing mass transfer between them. At high PHTS pressure, the pressure tube is assumed to fail when it starts to deform or balloon. At low PHTS pressure (<1.0 MPa(a)), fuel channels in the reactor are susceptible to failures due to specific thermal effects, namely local melt through or sagging of the pressure and calandria tubes. Fuel channel melt through occurs if specific temperature conditions are met. The local volume weighted average temperature of both the pressure tube and calandria tube is compared to the melting point of oxygenated zirconium. Alternatively, if either the pressure tube or the calandria tube temperature exceeds a user defined temperature, which is set at 2,125 K (1,852°C), fuel channel melt through is assumed. The MAAP-CANDU input parameter TZRFAIL is used to specify this user defined temperature threshold. Fuel channel failure by sagging is determined based on temperature conditions. The volume weighted average temperature of the pressure tube and calandria tube is compared to a threshold of 1,473 K (1,200°C). If this average temperature exceeds the threshold, the fuel channel is assumed to fail due to sagging. The MAAP-CANDU input parameter TSAGFAIL represents this temperature threshold.

2.5.1.3. Fuel channel disassembly

Disassembly refers to a process where fuel and channel structural materials are separated from their original positions within a fuel channel. These separated materials relocate downward, either to the suspended debris region or to the terminal debris bed located at the bottom of the calandria vessel. When a core collapse occurs (massive relocation of suspended debris and some intact fuel channels to the bottom of the calandria vessel), the suspended debris bed transfers to the calandria vessel's bottom. Disassembly is triggered by specific temperature conditions of the pressure tube and calandria tube. For an uncovered fuel channel, an axial segment of the fuel channel is considered disassembled when the average temperature of the pressure tube and calandria tube reaches 1,473 K (1,200°C). The MAAP-CANDU input variable TSAGFAIL represents this temperature threshold.

2.5.1.4. Core collapse

The core collapse is a critical event during a severe accident scenario where a substantial amount of debris and intact fuel channels relocate to the bottom of the calandria vessel. The accumulation of core debris and materials above the supporting channels leads to the potential collapse of these channels, allowing the debris bed to fall. The mass of the debris bed determines whether core collapse occurs, with specific conditions and failure mechanisms taken into account. The suspended debris is assumed to be supported by the calandria tubes rather than the pressure tubes due to the potential for the latter to be hot and weakened by the severe accident conditions. Under the conditions of core collapse, two main calandria tube failure mechanisms are considered: pulling out (the supporting calandria tubes can potentially pull out from the rolled joints), and shear (the supporting calandria tubes can fail through shear mechanisms). Core collapse is determined by the mass of the suspended debris bed. When the mass of the suspended debris bed exceeds a specific threshold of 25,000 kg per one PHTS loop (the MAAP-CANDU input variable MLOAD(1)), core collapse is assumed to occur. This mass is equivalent to 70 channels, based on the assumption that seven consecutive channels above a submerged channel can support the accumulated mass [3]. In certain conditions, partial core relocation may occur. This can happen as molten core material relocates, potentially reducing the mass available for accumulation in the suspended debris bed. Such a reduction may prevent the accumulation from reaching the core collapse criterion (25,000 kg).

2.5.1.5. Calandria vessel failure

The calandria vessel's failure criterion is tied to the water level in the calandria vault. When the water level drops to the level of the top of the calandria vessel's terminal debris bed, the assumption is that there is inadequate cooling in that region, which can lead to calandria vessel failure. The failure is conservatively assumed to occur at the bottom of the vessel, resulting in the rapid release of the terminal debris into the calandria vault. As a result of this failure, no debris is assumed to remain within the calandria vessel after the failure has occurred.

2.5.1.6. Calandria vault failure

The study accounts for two modes of failure for the reactor vault: pressure induced failure due to internal pressurization and temperature induced failure involving corium concrete interaction. The failure criteria involve specific conditions such as pressure differentials, concrete breach or remaining thickness, and

rupture disk failure. The interaction between the corium and the reactor vault's concrete floor results in erosion, and the reactor vault is considered failed when the eroded concrete thickness reaches a specified value. The pressure induced failure results from internal pressurization. This mode involves a gradual increase in pressure, and no dynamic load analysis is needed. The temperature induced failure is when the concrete of the calandria vault's bottom or sidewall can be penetrated by corium (molten core debris). This penetration facilitates the relocation of core debris out of the vault.

The failure criteria for the calandria vault include the following scenarios:

— Over pressurization: calandria vault is considered to have failed if a predetermined pressure differential between the exterior and interior is achieved;
— Corium concrete interaction: calandria vault is deemed to have failed if its wall is breached or if a certain thickness of concrete remains;
— Rupture disk failure: if there is a differential pressure of 70 kPa across the calandria vault rupture disk, the vault can be deemed to have failed.

After the calandria vessel failure and the relocation of core debris or corium into the reactor vault, core concrete interaction occurs. The interaction between the corium and the reactor vault's concrete floor results in erosion of the concrete. The thickness of the original reactor vault concrete floor is 2.45 m. The reactor vault is considered to have failed when the eroded concrete thickness reaches a user specified value; this eroded concrete depth is set to 2 m.

2.5.1.7. Containment failure

The containment failure criterion is based on the failure of the airlock seal, leading to a blowout that connects the containment to the environment. Additionally, a containment leakage model is used to account for potential leaks proportional to the pressure differential. No other model or criterion for large-scale containment failure is used in the analysis. The containment failure criterion is based on the failure of the containment equipment airlock seal. The seal is considered to fail at a containment pressure of 334 kPa (a) (absolute pressure) when the opening cross sectional area of the seal is 0.01858 m^2. This failure involves the inflatable seals that are typically present within the airlock. The airlocks connect the reactor building (containment) with the service building. For the analysis, it is conservatively assumed that the seals on both the inner and outer airlock doors fail together. There is no time delay assumed to pressurize the airlock volume between the doors. This assumption results in an airlock seal blowout, creating a connection between the containment and the environment. This event is assumed to occur as soon as the containment pressure reaches the specified threshold of 334 kPa (a). This assumption considers scenarios where an airlock door might be open during the accident. In addition to the airlock seal blowout model, another containment leakage model is used. The containment is assumed to leak at a maximum rate of 5% of the containment volume in 24 h when pressurized to 224 kPa (a). The leakage rate is proportional to the pressure differential between the containment and the environment.

2.5.2. Polytechnic University of Bucharest

The following sections describe the failure criteria used in the UPB analysis.

2.5.2.1. Fuel sheath failure

The SCDAPSIM/RELAP5/MOD3.6 calculates the cladding ballooning and rupture based on the mechanistic model to estimate the elastic-plastic deformation applying Hill and the Prandtl-Reuss equations [14].

2.5.2.2. Fuel channel failure

The fuel channel is considered to have failed when a specified pressure tube failure strain is reached. This criterion is used to assess the integrity of the fuel channel's pressure tube under severe conditions. For fuel channels with relatively uniform temperature distribution, a specific value is provided for the average creep strain that corresponds to pressure tube failure; specifically, 22% for the average creep strain associated with pressure tube failure [5, 13].

2.5.2.3. Fuel channel disassembly

The SCDAPSIM/RELAP5/MOD3.6 models the sagging of an entire fuel channel assembly. It is modelled as one beam with two fixed ends before the channel contacts the lower assembly and after channel-to-channel contact, the interaction force between the two channels are considered [5]. One of the following criteria are used to determine disassembly of a fuel channel or a segment of the channel assembly [5]:

- Axial node disassembles when the calandria tube temperature exceeds the Zircaloy melting temperature (2,033 K);
- Axial node disassembles, when the longitudinal strain exceeds 20%;
- Channel sagging exceeds two lattice pitches.

2.5.2.4. Core collapse

The mechanistic core collapse criterion (which is a function of unloaded length and ultimate tensile stress of the calandria tube) is based on the static beam theory, as stated in reference [5]. The RELAP/SCDAPSIM/MOD3.6 code calculates the maximum load on a single channel at each time step. The intact lower channel supports the segments of the disassembled channel from above (from the same column) as a suspended debris bed, until the core collapse is predicted to occur.

2.5.2.5. Calandria vessel failure

The core collapse criterion is based on static beam loading calculation and is a function of unloaded length and ultimate tensile stress of the calandria tube.

2.5.3. Korea Atomic Energy Research Institute

The following sections describe the failure criteria used in the KAERI analysis.

2.5.3.1. Fuel sheath failure

The fuel sheath temperature is set to 1,073 K (800°C).

2.5.3.2. Fuel bundle slumping

The bundle is assumed to have failed when the cladding temperature exceeds 1,173 K (900°C).

2.5.3.3. Fuel channel failure

The following criteria are used to determine disassembly of a fuel channel or a segment of the channel assembly:

- Larson-Miller creep-rupture model;
- Local thermal failure of pressure tube and calandria tube, when the local temperature of pressure tube and calandria tube exceeds the critical melting temperature 1,673 K (1,400°C);
- Global thermal failure of pressure tube and calandria tube, when the average temperature of pressure tube and calandria tube exceeds the user defined temperature 1,273 K (1,000°C), which needs a sensitivity study;
- Ultimate tensile strength by the fuel channel sagging, when the bending moment on a beam (fuel channel) exceeds maximum bending moment at entire cross section, with a consideration of additional load by a relocated debris bed on an intact fuel channel.

2.5.3.4. Fuel channel sagging to the channel below

Beam theory is used based on the bending momentum with sliding end supports. Sagging is governed by a weight of fuel channel itself and a load increase by a sagging of fuel channel above, together with a property change according to a fuel rod temperature.

2.5.3.5. Fuel channel disassembly

Fuel channel disassembly is assumed to occur at the same time with a fuel channel failure.

2.5.3.6. Core collapse

Since the fuel channel degradation in each node of calandria vessel is step by step progressed by the fuel channel failure mechanisms, the assumption of core collapse is not used in the CAISER simulation.

2.5.3.7. Calandria vessel failure

Calandria vessel failure criterion is based on the Larsen-Miller parameter with a consideration of ablated calandria wall thickness. The melting temperature of calandria vessel wall is set to 1,873 K (1,600°C).

2.5.3.8. Containment failure

Containment equipment airlock seal failure is at 334 kPa(a). The opened area of containment by airlock seal failure is 0.027871 m^2. Containment pressure is 500 kPa(a). The opened area of containment by gross failure is 0.1 m^2.

2.6. KEY MODELLING ASSUMPTIONS

Common assumptions adopted for the analysis of CANDU 6 SBO are described in Section 2.3.2. Specific analysis/modelling assumptions are however described in the following sections per participating organization.

2.6.1. Canadian Nuclear Laboratories

The following are the specific modelling assumptions adopted in the CNL analysis:

1. PHTS loop isolation is not assumed due to the requirement for powered isolation valves;
2. Steam generators are interconnected by a common steam header. Upon loss of Class IV power, the turbine emergency stop valve closes, isolating the turbine from the steam generator common header. Loss of condenser circulating water pumps disables the condenser and prevents the condenser steam discharge valves from opening, causing steam generator pressure to rise. No models of the secondary side downstream of steam generators were used, but each steam generator's behavior was assumed to be similar after power loss. Main steam isolation valves were used to separate steam generators from each other and from the turbine and condenser;
3. Atomic Energy of Canada Ltd. type total of 19 PARs were distributed in different containment nodes: 8 in containment Node 1 (basement), 1 in Node 2 (stairwell to steam generator room), 1 in Node 5 (portions of floors 1, 2, 3 and 4), 8 in Node 8 (lower steam generator room), and 1 in Node 9 (moderator service area);
4. LRVs and pressurizer relief valves were modeled to discharge primary coolant directly to containment, as the degasser condenser was not modeled. The degasser condenser would have provided additional 20 m^3 volume for high pressure PHTS steam or liquid containment, delaying, and reducing coolant venting into containment. This assumption is conservative. Some fission products could be deposited in the degasser condenser prior to loop rupture, although fission product releases from the fuel were low until core disassembly;
5. Moderator cover gas system bleed valves connecting calandria vessel and vapor recovery system were assumed to be operable but failed open after 7,200 s;
6. Steam generator MSSVs were available and operated as per their set point (5.11 MPa) to relieve steam generator secondary side pressure;
7. Effective containment isolation was assumed from time = 0 s. In reality, containment isolation would activate if containment pressure reached a threshold of 3.5 kPa (g). Containment leakage was modeled with a specific rate based on pressure difference; in the SBO simulations the containment pressure increased to 3.5 kPa (g) at time = ~200 s and containment leakage by an opening to environment that allowed 2.5% of containment volume to leak out per 24 hours, given a pressure difference of 124 kPa;
8. Primary coolant was initially modeled as single phase liquid in PHTS loops. As loop void fraction

increased due to LRVs opening, coolant was modeled as a homogeneous two phase fluid. Above a certain void fraction, primary coolant separated into water and steam, and water was tracked in separate pools corresponding to PHTS nodes and fuel channels; when the loop void fraction exceeded 50% (a user input), the primary coolant in that loop separated into water and steam. The water was tracked in separate pools corresponding to PHTS nodes and fuel channels;

9. In the current study, IFPRELCT=1 (flag to allow fission product release from calandria vessel terminal debris bed). This implies that the model was "ON" (as reported in [2]). The assumption to allow the fission product releases from the calandria vessel terminal debris bed is believed to be more realistic, what is why it was implemented in the current analysis. The difference in results of this study and the ones in [2] is not expected to be significant for major event timings and hydrogen releases, but could be noticeable for the fission product releases to environment;
10. Heavy water thermophysical properties are not modelled in PHTS and in calandria vessel (heavy water is modelled as light water).

2.6.2. Polytechnic University of Bucharest

The modelling assumptions used for CANDU 6 SBO analysis are consistent with the assumption presented in [2, 15] for the new mechanistic channel deformation models. Some of the key modelling assumptions are as follows:

1. Fission products are not modelled in this study (although SCDAP can calculate the fission products released from fuel, the RELAP5/SCDAPSIM code has not a model for fission product transport. Therefore, the release of fission products was not considered in this current study);
2. LRVs and pressurizer relief valves were modelled to discharge primary coolant directly to containment. These valves discharge into the degasser condenser, which was not modelled in this analysis;
3. PARs are not modelled;
4. Moderator cover gas system bleed valves, being part of the moderator cover gas system, connect the calandria vessel (reactor) to a vapor recovery system. Initially, these valves were assumed to be operable; after 7,200 s it was assumed that these valves would fail open. The reason for their failure was attributed to the depletion of air reservoirs associated with these valves. As a result of this failure, some of the moderator substance (water or steam) present within the calandria vessel could leave the vessel through these valves;
5. SBO occurs at time zero. This led to the loss of moderator cooling, shield tank and end-shield cooling and the loss of emergency core cooling;
6. Four representative channels per core pass, at different vertical elevation, were considered to simulate the thermal response of fuel channels. All fuel elements which belong to the same fuel bundle are considered to have the same power;
7. There are three limits for the Zircaloy oxidation in RELAP/SCDAPSIM:
    - Oxidation is terminated when the material is fully oxidized;
    - Oxidation is limited by the availability of steam;
    - Oxidation is limited by the diffusion of water vapour.
8. After fuel cladding rupture or breach of pressure tube/calandria tube, both the inside and outside surfaces oxidize at the same rates;

9. Trip valves are used for the hydraulic connection between the fuel channel and moderator; they remain closed until fuel channel rupture occurs;
10. Bundle slumping and fuel relocation inside channel are not considered;
11. Loads applied to the pressure tube and to the fuel channel are assumed to be uniformly distributed;
12. In the pressure tube sagging model, the four garter springs are assumed to be evenly and located in the centre of the channel;
13. Contact between pressure tube and calandria tube sagging and between channels is considered by assuming constant contact area and conductance applied at the point of contact;
14. Heavy water thermophysical properties are not modelled in PHTS and in calandria vessel (heavy water is modelled as light water).

2.6.3. Korea Atomic Energy Research Institute

The following are the key modelling assumptions for user inputs and failure criteria employed in the CAISER models:

1. Degasser condenser tank, the degasser condenser relief valves, and PHTS liquid relief valves are directly modelled in the current analysis;
2. Heavy water thermophysical properties are modelled in the PHTS. Moderator in calandria vessel is modelled as light water;
3. Moderator cover gas system bleed valves, connecting calandria vessel and vapour recovery system, are not modelled in the current analysis
4. PARs are not modelled;
5. Fuel rod degradation module has the three dimensional Cartesian coordinate system of [*M*, *N*, *K*]. The fuel rod temperature is calculated by solving the energy change for the representative fuel rod, with a consideration of the number of fuel rods in each node;
6. Fuel channel degradation module also has the three dimensional Cartesian coordinate system of [*I*, *J*, *K*]. The fuel channel temperature is secured by solving the energy change for the representative fuel channel, with a consideration of the number of fuel channels in each node;
7. In a high temperature condition, fuel rods in a fuel channel experience a slumping phenomenon, in which fuel rods are compactly gathered in the lower part of fuel channel. The slumping phenomenon in CAISER code is modelled by the correlation, which is a function of a fuel rod temperature. The sensitivity constant in the correlation is given by user input, which enables the code user to do a parametric study for the slumping correlation;
8. Fuel channel failure is determined by four failure mechanism as follows:
    - Larson-Miller creep rupture model;
    - Local thermal failure of pressure tube and calandria tube, when the local temperature of pressure tube, $T_{\theta,k}^{PT}$, and calandria tube, $T_{\theta,k}^{CT}$, exceed the critical melting temperature;
    - Global thermal failure of pressure tube and calandria tube, when $\left(\overline{T_{\theta}^{PT}} + \overline{T_{\theta}^{CT}}\right)_k/2$ exceeds the user defined temperature, which needs a sensitivity study;
    - Ultimate tensile strength by the fuel channel sagging when the bending moment on the beam (fuel channel) exceeds maximum bending moment at entire cross section. This condition is determined in the fuel channel degradation module, while other three conditions are determined in the fuel rod degradation module.

3. UNCERTAINTY AND SENSITIVITY ANALYSIS METHODOLOGY

Uncertainty propagation methodology in severe accident analysis involves quantifying and assessing the uncertainties associated with input parameters, models, and assumptions used in the analysis. This is crucial for understanding the range of possible outcomes and making informed decisions regarding safety measures and risk mitigation.

The techniques employed for uncertainty and sensitivity analysis are outlined in this section, providing insights into the specific methodologies adopted by the participating organizations.

3.1. UNCERTAINTY PROPAGATION METHODOLOGY

This section describes methodologies used by each participating organization for uncertainty analysis while Section 3.2 provides details about the methodologies used in sensitivity analysis.

3.1.1. Canadian Nuclear Laboratories

The ordered statistics approach [16], also known as the GRS method, for the determination of uncertainties (developed in Germany) is used with some best estimate thermal hydraulics codes such as ATHLET (Analysis of Thermal hydraulics of LEaks and Transients with core degradation) [17]. This approach utilizes the full computational/numerical model and applies non-parametric simple random sampling and the Wilks' formula [18] (the minimum number of runs, i.e. the minimum size of the random sample of input uncertainties, is determined by Wilks' formula). Therefore, the number of computer code runs is much less than required by other methods such as the Monte Carlo method [19]. The Monte Carlo method requires numerous evaluations with randomly selected model input, followed by an assessment using the results of these evaluations as a random population, from which the analyst derives statistical attributes of the output variable. Experience has demonstrated that it can take roughly 10,000–100,000 margin parameter calculations to achieve convergence in the output parameter distribution metrics. This level of computational efforts is currently not suitable for most integrated computer codes used in nuclear reactor severe accident analysis. The GRS approach allows to evaluate the effects of uncertainties in the code models, initial and boundary conditions, and solution algorithms, upon simulation results (output).

The ordered statistics approach method assumes that the state of knowledge about all parameters that were identified to have significant effects upon the results and to have uncertainties can be described by their probability distributions and ranges.

To generate information about the uncertainty of computer code results, a number of code runs has to be executed. For each of these simulation runs, all identified uncertain parameters are varied simultaneously. Uncertain input parameters include nuclear power plant coolant and fuel inventories, geometry values, model control and model selection such as user-input flags, boundary and initial conditions, and numerical values like convergence criteria and maximum/minimum time step size.

The selection of values of parameter, with respect to their defined probability distributions, their correlation/combination, and the evaluation of the simulation results are based on statistical and probabilistic methods. The advantage of the GRS method is that the number of code runs required is not dependent of

the amount of uncertain parameters. In each code simulation, all uncertain parameters are varied at the same time, and the impact of these variations on the outcome is derived using statistical methods. Because the number of runs is not dependent from the number of uncertain parameters, no initial ranking of input parameters is required to minimize their number to reduce the computational costs. The number of code runs depends on the probability content (coverage probability) and confidence level of the tolerance limits (statistical) used as uncertainty bounds of the simulation results. The required (minimum) number, n, of these simulation runs is provided by Wilks' formula [16]. The number of runs necessary for one-sided tolerance limits (a×100 %/ b×100 %) is as follows:

$$1-a^n \geq b \tag{1}$$

where a×100 (%) is the coverage probability and b×100 is the confidence level (in %) necessary for the tolerance limit to be derived and compared with the acceptance criteria.

The confidence level is typically used to assess the influence of the sampling error since the tolerance limits are normally obtained from a random data sample of limited size. For two sided (a×100 %/ b×100 %) tolerance (statistical) intervals, the necessary number of simulations becomes:

$$1-a^n-n\times(1-a)\times a^{n-1} \geq b \tag{2}$$

The minimum number of simulations for various tolerance limits is presented in Tables 9 and 10. It is also proposed by the ordered statistics method that the number of code calculations be greater than the number of uncertain parameters to perform an appropriate sensitivity analysis in the next step.

TABLE 9. MINIMUM NUMBER OF CALCULATIONS FOR ONE SIDED STATISTICAL TOLERANCE LIMITS [16]

Confidence Level *b*	**Probability Content *a***			
	90%	**95%**	98%	99%
90%	22	45	114	230
95%	29	**59**	149	299
98%	38	77	194	390
99%	44	90	228	459

TABLE 10. MINIMUM NUMBER OF CALCULATIONS FOR TWO SIDED STATISTICAL TOLERANCE LIMITS [16]

Confidence Level b	**Probability Content *α***			
	90%	**95%**	98%	99%
90%	38	77	194	388
95%	46	**93**	236	473
98%	56	115	290	581
99%	64	130	330	662

A total number of n code simulations are performed, simultaneously changing the values of all input (uncertain) parameters, according to their probability distribution functions. The n values Y(n) of the calculated output parameters are ordered as:

$$Y(1) < Y(2) < Y(n-1) < Y(n) \quad (3)$$

This equation explains why the order statistics name is used for Wilks' formula. On the basis of this approach (ranking), the one sided upper tolerance limit (95 %, 95 %) is derived by selecting Y(n) with n=59. Similarly, the one sided lower tolerance limit (95 %, 95 %) could be obtained by selecting the value of Y(1) with n=59. The two sided tolerance limits could be calculated by selecting Y(1) and Y(n) with n=93.

Another important and distinguishing feature of the ordered statistics approach is that analyst can assess the magnitude contribution of every input parameter uncertainty to the uncertainties of the simulation results (i.e., figure of merit) based on the data produced for the uncertainty analysis. This sensitivity analysis provides a ranking of the uncertain input parameters. This information provides guidance on how to improve the state of knowledge (e.g., analysis, or experiments) to reduce the output uncertainties in the most efficient way, or where to update the models in the simulation code. The uncertain parameter sensitivity measures can be derived using rank correlation coefficients, standardised rank regression coefficients, and correlation ratios, to allow a ranking of uncertainties in input data, model formulations.

The ordered statistics approach developed by GRS uses only actual code simulations without the use of methods like fitted response surfaces. The ordered statistics approach has been used in various nuclear power plant safety applications by a number of international organizations including licensing. The steps of the uncertainty and sensitivity analysis, according to the ordered statistics approach, are implemented by use of the SUSA code [20] developed by GRS. The SUSA code provides a number of various statistical tools that could be applied during the uncertainty and sensitivity, and is briefly described in Section 3.2.

3.1.2. Polytechnic University of Bucharest

The uncertainty analysis methodology employed by the UPB, in collaboration with the Spanish regulatory body and the Technical University of Catalonia, is statistical technique where the uncertainties are characterized using probability density functions (PDFs); these uncertainties are subsequently propagated through simulations by varying a predefined set of input parameters. This methodology is built upon the framework introduced by the code scaling, applicability, and uncertainty approach, distinguished by three key aspects as follows [21]:

- Requirements and code capabilities: analysis begins by defining the specific NPP, scenario, safety criteria, selected computer code, and its applicability to the chosen scenarios. This involves establishing the capabilities of the code to predict pertinent processes and phenomena, as well as determining the associated uncertainties linked to code parameters;
- Assessment and selection of parameters: involves evaluating the code's predictive abilities with regard to significant processes and phenomena relevant to the scenario. The uncertainty associated with code parameters is determined;
- Sensitivity and uncertainty analysis: consisting in setting up, executing and evaluating the uncertainty of the scenario.

According to [21], the uncertainty analysis employs a simultaneous random sampling approach for input parameters based on their respective PDFs, resulting in the generation of a defined number of input samples for uncertainty calculations. The Wilks' formula, as detailed in Section 3.1.1, is utilized to establish the

required number of input samples, which is determined by the desired percentile coverage and the confidence level associated with the estimate. Importantly, the count of input parameters characterized by uncertainties remains unaffected by the number of code runs. Thus, there are no constraints on the quantity of input parameters considered. For instance, using the Wilks' formula in a first order context, a minimum of 59 code runs is recommended for the one sided (95%, 95%) and (5%, 95%) tolerance limits used to conduct an uncertainty analysis for an in-vessel SBO scenario in a CANDU 6 reactor. The (95%, 95%) and (5%, 95%) values represent the 95^{th} and 5^{th} percentiles, respectively, of the output parameter under investigation. These values are with a confidence level of 95%.

3.1.3. Korea Atomic Energy Research Institute

KAERI adopted a statistical approach using Monte Carlo method with 100 random samplings. Probabilistic and statistical methods are used in this study to quantify the relevant code uncertainties, i.e., the simple random sampling of input parameter values, according to their specified PDFs, and their random combination for n code runs. All relevant uncertainty inputs are assumed to be mutually independent and uncorrelated in the study. Then the uncertainty analysis results of n code runs are summarized as typical statistical values such as the 95^{th} and 5^{th} percentiles, median and mean values, and standard deviation. Differently with CNL and UPB, KAERI does not explicitly take advantage of the Wilks' formula, considering a possibility of code crashes that may take place relating to settings of the sampled input parameters. Considering the situation in which the order of hours per sample calculation is required, the random sample of n=100 was primarily tested to obtain relevant insights into the analysis results of interest.

For the uncertainty analysis in the current study, the MOSAIQUE (Module for Sampling Input and QUantifying Estimator) code was utilized [22], which was developed by KAERI.

3.2. SENSITIVITY ANALYSIS METHODOLOGY DESCRIPTION

Sensitivity analysis as a technique in assessing the impact of varying input parameters on the outcomes of a severe accident analysis is outlined in this section per participating organization in pointing to the parameters that have the most significant influence on the results.

3.2.1. Canadian Nuclear Laboratories

The sensitivity analysis with SUSA code can be performed with the same sample data as already generated for the uncertainty analysis [20]. Like the uncertainty analysis, it can be performed for scalar as well as time/index-dependent computational results. Different groups of correlation related sensitivity indices could be implemented (Pearson, Spearman, Kendall, Blomqvist, etc.). Within each group, SUSA can calculate the ordinary and partial correlation coefficient as well as the standardized regression coefficient. The (sample) coefficient of determination (R^2) could be provided as well to inform on the usefulness of the calculated coefficients as sensitivity indices. Therefore, the Pearson`s and Spearman´s correlation coefficients are implemented.

3.2.2. Polytechnic University of Bucharest

The sensitivity analysis performed by UPB was based on two different correlations: Pearson's correlation coefficient and Spearman's correlation coefficient, both approaches being applied for the sensitivity study using the Microsoft Excel specific functions. In order to determine the Pearson's and Spearman's correlation coefficients the following procedure was used:

- Step 1: uncertainty parameters coefficients extraction from the weight files generated in the setup phase of the uncertainty analysis for each set of runs including the reference case for which the specific coefficients of each uncertain parameter are considered equal to 1.0 (reference case scenario);
- Step 2: addition of the FOMs resulted values for each set of code runs after the execution phase of the uncertainty analysis, including the reference case scenario (base case with no uncertainties considered) resulted value;
- Step 3: FOMs coefficient calculation normalized to the base case resulted values;
- Step 3x (only for Spearman's correlation): Ranking of the uncertainty parameters coefficients and the FOMs coefficients using the RANK.AVG function available in the Microsoft Excel software;
- Step 4: Pearson's and Spearman's correlation coefficients calculation using the PEARSON and CORREL functions available in the Microsoft Excel software.

Pearson's correlation coefficient methodology returns the Pearson product moment correlation coefficient, which is a dimensionless index that ranges between −1.0 and +1.0 inclusive, and reflects the extent of a linear relationship between the two data sets.

The methodology for computing the Pearson's coefficient, known as Pearson's product moment correlation coefficient [23], starts from a bivariate set of data (x_1, y_1), (x_2, y_2), …, (x_n, y_n), with $r = {s_{xy}}/{s_x s_y}$, where:

s_{xy} : covariance of x and y values (or scores);
s_x, s_y : standard deviation of x and y values (or scores) respectively.

The Pearson's product moment correlation coefficient, ρ, can be then written as follows:

$$\rho = \frac{\frac{1}{n}\sum xy - \bar{x}\bar{y}}{\sqrt{\left(\frac{1}{n}\sum x^2 - \bar{x}^2\right)} \cdot \sqrt{\left(\frac{1}{n}\sum y^2 - \bar{y}^2\right)}} \quad (4)$$

where:

n : number of pairs of values / scores (code runs in the uncertainty analysis);
$\sum xy$: sum of products of x and y;
$\bar{x}, \bar{y}$: mean of the x values (or x scores) and y values (or y scores) respectively;
$\bar{x}\bar{y}$: product of the mean values or scores of x and y;
$\sum x^2, \sum y^2$: sum of the square values of x and the square values of y respectively.

Guidelines to interpreting Pearson's correlation coefficient according to reference [24] are given in Table 11.

Spearman's correlation coefficient methodology can be defined as Pearson's correlation coefficient between the rank variables [25] rather than the linear relationship between two parameters, as defined by the Pearson's correlation coefficient. For a sample of size n, the n raw scores x_i, y_i are converted to ranks (basically, each value from the sample x_i is sorted/ranked, and similar for the sample y_i), and the Spearman's correlation coefficient, r_S, can be computed according to the specific ranks, rg_{x_i} and rg_{y_i}:

$$r_S = \rho_{rg_x, rg_y} = \frac{cov(rg_x, rg_y)}{\sigma_{rg_x}\,\sigma_{rg_y}} \tag{5}$$

where:

ρ : Pearson's correlation coefficient determined for the rank of variables;
$cov(rg_x, rg_y)$: covariance of the rank variables;
$\sigma_{rg_x}\,\sigma_{rg_y}$: product of the standard deviation of the rank variables of samples *x* and *y*, respectively.

TABLE 11. GUIDELINES TO INTERPRETING PEARSON'S CORRELATION COEFFICIENT

	Coefficient, *r*	
Strength of association	**Positive**	**Negative**
No influence	0.0 to 0.1	–0.1 to 0.0
Low influence	0.1 to 0.3	–0.3 to –0.1
Moderate influence	0.3 to 0.5	–0.5 to –0.3
High influence	0.5 to 1.0	–1.0 to –0.5

The most common used formula for Spearman's correlation coefficient, when all n ranks are distinct integers, is:

$$r_S = 1 - \frac{6\sum d_i^2}{n(n^2-1)} \tag{6}$$

$$d_i = rg_{x_i} - rg_{y_i} \tag{7}$$

where:

d_i : difference between two ranks of each observation;
n : number of pairs of values.

For both sensitivity analysis methodologies, it was considered that –1.0 and +1.0 coefficient indicate a perfect negative and positive correlation coefficient respectively, whereas a correlation of 0 implies no correlation between the parameters, or zero relationship. Moreover, a correlation coefficient of lower than 0.30 (whether negative or positive 0.30) indicates low influence of the uncertain parameter on the FOM, between 0.30 and 0.50 (respectively, between –0.50 and –0.30) indicates a moderate relationship, and any value higher than 0.50 (or lower than –0.50) indicates a high influence of the selected uncertain parameter on the FOM.

3.2.3. Korea Atomic Energy Research Institute

Pearson`s and Spearman´s correlation coefficients are used in the analysis. Pearson correlation describes the linear correlation between the two variables and its value is limited between −1 and +1. If the resultant correlation is negative it means that an increment of x variable leads to a reduction in *y* variable. Similarly, if the resultant correlation is positive, it means that an increment of *x* variable leads to an increment in *y* variable. If the resultant is zero, there is no correlation between the two variables. The simplified Pearson correlation between two variables *x* and *y* can be expressed as follows:

$$\rho = \frac{\sum_{i=1}^{n}(x_i - x_m)(y_i - y_m)}{\sqrt{\sum_{i=1}^{n}(x_i - x_m)^2 \sum_{i=1}^{n}(y_i - y_m)^2}} \tag{8}$$

Spearman correlation is a measure of monotonic correlation between two variables. The R_i and S_i are ranks of randomly chosen input parameter values and simulation results. Ranks are assigned in ascending order. For matching values an average rank should be assigned. If absolute value of ρ_s is less than critical value (R), there exists no correlation. Critical value $\bar{R}$ is a function of sample size N and confidence level:

$$r_S = \frac{\sum_{i=1}^{N}(R_i - \bar{R})(S_i - \bar{S})}{\sqrt{\sum_{i=1}^{N}(R_i - \bar{R})^2 \sum_{i=1}^{N}(S_i - \bar{S})^2}} \tag{9}$$

$$\bar{R} = \bar{S} = \frac{N+1}{2} \tag{10}$$

3.3. DESCRIPTION OF THE UNCERTAINTY TOOLS USED FOR THE ANALYSIS

The description of main codes used in the overall analysis are provided in Section 2. In this Section, a brief overview is provided on how the uncertainty tools are used in connection to severe accident modelling and simulation.

3.3.1. Canadian Nuclear Laboratories

The SUSA code [20] is used by CNL for the uncertainty and sensitivity analysis. As described in Section 2.2.2, the code is intended to provide support in quantifying input parameter uncertainties with respect to PDFs and other dependence structures. Starting with the SUSA version 4.02, the code was upgraded to be compatible with MAAP-CANDU. This modification allowed SUSA to produce input data that are used in MAAP-CANDU runs, direct MAAP-CANDU to perform simulation runs, and process the output produced by these MAAP-CANDU simulations for statistical analysis.

The SUSA code serves as a guidance on the major steps when conducting an uncertainty and sensitivity analysis., These steps are generally consistent with both the best estimate analysis and uncertainty approach, adopted by the CANDU Owners Group and the GRS method. These two methods are based on the Wilk's approach [18]. The analysis steps are as follows:

1. Identification of related phenomena, analysis assumptions, and parameters that deemed to be important for the uncertainty of the simulation result, and representation of all uncertainty sources

by uncertain parameters;
2. Quantification of the uncertain input parameters in terms of their probability distribution functions and dependence measures;
3. Calculation of a set (sample) of values for the uncertain input parameters according to a probability distribution function which satisfies the input provided in step 2;
4. Execution of computer code simulations for each sample (set) of values sampled for the uncertain input parameters;
5. Quantification of the uncertainty of the calculation result (such as FOM) on the basis of the input parameters as an outcome from step 4 (so called uncertainty analysis);
6. Ranking (categorizing) of the uncertain input parameters according to their significance to the uncertainty of the computational result such as FOM (so called sensitivity analysis);
7. Documentation of the above steps for assessing the analysis results.

Generally, for SUSA, there are no limitations regarding the number of uncertain input parameters, output quantities, and computer code simulations. The following analysis actions are undertaken in order to produce MAAP-CANDU run results for the uncertainty and sensitivity analysis with SUSA:

1. Using SUSA, prepare the so called template for MAAP-CANDU input data file generation, together with the related PDFs for the input parameters that will be sampled (in the step 2) in the analysis;
2. Use SUSA to produce the MAAP-CANDU input data files for each of the simulations based on the (prepared in step 1 above) input file template. Each input data file produced with the aid of SUSA considers a single set of values (of the input parameters being considered) taken from the parameter sample distributions;
3. Use SUSA to run the MAAP-CANDU simulations for the input files produced in step 2;
4. Select results from the MAAP-CANDU the in step 3 to be assessed (via name/address of result) and utilize SUSA to produce a single file including the values of the selected results from various MAAP-CANDU output files (extension *.dnn) that were generated in step 3.

After execution of the steps 1–4, the analyst would have a combined file of all the simulation data set for the MAAP-CANDU analysis, which can be used by SUSA to perform the uncertainty and sensitivity analysis (Steps 5–7 from Section 3.2.1).

3.3.2. Polytechnic University of Bucharest

This section provides details on the uncertainty and sensitivity analysis of a SBO accident in a CANDU 6 reactor as performed by the Polytechnic University of Bucharest.

3.3.2.1. Uncertainty analysis tool

For the uncertainty analysis of a SBO accident in a CANDU 6 reactor focusing on in-vessel retention, the RELAP/SCDAPSIM/MOD3.6 code was selected as the analysis tool. This code incorporates a specialized uncertainty analysis package developed by the University Politechnica of Catalunya and Innovative Systems Software (USA). The uncertainty assessment capability is implemented through an alternative run mode called the uncertainty mode, which facilitates the automated execution of uncertainty analyses following a probabilistic approach. The complete uncertainty analysis with the RELAP/SCDAPSIM code involves three

interconnected phases, as depicted in Fig. 21, namely the setup phase, the simulation phase comprising multiple executions, and the post processing phase [21]. These phases are detailed as follows:

- Setup phase: the total number of sampled values, often referred to as weights, is generated. These weights play a role in associating uncertainty with code parameters by serving as scaling factors applied to base values. The setup phase also entails the calculation of the required number of code runs using the Wilks' formula or a user provided value. The setup information is stored in disk files, one for each simulation run, and another for post-processing purposes;
- Simulation phase: encompasses two primary runs. The base case run is performed without considering uncertainty options, while the set of uncertainty runs involves modifications to input data and sources. For each run during the simulation phase, the corresponding weight file generated in the setup phase is consulted. Information for post-processing is recorded in the restart plot file's plot records for each simulation run. Importantly, the input data remains consistent across the base run and each uncertainty run, aligning with the setup phase;
- Post processing phase: restart plot files generated in both the base case and uncertainty runs are examined. Rank matrices for specified output quantities outlined in the post processing input file are generated during this stage. These matrices organize the output parameter values based on their rank, forming the basis for establishing tolerance intervals. The post processing input file encompasses details on the simulation runs used for generating tolerance intervals.

Through these phases, the uncertainty analysis integrates probabilistic approaches with the RELAP/SCDAPSIM/MOD3.6 code to comprehensively assess the impact of uncertainties on the simulation outcomes for the specific SBO accident scenario in the CANDU 6 reactor.

The uncertainty data has to be supplied for the two types of parameters, the input treatable and the source correlation quantities. The required information is the probability distribution function and its characteristic parameters. Four distribution types are available:

- Uniform distribution: the required parameters are the minimum and the maximum values;
- Normal distribution: the required parameters are the mean and the standard deviation;
- Log-normal distribution: the required parameters are the mean and the standard deviation;
- Polynomial (or trapezoidal) distribution: the required parameters are defining the minimum and the maximum values with zero and maximum probability. This distribution may be used when the (uniformly distributed) uncertainty available seems to be rather narrow and the range is enlarged but without keeping the restrictive uniform shape.

For the input treatable parameters type, a second set of information is required to specify the input data card and the word number within that data card to be modified by the uncertainty multiplier. These fields in the setup input file allow the following options:

- Different or equal weights can be used for quantities with the same distribution function, that is, a sampling may be performed for each parameter or the first generated value is used for all specified parameters;
- Use entered bias instead of the computed weight;
- Normalization to the base case value: when this option is activated the code computes the sum of

the base case values for the marked parameters and renormalizes the modified values, i.e. values obtained after multiplying the base case values by the corresponding weights, so that their sum is equal to the base case values' sum;

— Maximum of 1 for the modified value: by activating this option the modified value is limited to 1. This feature might be useful when associating uncertainty to decay power tables built as multipliers to the nominal power.

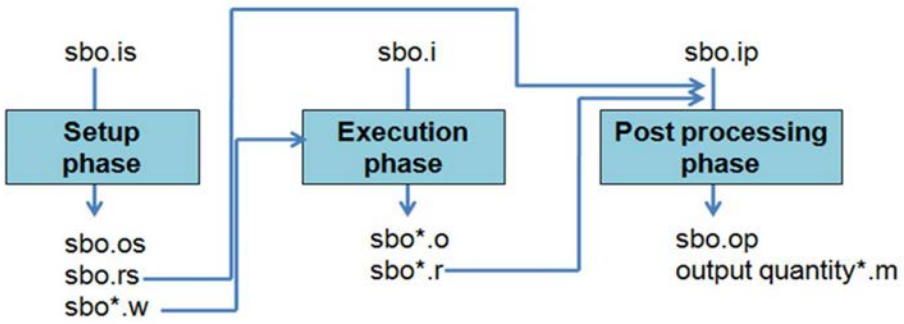

sbo.i – standard input file for reference SBO case scenario analysis where no uncertainties were considered;
sbo.is – specific input file for the SBO analysis with the uncertainty parameters and its PDFs (it is built upon sbo.i file);
sbo.os – readable format file that contains the Wilks' formula related data, the uncertainty data entered in the setup input file, and the list of the sampled (or specified) uncertainty multipliers for each uncertainty run calculation. It is a specific output file generated in the setup phase of the uncertainty analysis, which includes the set of sample values for each parameter according to the uncertainty analysis (each set of values for the selected parameters to be perturbed);
sbo.rs – binary format file that contains Wilks' related information needed in the post processing phase to derive the uncertainty bounds;
sbo*.w – binary format files that contain the multipliers to be used in the uncertainty runs. The number of weight files may be equal to the computed number by Wilks' formula, to the user-supplied value, or limited to a specified minimum and maximum run number.
sbo*.o – output print file which will be generated for each code run;
sbo*.r – restart plot file generated for each code run in the uncertainty analysis;
sbo.ip – specific input file for the post processing phase, containing the requested output quantities to be plotted;
sbo.op – specific output file for the post processing phase;
output quantity*.m – resulted output quantities resulted from the post processing phase.

FIG. 21. Uncertainty analysis files flow map.

The sampling technique implemented in the code is simple random sampling that generates sampled values from distribution functions defining the state of knowledge of each input parameter with associated uncertainty. The four types of distribution functions are available for the uncertainty package. The sampled values from the uniform function are directly obtained by using firstly the Fortran random generator and secondly scaling the generated [0; 1] value to the requested minimum and maximum values. The sampling from the polynomial distribution function uses the inverse method, and the normal based functions (normal and log-normal distributions) are sampled using the Box-Mueller method[2] [21].

[2] The Box-Muller method is a widely used technique for generating pairs of independent random numbers with a specified probability distribution, particularly for generating random numbers from a Gaussian (normal) distribution. This method is based on the concept of transforming uniformly distributed random variables into normally distributed random variables using mathematical transformations. The method is named after its inventors George E. P. Box and Mervin E. Muller, who introduced it in the 1950s.

3.3.2.2. Sensitivity analysis tool

The sensitivity analysis was conducted utilizing the Pearson and Spearman correlation coefficient functions which are readily available within Microsoft Excel. This Excel tool facilitates the sensitivity assessment by comparing two distinct datasets. The first dataset comprises the coefficients of a particular parameter extracted from the uncertainty parameters list generated during the setup phase of the uncertainty analysis, sourced from the sbo.os file. The second dataset encompasses values associated with the chosen FOM, such as H_2 mass generation during the in-vessel phase of the accident. This FOM's values are obtained subsequent to moderator depletion within the calandria vessel.

The methodology to perform the sensitivity analysis using the Pearson's correlation coefficient with Microsoft Excel involves the following steps:

A. Creating specific data sheets containing each uncertainty parameter selected for the uncertainty analysis with its specific assigned coefficient extracted from the sbo.os file (resulted from the setup phase of the uncertainty analysis, based on the Simple Random Sampling method);
B. Calculation of the normalized values of the selected FOM from the uncertainty runs to the base case resulted value. The normalization has been done to the base case value (the value resulted from the SBO accident analysis when no uncertainties were considered with best-estimate modelling assumptions) in order to determine the correlation coefficient of the resulted value from the uncertainty analysis to the best estimate value;
C. Determining the Pearson product moment correlation coefficient, for each FOM (H_2 mass generation after moderator depletion with respect to all 26 selected uncertainty parameters, first fuel channel failure time based on the first 19 selected uncertainty parameters, etc.) using the Pearson function available in Microsoft Excel.

The methodology to perform the sensitivity analysis using the Spearman's correlation coefficient with Microsoft Excel follows the same steps as the sensitivity study using the Pearson's correlation coefficient, with an intermediate action is needed, to rank the parameters coefficients (both for the uncertainty parameter and each FOM), followed using the available CORREL function available in Microsoft Excel, which defines the Spearman's correlation coefficients.

3.3.3. Korea Atomic Energy Research Institute

The MOSAIQUE (Module for Sampling Input and QUantifying Estimator) code developed by KAERI is used for the uncertainty analysis [22]. MOSAIQUE has two unique features. One involves the utilization of a spreadsheet to facilitate the assignment of uncertainty parameters within electronic input files, simplifying the generation of sampling inputs.

The other feature relates to the sampling calculations, wherein an intranet network of personal computers is connected to simultaneously execute sampling calculations across multiple units. To perform an uncertainty analysis using a simulation code, it is needed to generate sampling inputs, to perform sampling calculations, and to process outputs from sampling calculations. MOSAIQUE can consistently to incorporate all processes needed for the uncertainty analysis. The overall structure of MOSAIQUE shown in Fig. 22 is composed of three main units (or modules): the master unit for generating sampling inputs, the client unit

for distributing calculations among the personal computers linked to the intranet, and the plot unit for post processing the output from the sampling calculations.

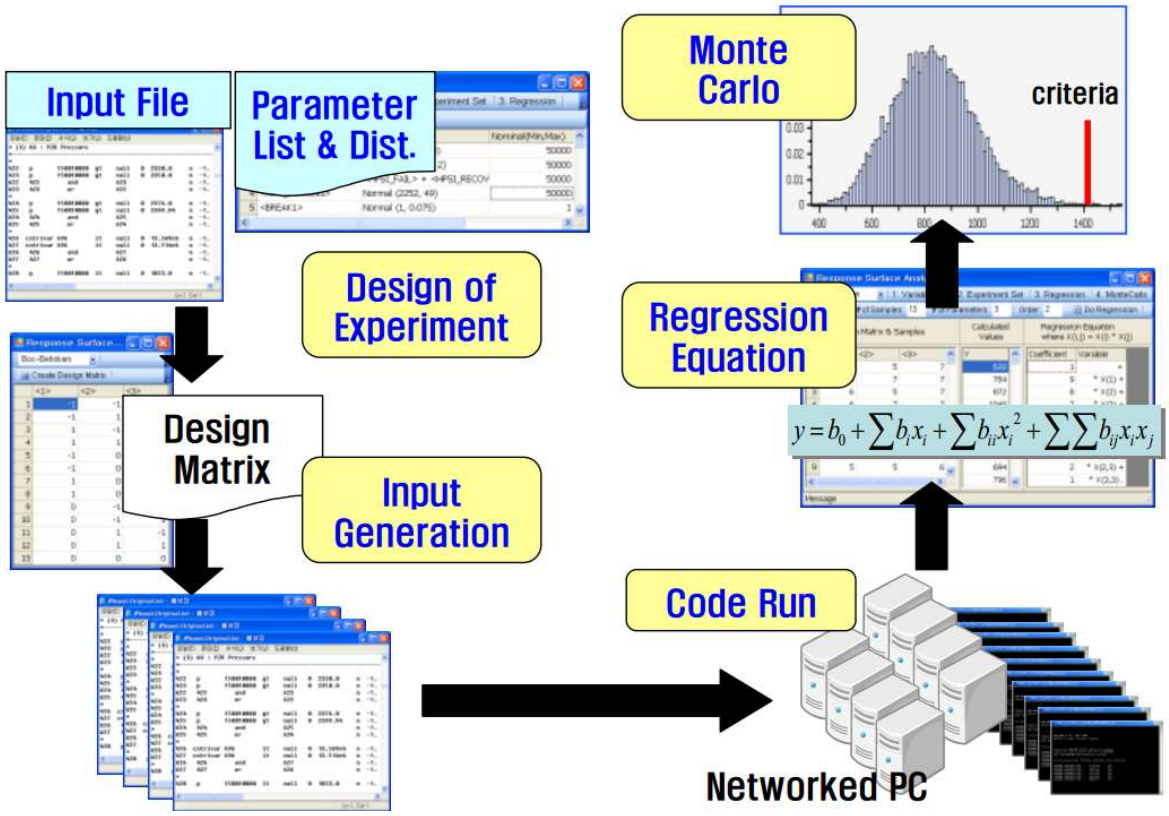

FIG. 22. Uncertainty analysis process in the MOSAIQUE software.

The master unit has the following functions:

- Read an input file and transform it into a spread sheet in which user can choose a cell containing input parameter to assign the PDF for an uncertain parameter;
- Assign statistical information for a parameter;
- Generate sample input files;
- Save run information to master file.

The client unit has the following functions:

- Read run information from the master data base and assign each calculation to the personal computers on the intranet;
- Return calculation results to master personal computer.

The plot unit has the following functions:

- Read output files from a folder where all individual calculation results are agglomerated;

— Select and plot a parameter from the template generated by the code and provide the statistical estimators.

Using these three units, an uncertainty/sensitivity calculation can be fully automated and computational costs can be reduced considerably.

3.4. UNCERTAIN PARAMETERS AND DISTRIBUTIONS

In this section, the focus is on detailing the uncertain input parameters and their associated PDFs specific to each participating organization. Subject matter experts within each organization were selecting these parameters. The selection process mirrored the methodology commonly utilized in the phenomena identification and ranking table process. This approach ensured the identification of the most critical uncertain parameters.

Notably, the utilization of three distinct and independent codes, as outlined in Section 2.2, was a unique aspect. These codes, employed by each CANDU participating organization, incorporated diverse models to represent the intricate multi-disciplinary processes inherent in severe accidents. As a result, the uncertain parameters varied among the participating organizations due to the inherent differences in the codes and models employed by each organization.

3.4.1. Canadian Nuclear Laboratories

A list of uncertain input parameters used by CNL is presented in Table 12. This list is comprised from parameters that are deemed to be most important based on currently available information/knowledge. Some of the parameters are truly phenomenological model parameters (such as ENT0, EANN, GSHAPE, EPSPB, etc.). Others (such as VFSEP, WSTDSO, HDRDELP, etc. are tuning MAAP-CANDU input parameters that are designed to allow for a simplistic representation of very complex processes during severe accident progression or alignment of various MAAP-CANDU modelling with that of a much more detailed (such as thermal-hydraulic etc.) codes that can provide a better estimate of the behaviour (such as thermal-hydraulics). It is important to better understand the impact of various input parameters (both phenomenological and tuning) and their uncertainties on the analysis outcome. This list of uncertain input parameters can be refined in the future with more information becoming available.

A sample histogram type of cumulative distribution function (CDF) and PDF derived based on the expert's opinion for the selected input parameters (MLOAD (1)) example is shown) are presented in Fig. 23.

TABLE 12. MAAP-CANDU MODEL PARAMETERS AND PDFs FOR THE UNCERTAINTY ANALYSIS

Parameter number	Parameter	Units	Range	Reference Value	Details	PDF
1	MLOAD(1)	kg		25000	Total debris mass in the suspended debris bed, per PHTS loop, that will trigger a core collapse.	Histogram Fig. 23
2	VFSEP			0.5	Void fraction in the PHTS above which the two-phase mixture characteristics no longer lead to the carrying of water over the highest point in the PHTS.	Histogram
3	TIMKDEB	s	10–100	50	Time delay for the remainder of un-oxidized pressure tube/calandria tube to go to molten Zr bin for spilling to terminal debris bed	Uniform
4	EANN		0.325–0.55	0.55	Emissivity of surfaces in pressure tube/calandria tube in intact annulus	Uniform
5	EPSZR			0.75	Emissivity of ZrO_2 (used if EMISSI=0)	Histogram
6	TSAGFAIL	K		1473	Disassembly temperature of channel segment in dry calandria vessel	Histogram
7	TCONT	K		1273	Pressure tube temperature trigger for fuel/pressure tube/calandria tube contact	Histogram
8	TCLRUP	K		2123	Sheath melting temperature (melt relocation temp.)	Histogram:
9	TRELOC	K		2123	Sheath melting temperature (melt relocation temp.)	Histogram
10	LHEU	J/kg	2×10^5–3×10^5	2×10^5	Latent heat of U-Zr-ZrO2 eutectic	Uniform
11	TEU			2500	The core node eutectic melting temperature	Uniform
12	FXEGAP			0.05	Fraction of the xenon inventory in the pellet-cladding gap due to long-term operation.	Histogram
13	TFAIL	K		1473	Temperature of calandria tube above which calandria tube is defined as hot and therefore can perforate	Histogram

TABLE 12. MAAP-CANDU MODEL PARAMETERS AND PDFs FOR THE UNCERTAINTY ANALYSIS (Cont.)

Parameter number	Parameter	Units	Range	Reference Value	Details	PDF
14	TZRFAIL	K		2125	User input temperature at which the channel section disassembles and is added to the debris.	Histogram
15	HDRDELP	Pa	20–300	100	User specified pressure differential between the inlet and outlet headers, across the characteristic channel, feeder and end fitting.	Uniform
16	WSTDSO	kg/s	10^{-4}–10^{-3}	0.0005	User input steam flow rate to flow into the fuel channel annulus of every channel node located between the first and last perforated axial channel nodes.	Uniform
17	XDBSOLID	m	0.005–0.002	0.0132	User input characteristic dimension of suspended debris.	Uniform
18	XDBGAP2	m	0.0005–0.0015	0.001	User input reduced gap dimension {m} of suspended debris.	Uniform
19	XDBGAP1	m	0.001–0.003	0.002	User input nominal gap dimension {m} of suspended debris.	Uniform
20	ZDBCLOSE	m	0.05–0.15	0.1	Height of debris at which debris compacts and ZSPACE closes from user input XDBGAP1 to user input XDBGAP2.	Uniform
21	TDBCLOSE	K	2100–2800	2600	User input average debris temperature, above which suspended debris compacts.	Uniform
22	ENT0			0.045	Jet entrainment coefficient for the Ricou-Spalding correlation.	Histogram
23	ENT0C			0.045	Jet entrainment coefficient for the Ricou-Spalding correlation.	Histogram
24	EPSPB			0.4	Assumed porosity of the particulate debris bed in the calandria vessel terminal debris bed	Histogram
25	GSHAPE			2.5	Gamma shape factor to account for non-spherical shapes in the aerosol coagulation calculations.	Histogram

TABLE 12. MAAP-CANDU MODEL PARAMETERS AND PDFs FOR THE UNCERTAINTY ANALYSIS (Cont.)

Parameter number	Parameter	Units	Range	Reference Value	Details	PDF
26	CSHAPE			1	The chi shape factor to account for non-spherical shapes of the aerosols in Stokes' law for gravitational settling	Histogram

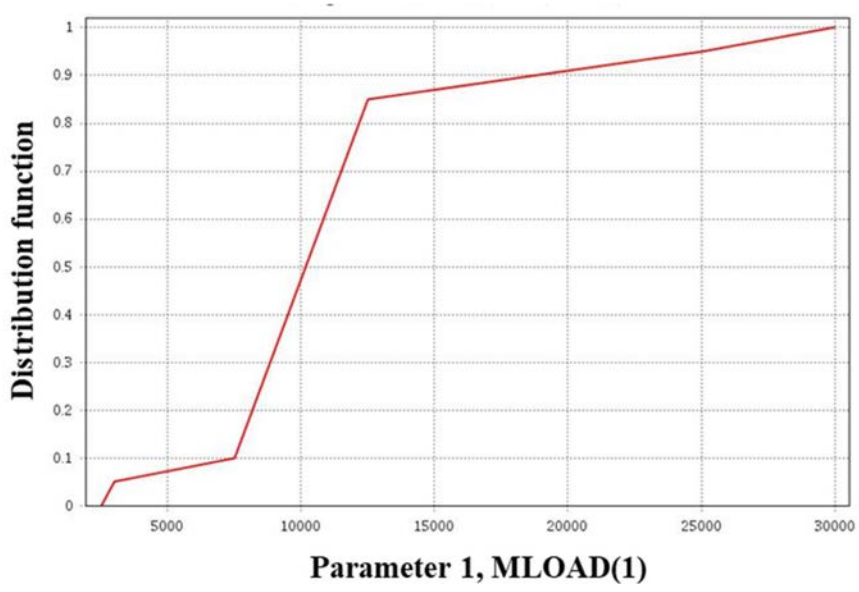

(a)

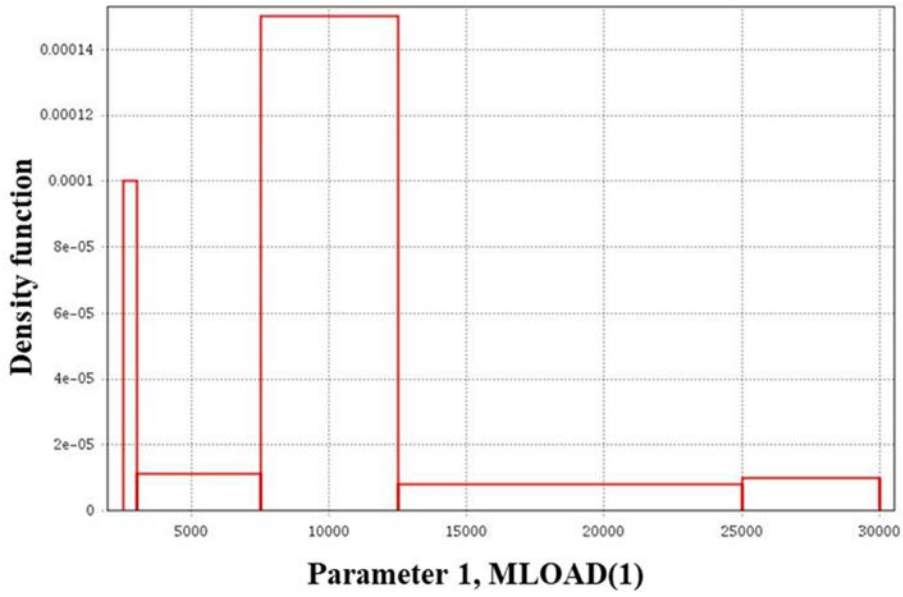

(b)

FIG. 23. (a) CDF and (b) PDF constructed for the input parameter #1, MLOAD (1).

3.4.2. Polytechnic University of Bucharest

As shown in Table 13 total of 26 uncertain parameters were selected for the uncertainty analysis of a SBO accident. Among these 26 uncertain parameters, 9 parameters are identified as source correlation parameters (7^{th} to 15^{th} parameter in Table 13). These correlations are applied to the heat transfer coefficients from the heat transfer correlations available in the code from wall structures to fluids, i.e. heat transfer from the steam generators U tubes to the secondary side water, heat transfer from the fuel bundles to the primary coolant). The remaining 19 parameters are input treatable parameters, which allow the perturbation to thermal hydraulics parameters for different components, in addition governing the behaviour of fuel channels during the core disassembly phase of the accident.

TABLE 13. SELECTED UNCERTAINTY PARAMETERS FOR SBO ANALYSIS

Uncertainty parameters for SBO analysis (in-vessel retention / calandria vessel dry-out)				
#	**Phenomena**	**Parameter**	**PDFs**	**Comments**
1	UO_2 behavior [26]	Heat capacity (T≤1800K)	ND*	Multiplier applied to the heat capacity when T≤1800K
2		Heat capacity (T>1800K)	ND	Multiplier applied to the heat capacity when T>1800K
3		Thermal conductivity (T≤1800K)	ND	Multiplier applied to the thermal conductivity when T≤1800K
4		Thermal conductivity (T>1800K)	ND	Multiplier applied to the thermal conductivity when T>1800K
5		Density (T≤1800K)	ND	Multiplier applied to the density when T≤1800K
6		Density (T>1800K)	ND	Multiplier applied to the density when T>1800K
7	Heat transfer to fluids (coolant) [26]	Heat transfer coefficient (HTC)	ND	Multiplier applied to the HTC from heat transfer source correlation when single phase liquid is assumed
8		HTC	UD*	Multiplier applied to the HTC from heat transfer source correlation when subcooled nucleate boiling is assumed
9		HTC	UD	Multiplier applied to the HTC from heat transfer source correlation when saturated nucleate boiling is assumed
10		HTC	TD*	Multiplier applied to the HTC from heat transfer source correlation when subcooled transition boiling is assumed
11		HTC	TD	Multiplier applied to the HTC from heat transfer source correlation when saturated transition boiling is assumed
12		HTC	TD	Multiplier applied to the HTC from heat transfer source correlation when subcooled film boiling is assumed
13		HTC	TD	Multiplier applied to the HTC from heat transfer source correlation when saturated film boiling is assumed
14		HTC	UD	Multiplier applied to the HTC from heat transfer source correlation when single phase vapor is assumed

TABLE 13. SELECTED UNCERTAINTY PARAMETERS FOR SBO ANALYSIS (Cont.)

Uncertainty parameters for SBO analysis (in-vessel retention / calandria vessel dry-out)				
#	**Phenomena**	**Parameter**	**PDFs**	**Comments**
15		HTC	UD	Multiplier applied to the HTC from heat transfer source correlation when condensation with void less than 1 is assumed
16	Reactor thermal power	Power after scram	ND	±10% decay heat, according to [27, 28]
17	Core pressure [26]	Form loss coefficients	UD	Multiplier applied to the junctions of the pipes modelling the core
18	Flow rate at LRVs	Discharge coefficient	ND	Multiplier applied to discharge coefficient: subcooled discharge coefficient best-estimate 0.89 with standard deviation 0.0348 [29]
19		Discharge coefficient	ND	Multiplier applied to discharge coefficient: two-phase discharge coefficient - BE 1.07 with standard deviation 0.1189 [29]
20	Moderator expulsion through calandria vessel rupture disks	Discharge coefficient	ND	Multiplier applied to discharge coefficient: subcooled discharge coefficient best-estimate 0.89 with standard deviation 0.0348 [29]
21		Discharge coefficient	ND	Multiplier applied to discharge coefficient: two-phase discharge coefficient - best-estimate 1.07 with standard deviation 0.1189 [29]
22	Fuel channels behaviour	Pressure tube failure strain	UD	Best estimate 22%, min. value 19% and max. value 24% [13]
23		Contact angle for channel-to-channel contact	UD	Best estimate 30 deg (between 20 deg and 40 deg)
24		Contact conductance for channel-to-channel contact heat transfer calculation	LN*	Best estimate 5000 W/m^{2}K (between 2,800–11,000 W//m^{2}K)
25		Contact angle for pressure-tube-to-calandria-tube sagging contact	UD	Best estimate 20 deg (min. 10 deg and max. 30 deg)
26		Channel rupture area	UD	Best estimate assumed as the flow area of an individual channel (50–100% channel rupture area)

* ND: normal distribution; UD: uniform distribution; TD: trapezoidal distribution; LN: log-normal distribution

3.4.3. Korea Atomic Energy Research Institute

As provided in Table 14, total of 13 uncertain input parameters, which are mainly related to in-vessel accident progression phase, were selected. For each parameter, the possible range and probability distribution were derived based on the expert judgment and relevant material properties.

TABLE 14. UNCERTAINTY INPUTS AND RELEVANT PDFS (CAISER, 13 PARAMETERS)

#	FOM	Parameter	Range	Comments	Distribution (PDF)
1	Hydrogen mass generation	db_porosity	Mean: 0.3 S.D: 0.1	Effective oxidational surface area of suspended debris bed available for oxidation	Normal
2		eta_db	0.0001~0.01	Effective contact area with the intact fuel channel	Uniform
3		w_fc_db_1	0.2~0.6	Mass fraction of accumulated debris bed generated by a fuel channel failure	Uniform
4		DH_DB	Mean: 0.1 S.D: 0.03	Hydraulic diameter of debris bed	Normal
5		factor_quench	Mean: 5.0 S.D: 1.0	Quenching heat transfer coefficient	Normal
6	Fuel channel failure time	H_sagging	0.1~0.5	Sagging failure criterion	Uniform
7		Vfactor_side	0.01~0.1	View factor for a radiation heat transfer	Uniform
8		Vfactor_PT	0.01~0.1	Effective contact area with fuel rods because of the fuel rods slumping	Uniform
9		pt_local	Mean: 1800 S.D: 100	Local temperature of pressure tube for the pressure tube perforation	Normal
10		ct_local	Mean: 1800 S.D: 100	Local temperature of calandria tube for the calandria tube perforation	Normal
11		pt_avg	Mean: 1200 S.D: 100	Average temperature of pressure tube for the fuel channel failure	Normal
12		ct_avg	Mean: 1200 S.D: 100	Average temperature of calandria tube for the fuel channel failure	Normal
13	Calandria vessel failure time	A_FC_fail	0.5~1.5	Moderator pop-up due to a fuel channel failure	Uniform

4. SUMMARY RESULTS

This section summarizes overall contributions from the three participating organizations from three Member States. Each contribution is presented in the same way describing summary results for the steady state and the reference case, uncertainty, and sensitivity analysis. The lessons learned and best practices are discussed in Section 5.

Table 15 shows significant event timings for the reference case analysis for three participating organizations in developing the SBO analysis.

TABLE 15. SIGNIFICANT EVENT TIMINGS FOR IN-VESSEL HYDROGEN PRODUCTION FOR A GENERIC CANDU 6 SBO SCENARIO

Time (h)			Events
UPB	**KAERI**	**CNL***	
0	0	0	Class IV and Class III Power loss and reactor shut down
2.36	2.97	2.4	Liquid Relief Valves first open
2.15	2.58	2.65	steam generator secondary sides are dry, Loops 1&2
N/A*	N/A	2.98	Reactor vault rupture disk bursts
N/A	4.71	3.1	Moderator in calandria vessel reaches saturation temperature
3.23	3.53	3.41	Pressurizer empty
2.93	3.42	5.01	First channel is dry
4.65	6.04	5.03	Pressure and calandria tubes rupture
4.55	6.04	5.08	Calandria vessel rupture disk 1 bursts
4.85	6.22	5.48	Beginning of core disassembly
11.24	10.95	8.5	Core collapse (Loop 2)
11. 26	10.40	9.45	Core collapse (Loop 1)
N/A**	N/A**	7.77	Containment fails
11. 26	12.27	11.24	Water is depleted inside calandria vessel
N/A**	N/A**	14.81	Water in reactor vault reaches saturation temperature
52.78	N/A**	48.05	Calandria vessel fails and debris relocation starts into reactor vault
N/A**	N/A**	51.2	Water is depleted inside reactor vault
N/A**	N/A**	55.22	Molten corium-concrete interaction begins in reactor (calandria) vault
			In-vessel hydrogen production (in two PHTS loops), kg
157.0	315	182.7	In-vessel hydrogen production, kg

*CNL Simulation ID: SUSA500A-2
** The associated model is not available in the assessment conducted by participating organization.

4.1. CANADIAN NUCLEAR LABORATORIES

This section summarizes the results obtained by the Canadian Nuclear Laboratories.

4.1.1. Steady state and reference case

The steady state analysis results for the generic CANDU 6 reactor performed with MAAP-CANDU v5.00A are presented in Table 16. The simulations were run up to 500,000 s (139 h); a mission time of 72 h was required for the Level 2 PSA.

TABLE 16. STEADY STATE MAAP-CANDU SIMULATION RESULTS

Parameter	Units	Steady state results
Core thermal power	MW_{th}	2,155.9
PHTS pump power	MW	17.55
Heat loss to containment	MW	0.11
Heat load to moderator	MW	88.65
Thermal power to steam generators	MW_t	2,080.41
RIH temperature	°C	312.85
ROH temperature	°C	312.85
RIH pressure	MPa	10.3
ROH pressure	MPa	10.3
PHTS loop flow	kg/s	1925
Loop inventory (one loop)	kg	42,294.0
Pressurizer inventory	kg	27,986
Total primary inventory including pressurizer	kg	112,563
Steam generator pressure	MPa	4.7
Steam generator temperature	°C	259.85
Steam generator inventory (per steam generator)	kg	38,023
Moderator cover gas pressure	kPa	97.7
Moderator temperature	°C	68.83
Moderator inventory	kg	227,000
End shield pressure	kPa	117.5
End shield temperature	°C	62.38
End shield inventory	kg	14,118
Reactor vault pressure	kPa	117.4
Reactor vault temperature	°C	49.7

4.1.2. Uncertainty analysis

The two output parameters (FOMs) are considered. The MH2CR(1) is the integrated amount of hydrogen generated in-vessel (i.e., inside the calandria vessel) by the oxidation of PHTS Loop 1 zirconium (fuel sheaths, pressure tubes and calandria tubes), from both intact channels and suspended channel debris. The MAAP-CANDU output parameter MH2CR(2) corresponds to Loop 2. Hydrogen represents a major risk to containment integrity due to its high flammability and maintaining containment integrity is important to prevent radioactivity releases to the environment during the postulated severe accident progression. The second MAAP-CANDU output parameter (FOM) that was analysed represents the mass of fission products of group 2 (representing a CsI compound) released in environment. The MAAP-CANDU output variable name for this parameter is MFPREL(2). This fission product is released from damaged fuel/core debris during core disassembly, which can then migrate from the core/debris to the reactor/calandria vessel, then on into containment, and when containment fails, it could be released in the environment.

Uncertainty analysis related to the hydrogen generated in-vessel (i.e., inside the calandria vessel) is presented in Section 4.1.2.1, and uncertainty analysis related the release of the fission products of group 2 (CsI) into the environment is discussed in Section 4.1.2.2.

4.1.2.1. Figure-of-merit: hydrogen generated in-vessel

During severe accident progression and core disassembly, fuel channel debris migrates to the calandria vessel terminal debris bed, where it is usually quenched by moderator that is available at the bottom of the calandria vessel. After that, very little hydrogen is produced inside the calandria vessel, i.e., hot metal oxidation no longer contributes to MH2CR(loop). Therefore, typical MH2CR(loop) time evolution shows a rapid rise to a nearly a constant value, with the plateau suggesting that the fuel channels of that PHTS loop have completely disassembled to the terminal debris bed.

A selection of uncertainty and sensitivity analysis results, for generic CANDU 6 SBO (FOM: hydrogen generated in-vessel), is shown in Figs. 24–26. Figure 24 presents the results of the 100 MAAP-CANDU runs showing the hydrogen mass produced in PHTS Loop 1, MH2CR(1) as a function of time. Figure 25 presents the two sided (95%, 95%) tolerance limits for the hydrogen mass generated in PHTS Loop 1 as a function of time. The two sided (95 %, 95 %) tolerance limits, for the maximum MH2CR(1) value, are 7.5 kg and 134.7 kg, respectively. These values are calculated using ordered statistics approach and Wilk's formula (a=0.95 and b=0.95) and represent the lower and upper bounds of an interval covering at least 95% of the possible values of the maximum, with a statistical confidence of at least 95%. This represents the uncertainty of the output parameter (i.e., hydrogen mass), given the input uncertainties. Figure 26 illustrates cumulative distribution function for hydrogen mass MH2CR(1), produced in PHTS Loop 1, for 100 MAAP-CANDU SBO runs.

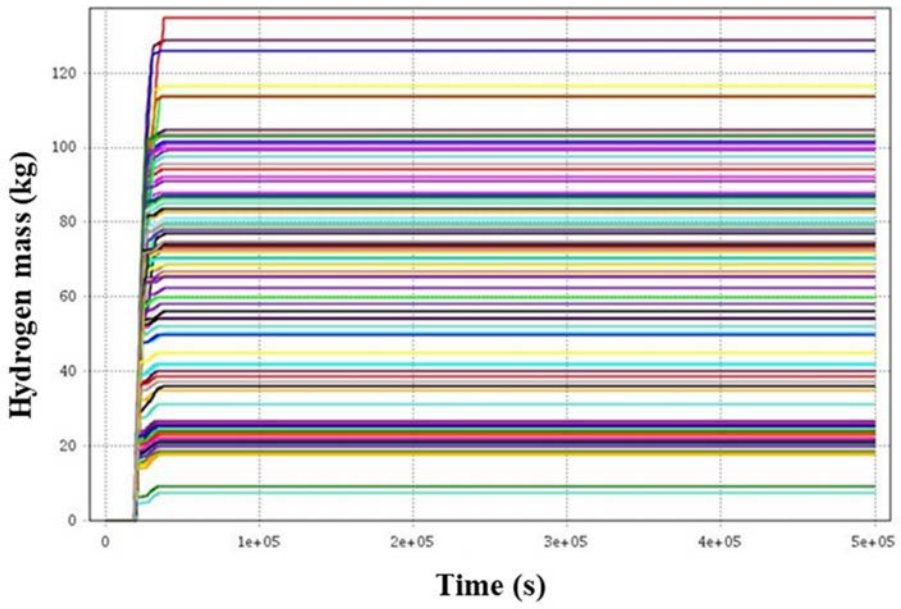

FIG. 24. Hydrogen mass produced in PHTS Loop 1, versus time 100 MAAP-CANDU SBO runs.

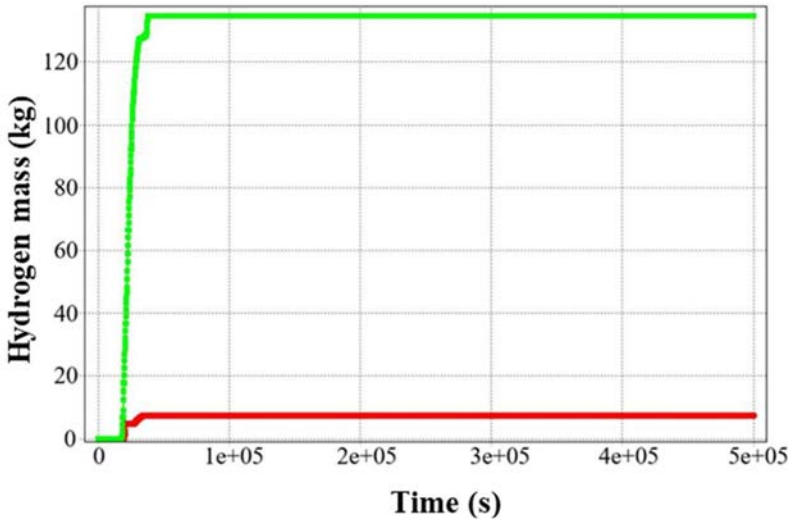

FIG. 25. Two sided (95%, 95%) tolerance limits for hydrogen mass produced in PHTS Loop 1, versus time for 100 MAAP-CANDU SBO runs.

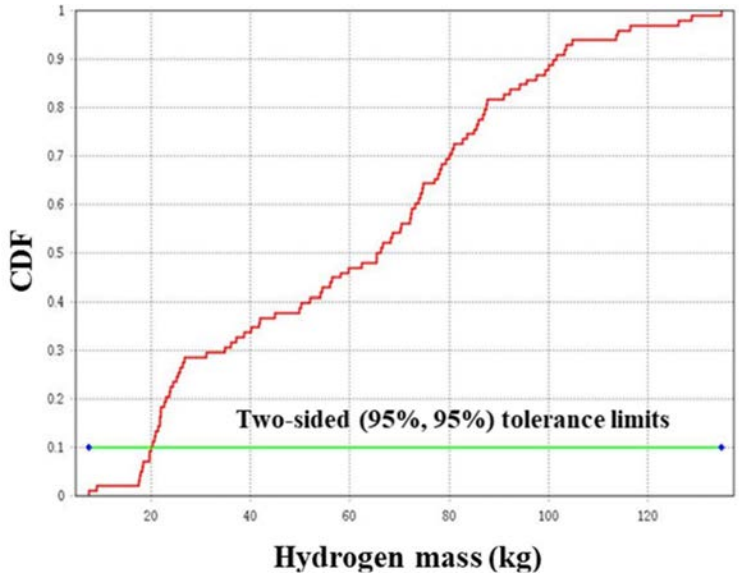

FIG. 26. Cumulative distribution function for hydrogen mass MH2CR(1) produced in PHTS Loop 1, for 100 MAAP-CANDU SBO runs.

4.1.2.2. Figure-of-merit: fission products (CsI) released into environment

During severe accident progression, when the reactor core is undergoing disassembly, fuel heats up. At the elevated temperatures, fuel/debris release fission products. At some point (in this analysis at ~9.5h=34,200s, as shown in Table 15), channel debris migrates (due to the core collapse) to the calandria vessel terminal debris bed, where it usually gets quenched by moderator that is available at the bottom of calandria vessel. After that, very little fission products are released inside the calandria vessel as shown in Fig. 27. Therefore, an MFPREL(2) time evolution curve shows a rise to a nearly constant value, with the plateau suggesting

that all the fuel channels completely disassembled to the terminal debris bed. Later, after calandria vessel fails (at ~48h=172,000s), debris relocates from the calandria vessel to the reactor vault, where the debris is quenched and cooled by water. When the rector vault water is evaporated, debris heats up again due to the decay heat, and fission products release starts again at ~48.5h=175,000s. Once most of the CsI inventory in the core is released from the debris bed in the reactor vault, the CsI release curve reaches the second plateau.

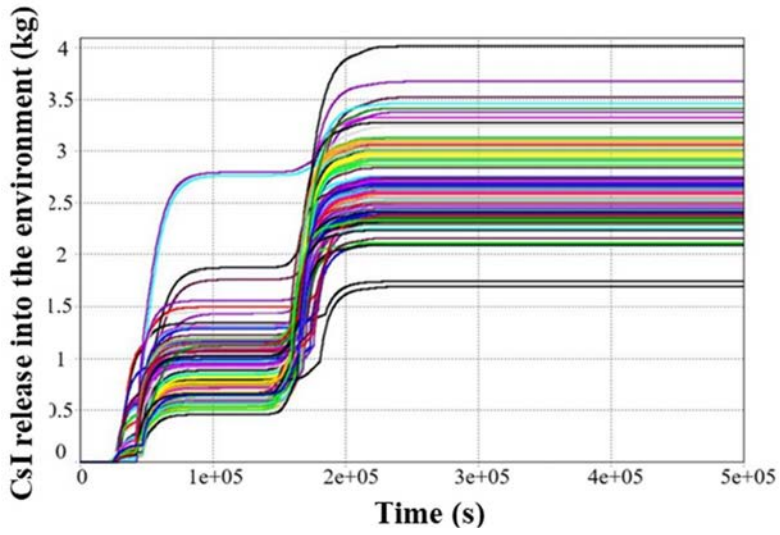

FIG. 27. Fission product group 2 (CsI) mass (MFPREL(2)) released to the environment vs time for each of 100 MAAP-CANDU SBO runs.

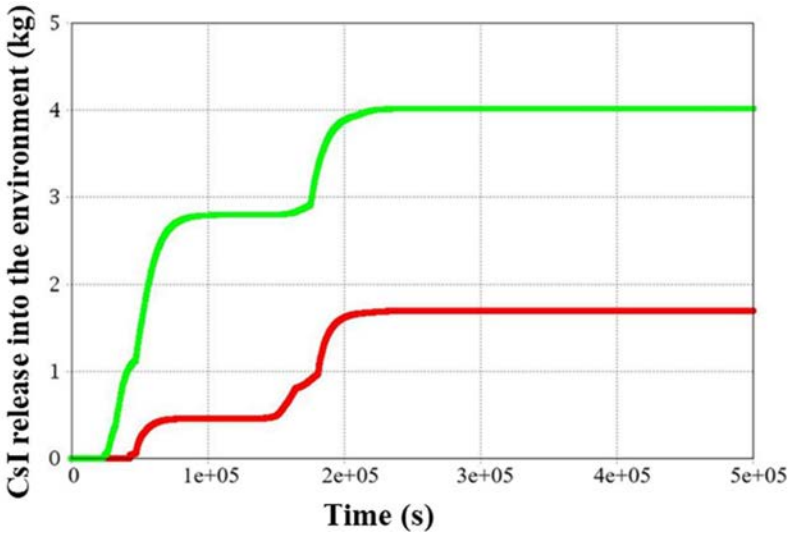

FIG. 28. Two sided (95%, 95%) tolerance limits for fission product group 2 (CsI) mass (MFPREL(2)) released to the environment vs time for 100 MAAP-CANDU SBO runs.

Figure 28 illustrates the two sided (95%, 95%) tolerance limits for the CsI mass, released to environment vs time, computed for 100 MAAP-CANDU runs. The two sided (95 %, 95 %) tolerance limits, for the maximum MFPREL(2) value, are 1.69 kg and 4.02 kg. These values are computed using ordered statistics

and Wilk's formula (a=0.95 and b=0.95) and represent the lower and upper bounds of an interval covering at least 95% of the possible values of the maximum, with a statistical confidence of at least 95%. This represents the uncertainty of the output parameter, given the input uncertainties. Figure 29 illustrates cumulative distribution function for CsI mass released to the environment for 100 MAAP-CANDU runs.

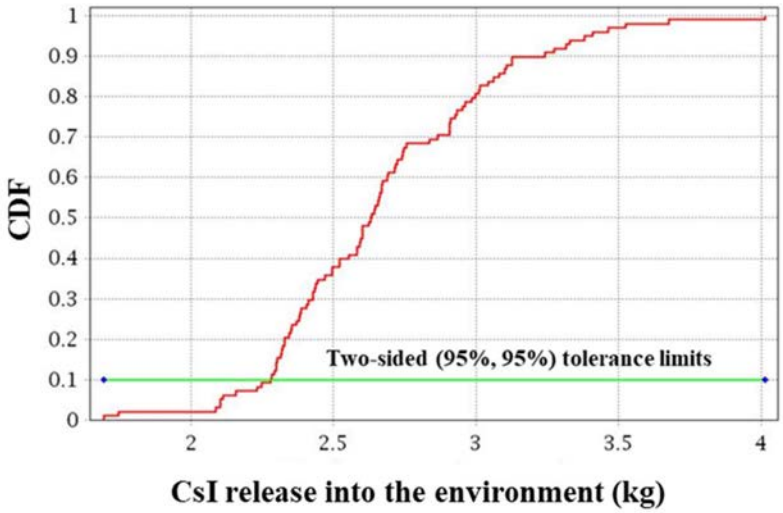

FIG. 29. Cumulative distribution function for the fission product group 2 (CsI) mass (MFPREL(2) released to the environment for 100 MAAP-CANDU SBO runs.

4.1.3. Sensitivity Analysis

The same two FOM parameters are considered in the sensitivity analysis as the one analysed within the uncertainty analysis framework as discussed in Section 4.1.2.

4.1.3.1. Figure-of-merit: hydrogen generated in-vessel

Figure 30 shows calculated Pearson's ordinary correlation coefficient as a sensitivity measure of the maximum hydrogen mass produced by zirconium oxidation in PHTS Loop 1 channels and core debris, MH2CR(1), with respect to 26 uncertain input parameters. This presents relative sensitivity of the output to each of the uncertain input parameters (for both Pearson' and Spearman's correlation coefficients, they are meaningful when they exceed the value of ~0.2). It can be concluded, using the Pearson's correlation assessment, that the first two MAAP-CANDU input parameters (of the 26 investigated) contribute the most variation of the MH2CR(1) maximum value obtained in the simulation (0–500,000s). MLOAD(1) (uncertain parameter 1) corresponds to the maximum allowable amount of suspended core debris in a loop, and VFSEP (parameter 2) determines the maximum PHTS void fraction where the primary coolant is modelled as a homogeneous two phase mixture. Figure 31 shows Spearman's ordinary correlation coefficients for maximum hydrogen mass produced in PHTS Loop 1 with respect to 26 uncertain parameters. From Figs. 30 and 31 can be concluded that the most significant input parameters predicted using two different criteria (Pearson's ordinary correlation coefficients and Spearman's rank correlation coefficients), are similar in both assessments.

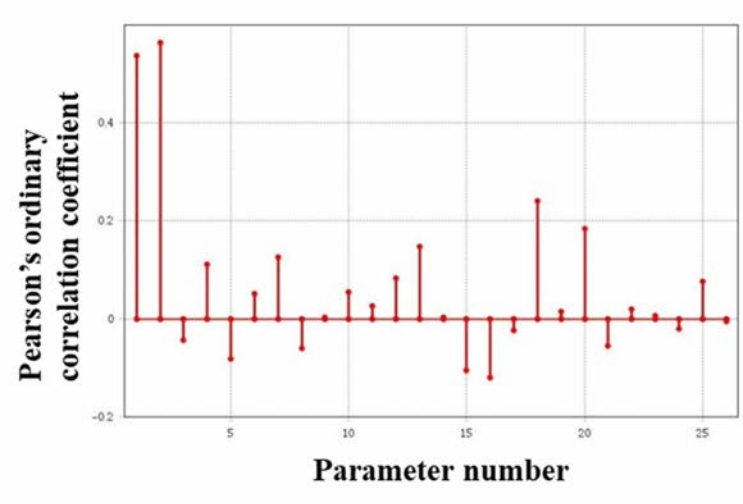

FIG. 30. Sensitivity measure: Pearson's ordinary correlation coefficients for the maximum hydrogen mass (produced in PHTS Loop) 1 with respect to 26 uncertain parameters.

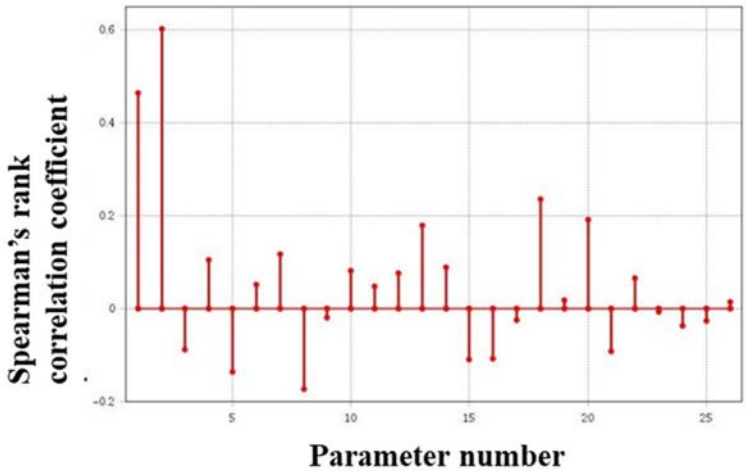

FIG. 31. Sensitivity measure: Spearman's rank correlation coefficients for the maximum hydrogen mass, (produced in PHTS Loop) 1 with respect to 26 uncertain parameters.

4.1.3.2. Figure-of-merit: fission products (CsI) released into environment

Figure 32 shows computed Pearson's ordinary correlation coefficient as a sensitivity measure of the maximum fission product (CsI, MAAP-CANDU fission product group 2) mass released to environment, MFPREL(2), with respect to the 26 uncertain input parameters. This presents the relative sensitivity of the output to each of the uncertain input parameters. It can be concluded from the sensitivity analysis of output parameter MFPREL(2), using the Pearson's correlation assessment, that the first two and last two MAAP-CANDU input parameters (of the 26 investigated) contribute the most variation, with parameters 25 and 26 being the most impactful, in the maximum value of the MFPREL(2) obtained in the course of simulation (0–500,000 s). MLOAD(1) (parameter 1, Table 12) corresponds to the maximum allowable amount of suspended core debris in a loop, and VFSEP (parameter 2, Table 12) determines the maximum PHTS void

fraction where the primary coolant is modelled as a homogeneous two-phase mixture. GSHAPE (parameter 25, the 2nd last MAAP-CANDU uncertain input parameter, Table 12) corresponds to the gamma shape factor to account for non-spherical shapes in the aerosol coagulation calculations, and CSHAPE (last, 26th MAAP-CANDU uncertain input parameter, Table 12) corresponds to the chi-shape factor to account for non-spherical shapes of the aerosols in Stokes' law for gravitational settling. Thus, the parameters defining the shapes of aerosols for coagulation and gravitational settling have an expected large effect on the CsI release to the environment as they will dictate the amount of deposition of CsI in the reactor vessel and containment (deposited fission products will not be released to the environment).

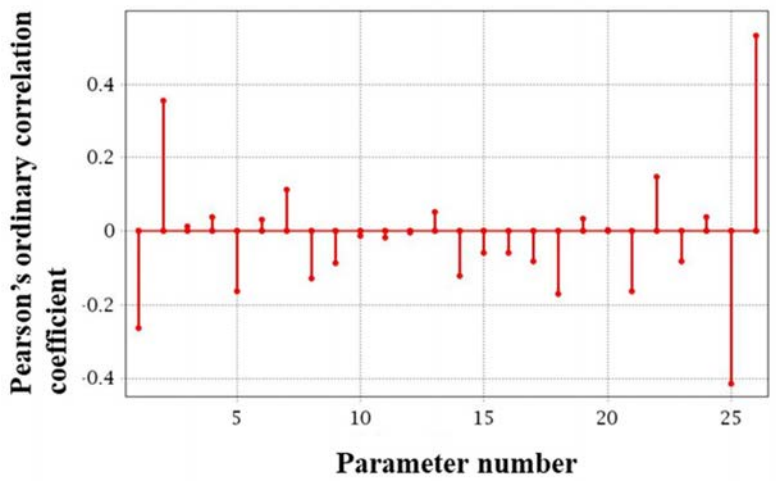

FIG. 32. Pearson's ordinary correlation coefficients as sensitivity measure for the maximum fission product mass, released to the environment with respect to 26 uncertain parameters.

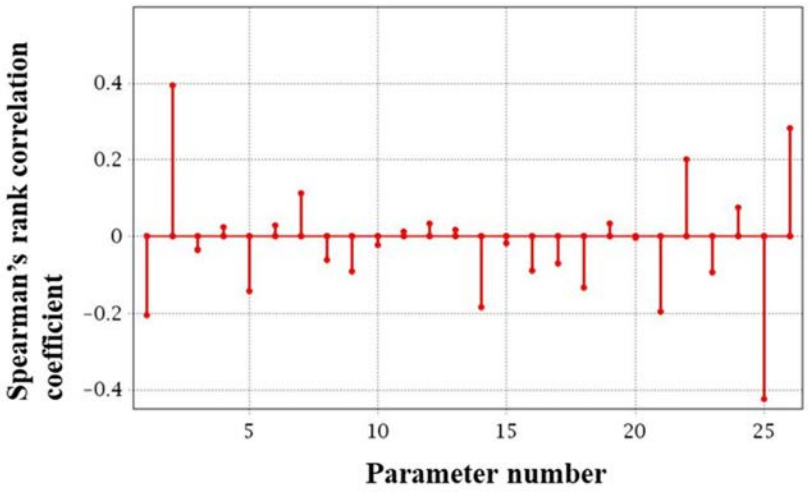

FIG. 33. Spearman's rank correlation coefficients as sensitivity measure for the released to the environment with respect to 26 uncertain parameters.

The Spearman's rank correlation (Fig. 33) shows similar relationship as the Pearson's rank correlation, though parameter 2, VFSEP, is more significant compared to parameter 1, MLOAD, and parameter 26,

CSHAPE. From Figs. 32 and 33 can be concluded that the most significant uncertain input parameters are similar.

4.2. POLYTECHNIC UNIVERSITY OF BUCHAREST

This section summarizes the results obtained by the Polytechnic University of Bucharest.

4.2.1. Steady state and reference case

The steady state analysis results for the generic CANDU 6 reactor performed with RELAP/SCDAPSIM/MOD3.6 are presented in Table 17. The significant event timings observed during this simulation are provided in Table 15.

TABLE 17. STEADY STATE RELAP/SCDAPSIM SIMULATION RESULTS

Parameter	Units	Steady state results
Core thermal power	MW_{th}	2072.9
PHTS pump power	MW	–
Heat loss to containment	MW	3
Heat load to moderator	MW	2.702[3]
Thermal power to steam generators	MW_t	2,071.8
RIH temperature	°C	267
ROH temperature	°C	311
RIH pressure	MPa	11.23
ROH pressure	MPa	10.02
PHTS loop flow	kg/s	1,917.78
Loop inventory (one loop)	kg	45,935.6
Pressurizer inventory	kg	25,803.1[4]
Total primary inventory including pressurizer (and from pipes between PHT and pressurizer)	kg	117,635.2
Steam generator pressure	MPa	4.7
Steam generator temperature	°C	260
Steam generator inventory (per steam generator)	kg	38,003.4
Moderator cover gas pressure	kPa	121.675
Moderator temperature	°C	69.8
Moderator inventory	kg	235,578
End shield pressure	kPa	101.3
End shield temperature	°C	53.9
End shield inventory	kg	14,647.04
Reactor vault pressure	MPa	101
Reactor vault temperature	°C	53.9
Reactor vault inventory	kg	534,975
Containment pressure	kPa	101
Containment temperature	°C	34

[3] Amount of heat transferred from the fuel channels to the moderator

[4] Inventory from pipes connecting ROH and pressurizer not included assuming there is no water in the dousing tank and reactor vault

The CANDU 6 nuclear power plant response during an unmitigated SBO scenario, initiated at time =0s, is briefly described as follows. During the unmitigated SBO accident fuel channel failures are expected to occur, due to the loss of all heat sinks; there are several hypothetical mechanisms for the fuel channel failure, such as large circumferential temperature gradient on the pressure tube during ballooning, asymmetric heat loads on the channel post contact, failure at a pre-existing flaw site or pressure tube embrittlement, failure due to calandria tube dry-out on its outer surface, or local overheating driven by fuel bundle slumping. The pressure tube is assumed to fail when the average strain reaches 22%, which is the typical measured average transverse creep strain at failure in pressure tube deformation tests with small circumferential temperature gradient, according to [30].

The initiation of the accident will trip the reactor and close the turbine stop valves with 20s delay. The PHTS loop isolation valves are not closed, so both loops show similar pressure behaviour, as seen in Fig. 34. After an initial decrease in PHTS pressure, the primary pressure remains roughly constant until the steam generators secondary side inventories are depleted. As the steam generators are no longer a heat sink to remove heat from PHTS, the pressure in the PHTS increases until it reaches the PHTS liquid relief valve set point (10.24 MPa (a)), at time =2.67h, and then it oscillates at the relief valve set point. The rupture of the pressure tube and calandria tube of fuel channels in each loop generates a rapid blow down from the PHTS into the calandria vessel and a fast depressurization of PHTS.

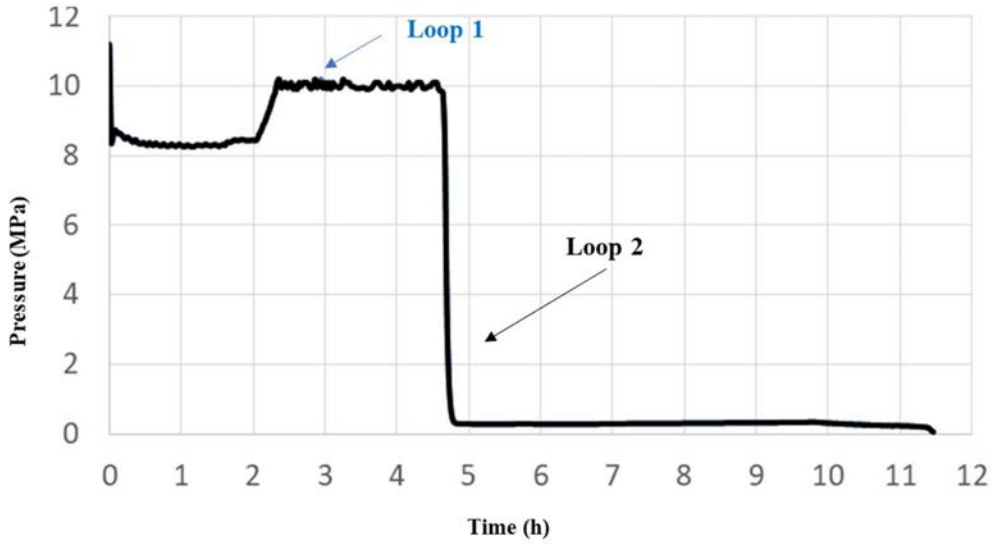

FIG. 34. PHTS pressure trend in both loops as a function of time.

Boil-off of the water on the secondary side of the steam generators secondary side results in continuously decrease of the steam generators mass inventories and water levels as can be seen in Fig. 35. The steam generator secondary sides are dry at time =2.15 h. The loss of steam generators as heat sink together with the continuous loss of inventory through the LRVs, result in a rapid increase of the average PHTS void fraction as shown in Fig. 36. The decay heat from the core boils off the coolant, eventually leading to dry-out of the fuel channels at ~4.24 h.

Figure 37 indicates a fast rise of the fuel channel temperatures occurs after the fuel channels dry-out.

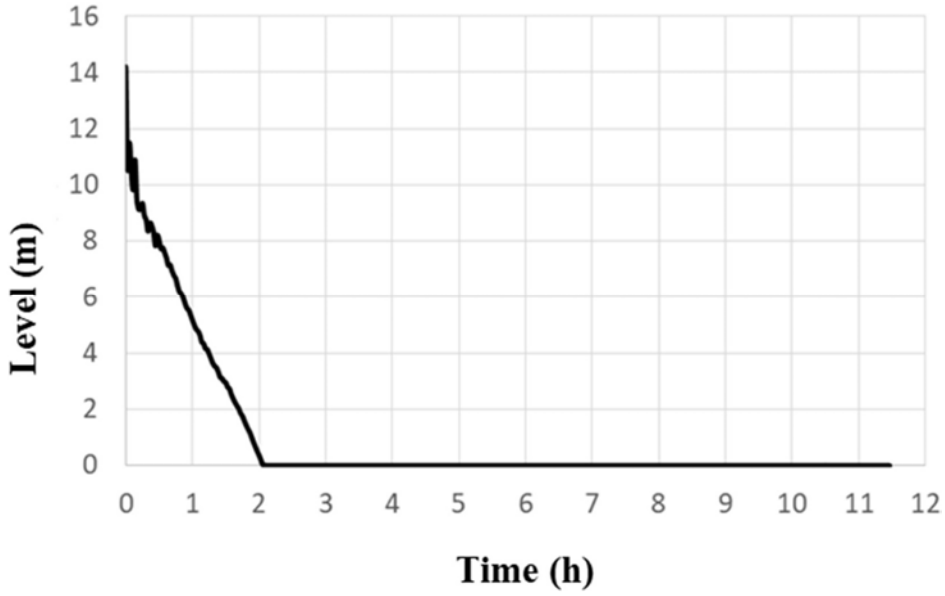

FIG. 35. Water level in the steam generators secondary side as a function of time.

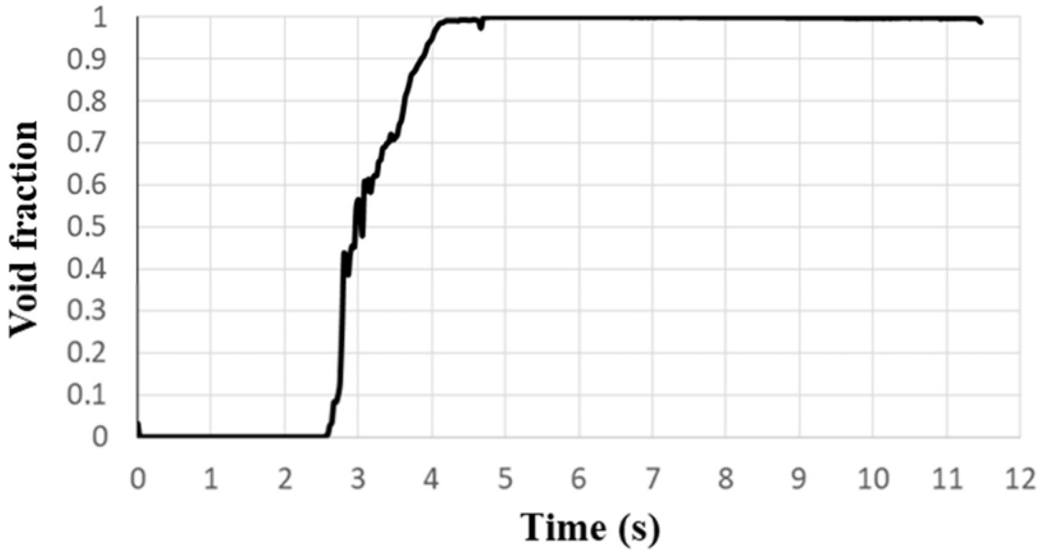

FIG. 36. Core average void fraction as a function of time.

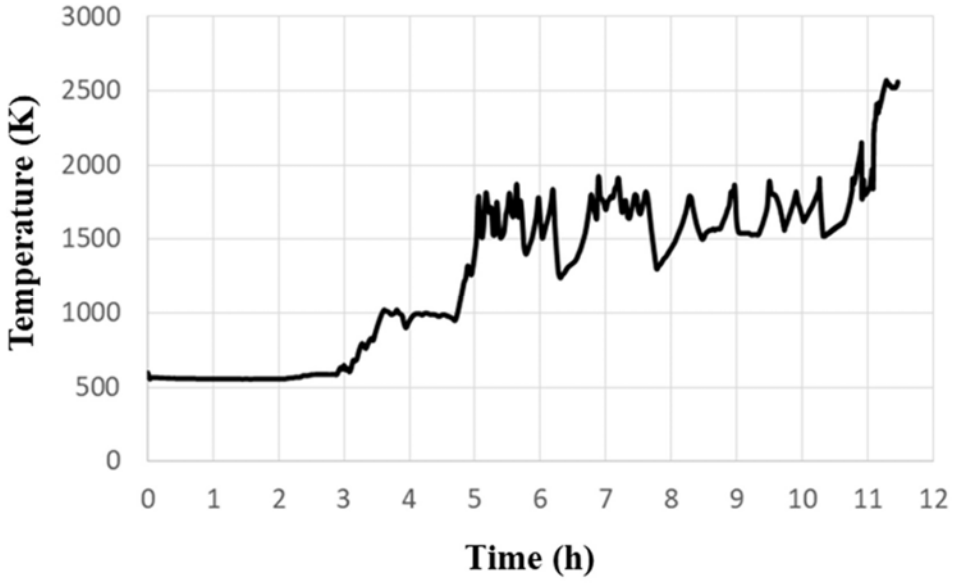

FIG. 37. Core maximum surface temperature as a function of time.

The boil-off of water in the calandria vessel increases the pressure inside the calandria vessel, as depicted in Fig. 38. The pressure increase causes the calandria vessel rupture disks to burst open at 4.55h, expelling some moderator (through flashing and carry over) into the containment. The decrease of the moderator level leads the upper row of channels to become uncovered. The pressure tube failure strain is exceeded in one of the channels after 4.65h and the fuel channel ruptures. The rupture of the fuel channel discharges PHTS inventory into the calandria vessel which generates a rapid increase in calandria vessel pressure and a large moderator inventory expulsion.

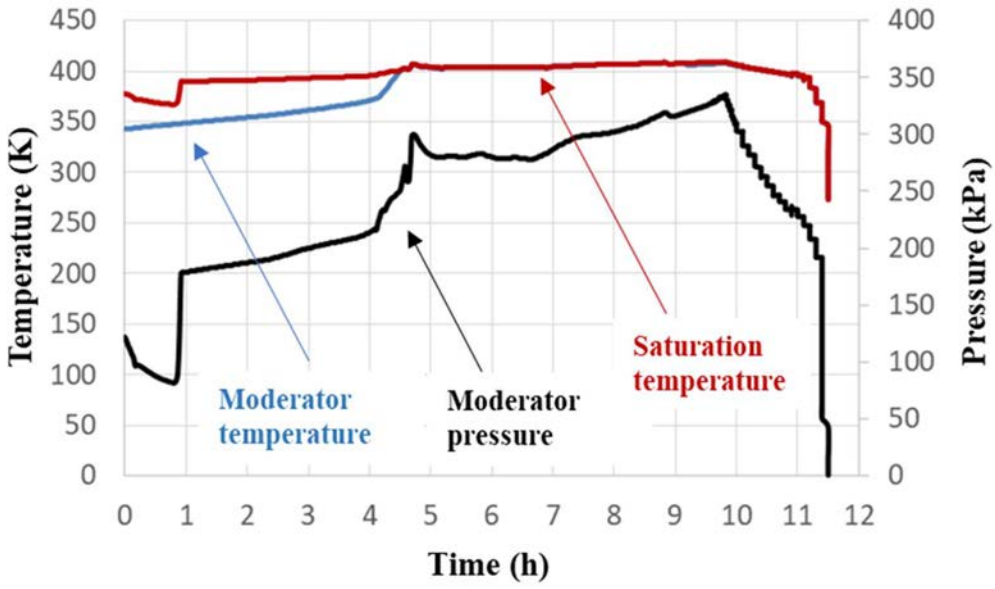

FIG. 38. Moderator pressure and temperature change wit time.

Figure 39 shows that after the sharp initial decrease, the moderator level continues to decrease gradually because of continued moderator boil-off due to the heat transfer from the core as seen in Fig. 40. Water is depleted inside calandria vessel at time =11.27h.

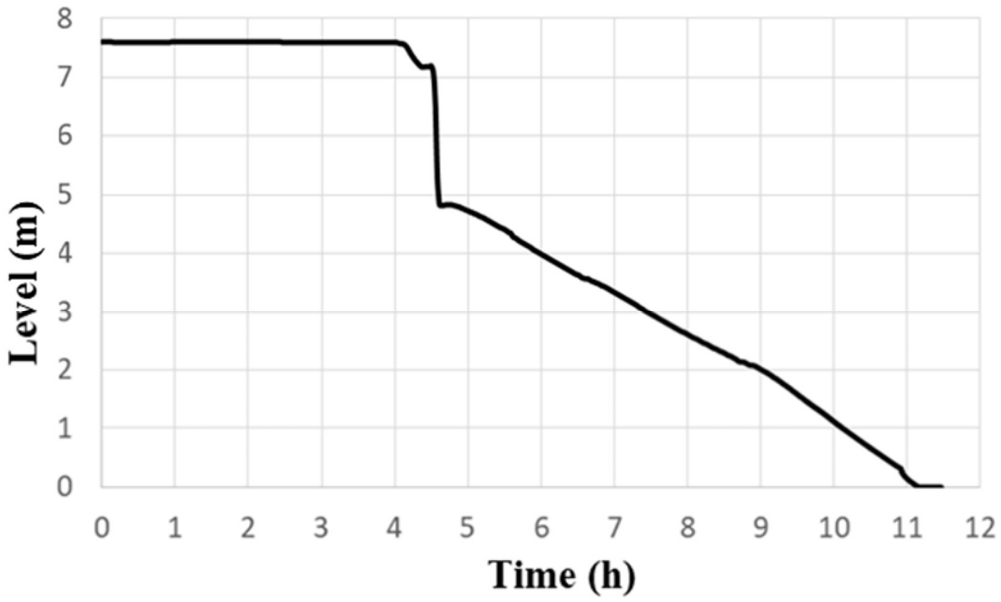

FIG. 39. Time dependence of a moderator level inside calandria vessel.

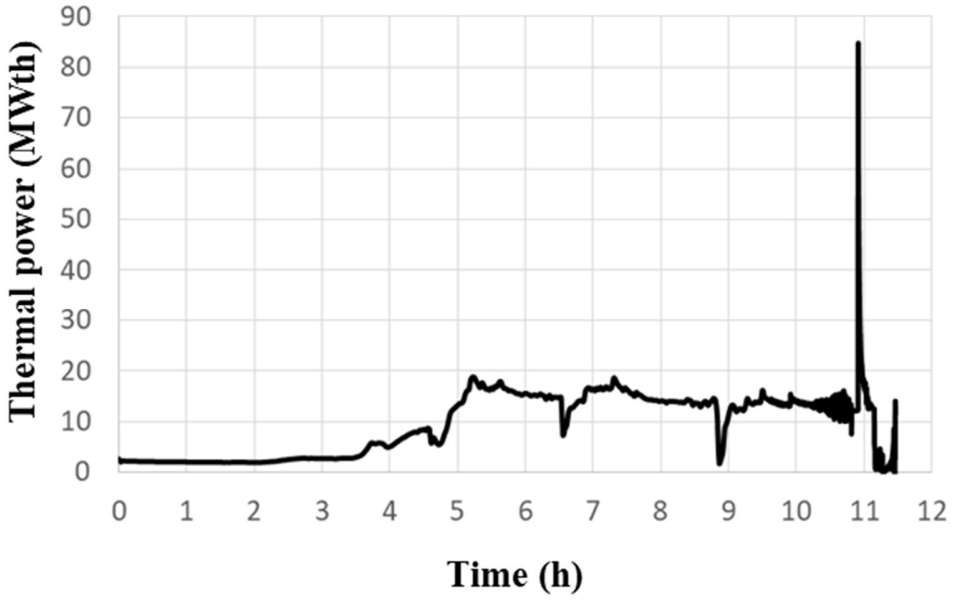

FIG. 40. Heat transferred from the fuel channels to moderator as a function of time.

Following the initial rapid moderator expulsion, about half of the fuel channels located in the upper portion of the calandria vessel become uncovered. Consequently, fuel, sheath, pressure tube and calandria tube temperatures in these channels increase rapidly.

The core disassembly starts at 4.85h with the fuel channel from the upper first row of pass 4 being the first to disassemble. The last channel disassembled, the channel from the bottom first row of pass 2, triggers the core collapse at 11.26h. The core disassembly progression is presented in Fig. 41.

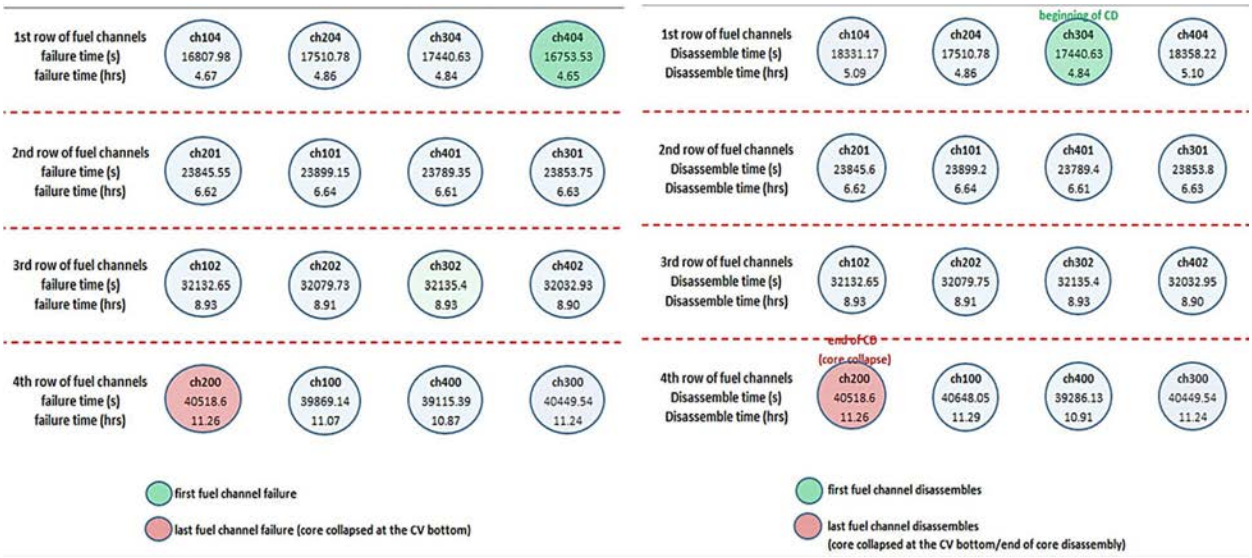

FIG. 41. Core disassembly map.

After the calandria vessel water is depleted, the debris relocated into the calandria vessel bottom (i.e. the terminal debris bed) heats up rapidly, starts to melt and begins to form a molten pool surrounded by a crust. The water in the reactor vault acts as a heat sink and cools the calandria vessel wall, maintaining the calandria vessel integrity. After a time, the reactor vault inventory reaches saturation temperature and starts to boil, and the reactor vault water level begins to decrease. Eventually, the water level in the reactor vault falls below the level of the molten pool in the calandria and the calandria vessel bottom heats up rapidly and fails due to creep, at ~52.78h.

The zircaloy oxidation starts during the initial core disassembly as channels are uncovered due to the sheath temperature increases and the fuel channel filling with steam (from the PHTS coolant boiling). The rate of hydrogen generated increases as the fuel channel temperatures increase and fuel channel disassembly occurs. Total amount of H_2 generated in the core is 157 kg, as seen in Fig. 42.

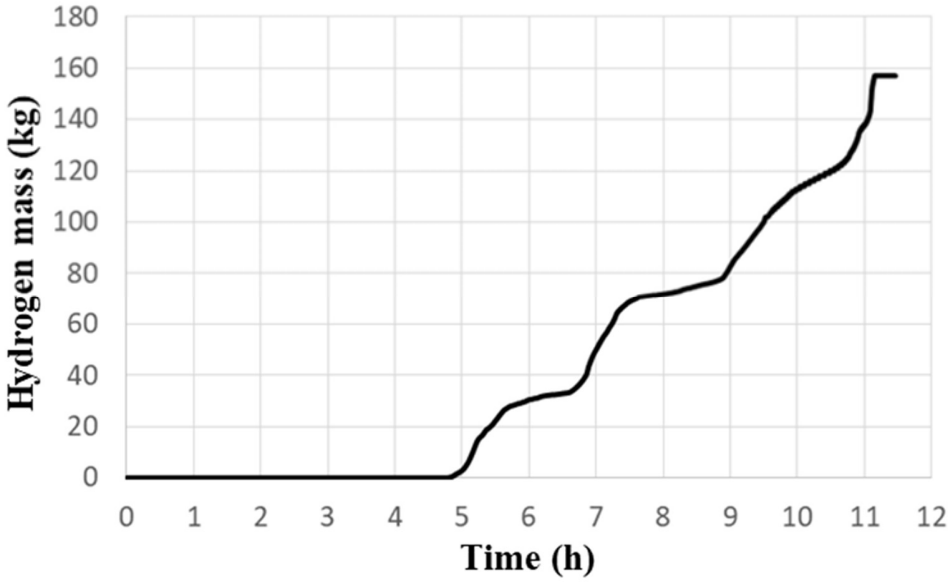

FIG. 42. Total amount of H_2 generated inside calandria vessel as a function of time.

4.2.2. Uncertainty analysis

The uncertainty analysis results based on the 59 code runs are summarized in Table 18. The major selected FOMs of relevance were the H_2 mass generation inside the calandria vessel and the events timing, such as the first fuel channel failure, beginning of core disassembly, core collapse and moderator depletion inside the calandria vessel.

The results of the uncertainty analysis show that the first fuel channel fails at 2.95–6.92 h from the initiation of the event, with the base case estimate indicating a failure time of 4.65 h. Almost immediately thereafter, the process of core disassembly takes place, estimated to occur in the time interval of 3.16–7.15 h for Loop 1, and 3.16–7.21 h for Loop 2. The final estimated time interval for the beginning of the core disassembly (spanning both loops) during the SBO is 3.16–7.21 h.

Continuous heat transfer from the hot fuel channels to the remaining moderator leads to a gradual decrease in the water level within the calandria vessel, attributed to ongoing moderator boiling. As the moderator boil-off uncovers the second row of fuel channels these channels start to heat up and gradually sag into contact with the underlying third row of equivalent fuel channels. This phenomenon initiates a heat transfer to the lower channels and contributes to the formation of suspended debris. Furthermore, a channel that has sagged and made contact with the channel beneath transfers its load to this newfound supporting channel. This process persists until the last row of fuel channels (situated at the lowest point within the core) either fails due to the elevated temperatures of the calandria tube, surpassing the melting point of Zircaloy, or when the longitudinal strain of a specific node exceeds a designated user defined threshold, or the sagging of a channel surpasses two to three lattice pitches. The estimated time interval for the entire CANDU 6 core collapse resulting from the uncertainty analysis is 7.14–16.99 h from the initiation of the event.

The suspended hot debris is surrounded by a steam environment due to the continuous moderator boil-off. This steam-rich environment is favourable to Zr-steam reactions. Once the suspended debris relocates to the bottom of the calandria vessel, it is quenched by the remaining moderator and no longer contributes to H_2 production. The total hydrogen production after the dry-out of the calandria vessel, as estimated from the uncertainty analysis ranges between132–258 kg. The estimated timed interval of the moderator depletion is around 7.19–16.87 h, which shows that the moderator complete boil-off can occur slightly before the moment of the entire core disassembly (i.e. core collapse).

TABLE 18. UNCERTAINTY ANALYSIS RESULTS

Events	**Events timing (s)**	**Events timing (h)**
Class IV and Class III Power loss	0	0
Reactor shutdown	0	0
Calandria vessel bleed valves open	3131.8–3294.5	0.870–0.915
LRVs first opening	5500–14000	1.53–3.89
Steam generator secondary side is dry Loops 1&2	5054.6–12417.6	1.40–3.45
Pressurizer empty	7468.7–18152.3	2.07–5.04
At least one channel is dry Loops 1 and 2 (complete boil-off)	7015.6–21625.65	1.95–6.01
Pressure and calandria tubes are ruptured	10,633.74–24,912.6	2.95–6.92
Calandria vessel rupture disks #1–4 open	10,351.94–23,443.93	2.88–6.51
Beginning of the core disassembly (Loops 1&2)	11,385.2–25,744.9 (Loop 1) 11,600–25,942.45 (Loop 2)	3.16–7.15 (Loop 1) 3.22–7.21 (Loop 2)
Core collapse (Loop 1)	25,691.46–61,061.79	7.14–16.96
Core collapse (Loop 2)	25,711.64–61,152.93	7.14–16.99
Water is depleted inside calandria vessel	25,886.02–607,40.79	7.1–6.87
Calandria vessel failed	N/A	N/A
H_2 mass production (kg): 132–258 kg		

Analysis results for hydrogen production inside the reactor vessel, moderator level, and CDF for hydrogen mass generation in core are shown in Fig. 43 and Fig. 44, and Fig. 45, respectively. The upper (95 %, 95 %) tolerance limit for the hydrogen mass generation in a core was calculated to be 258 kg. The uncertainty analysis results for the first fuel channel failure as a function of time is shown in Fig. 46, while corresponding CDF is shown in Fig. 47.

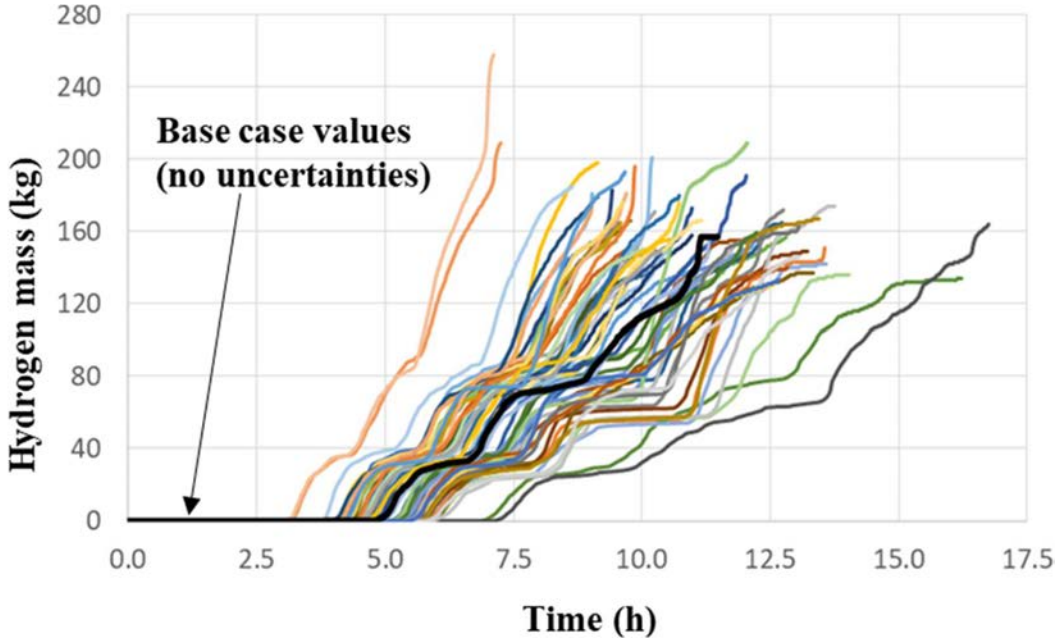

FIG. 43. H_2 generated inside calandria vessel as a function of time (uncertainty analysis).

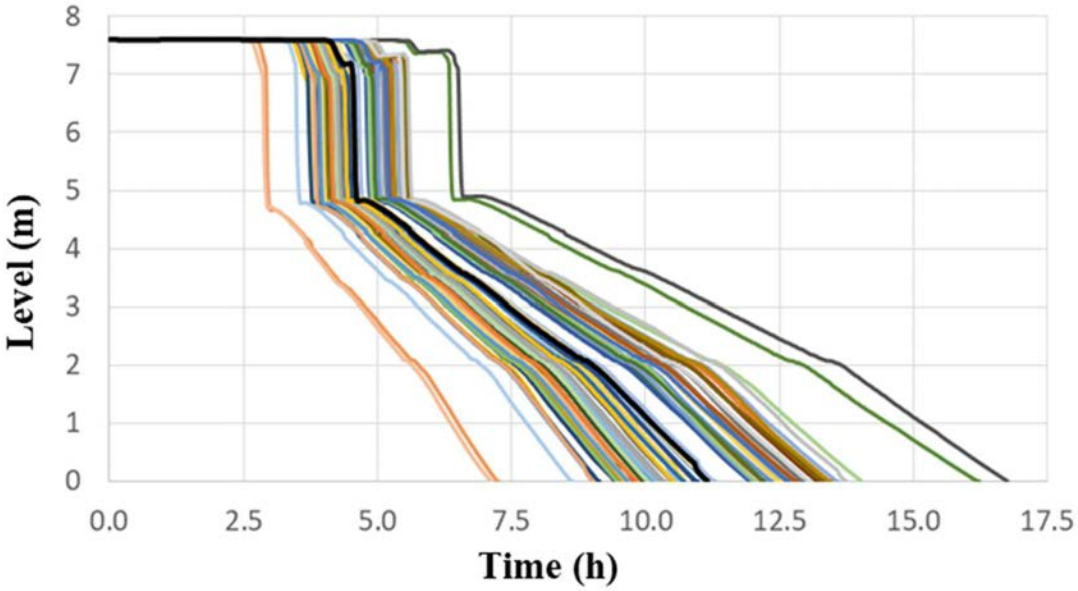

FIG. 44. Moderator level as a function of time (uncertainty analysis).

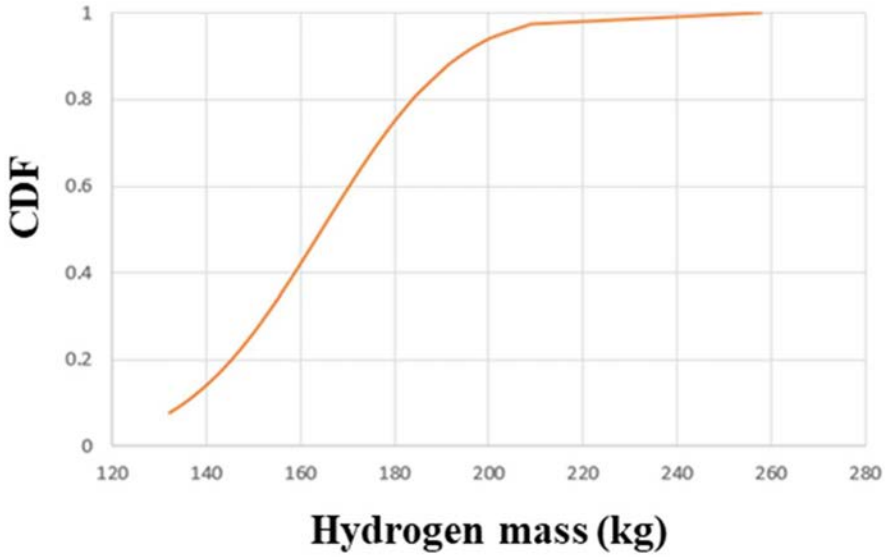

FIG. 45. CDF for hydrogen mass generation in a core.

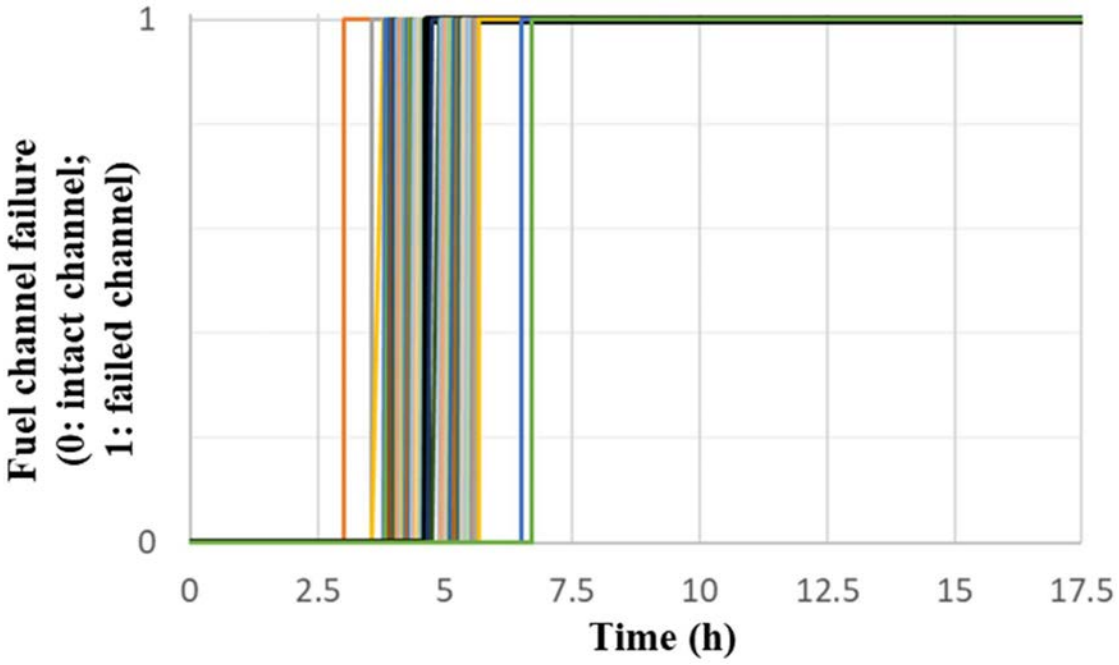

FIG. 46. First channel failure time (uncertainty analysis).

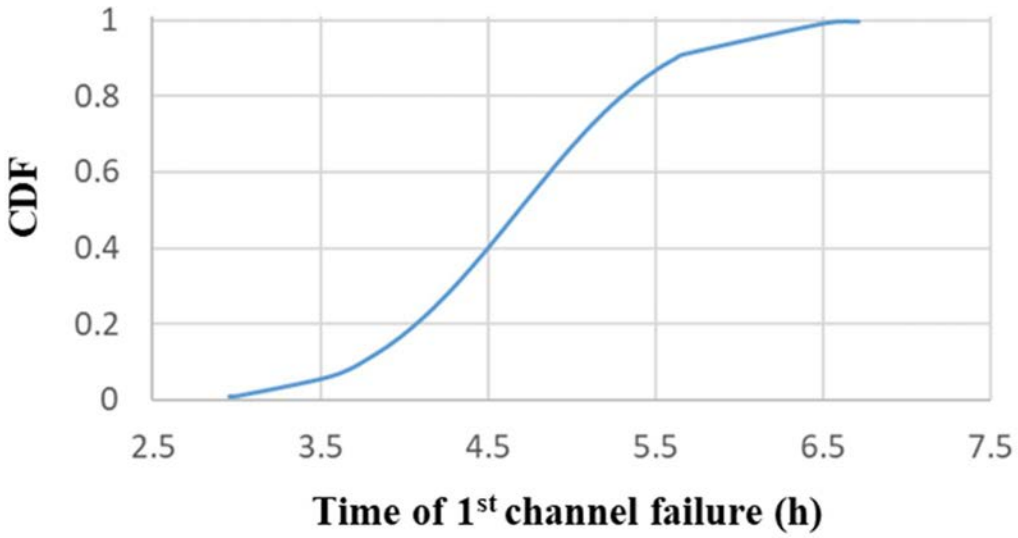

FIG. 47. CDF for the first channel failure time.

4.2.3. Sensitivity Analysis

The sensitivity analysis was performed using Microsoft Excel available functions (to determine the Pearson's and Spearman's correlation coefficients) in evaluating the influence of the selected uncertainty parameters on the FOMs. For the H_2 mass generation, the entire list of 26 uncertainty parameters was considered as being influential, and the correlation coefficients obtained are graphically represented in Fig. 48 and the calculated correlation coefficients are summarized in Table 19. Based on the results presented in Fig. 48 and Table 19, it can be concluded that the most influential parameters for hydrogen production are parameter 24 (contact conductance for channel-to-channel contact heat transfer calculation) and parameter 26 (the fuel channel rupture area).

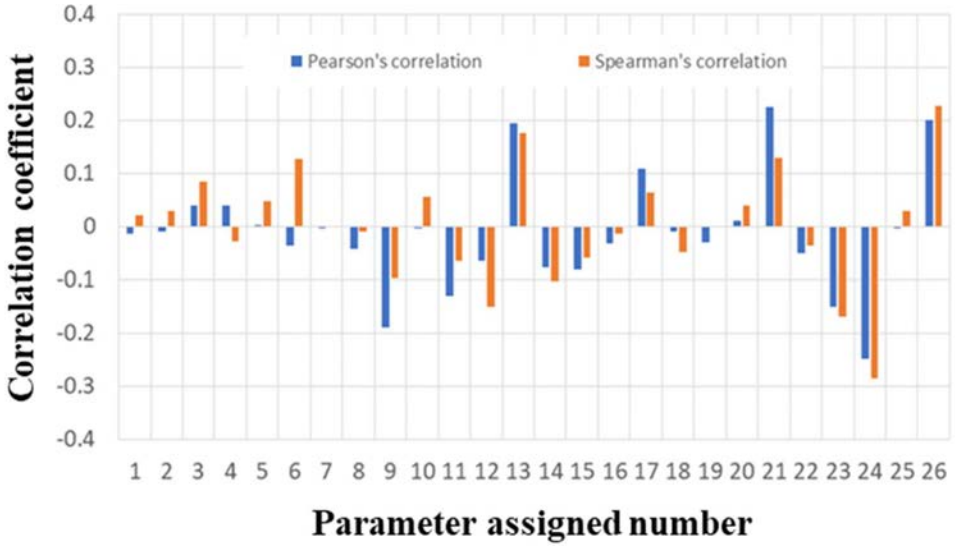

FIG. 48. Sensitivity analysis for H_2 generation during the SBO event.

TABLE 19. CALCULATED CORRELATION COEFFICIENTS FOR THEPARAMETERS INFLUENCING THE H_2 GENERATION DURING THE SBO EVENT

Number of calculations	Parameter	Pearson's correlation Coefficient (ρ)	Spearman's correlation Coefficient (r_s)
1	UO2.CP.LE1800K	-0.012576091	0.021079717
2	UO2.CP.GT1800K	-0.008184973	0.029266014
3	UO2.TH.LE1800K	0.039862882	0.0854591
4	UO2.TH.GT1800K	0.040370318	-0.026810125
5	UO2.RH.LE1800K	0.003091752	0.048066667
6	UO2.RH.GT1800K	-0.035967523	0.127033798
7	HTC single phase liquid	-0.003338571	0.000877103
8	HTC subcooled nucleate boiling	-0.041299363	-0.008624849
9	HTC saturated nucleate boiling	-0.188657897	-0.097155231
10	HTC subcooled transition boiling	-0.002289911	0.056076139
11	HTC saturated transition boiling	-0.128787924	-0.064730225
12	HTC subcooled film boiling	-0.064071389	-0.150452457
13	HTC saturated film boiling	0.195469575	0.175742269
14	HTC single phase vapor	-0.076217186	-0.102650326
15	HTC condensation with void < 1	-0.081162149	-0.05797653
16	Power after scram	-0.030803813	-0.013302734
17	Core form loss coefficients	0.108981907	0.064642515
18	Flow rate at LRVs - discharge coefficient (subcooled)	-0.008050543	-0.048036025
19	Flow rate at LRVs - discharge coefficient (two phase)	-0.028810444	0.001374129
20	Flow rate at calandria vessel rupture disk - discharge coefficient (subcooled)	0.010469512	0.040346753
21	Flow rate at calandria vessel rupture disk - discharge coefficient (two phase)	0.225021648	0.129915519
22	Pressure tube failure strain	-0.050704709	-0.036136657
23	Contact conductance for channel-to-channel contact heat transfer calculation	-0.150118539	-0.168900863
24	Contact angle for pressure-tube-to-calandria-tube sagging contact	-0.247509204	-0.284766212
25	Contact conductance for pressure-tube-to-calandria-tube sagging contact heat transfer calculation	-0.00372261	0.029090594
26	Fuel channel rupture area	0.201678705	0.228631599

For the sensitivity analysis for the predicted time of the first fuel channel failure, out of 26 uncertain parameters, only 20 parameters were considered (fuel behaviour specific parameters, heat transfer from heat structures to fluids, core power after accident initiation, core pressure loss, flow rate at LRVs and the pressure tube failure strain); the remaining six parameters specific to the core disassembly phase of the accident were not assessed (parameters 21–26 are referring to core disassembly phase).

The Pearson's and Spearman's correlation coefficients with the selected FOM are shown in Fig. 49 and summarized in Table 20 showing that the most influential parameters for the 1st fuel channel failure time are parameter 21 (flow rate at calandria vessel rupture disk - discharge coefficient (two phase)) and parameter 2 (fuel specific heat).

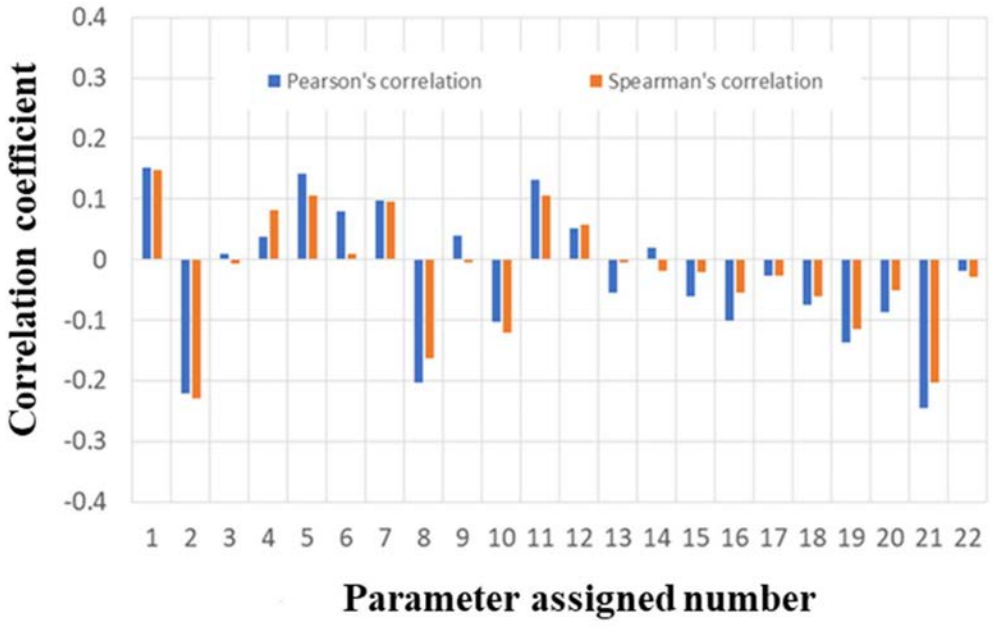

FIG. 49. Sensitivity analysis for the 1st fuel channel failure time.

TABLE 20. CALCULATED CORRELATION COEFFICIENTS FOR THE PARAMETERS OF INFLUENCE TO THE 1ST FUEL CHANNEL FAILURE TIME

Uncertain parameter number	Parameter	Pearson's correlation Coefficient (ρ)	Spearman's correlation Coefficient (r_s)
1	UO2.CP.LE1800K	0.152266493	0.147983635
2	UO2.CP.GT1800K	-0.220529567	-0.22817066
3	UO2.TH.LE1800K	0.009524877	-0.007247224
4	UO2.TH.GT1800K	0.038313244	0.081063705
5	UO2.RH.LE1800K	0.141270322	0.105350829
6	UO2.RH.GT1800K	0.079469119	0.009701929
7	HTC single phase liquid	0.098614446	0.094915254
8	HTC subcooled nucleate boiling	-0.202436335	-0.161893629
9	HTC saturated nucleate boiling	0.03976621	-0.004441912
10	HTC subcooled transition boiling	-0.101718482	-0.120806546
11	HTC saturated transition boiling	0.131063447	0.106487434
12	HTC subcooled film boiling	0.051989772	0.057568673
13	HTC saturated film boiling	-0.053766844	-0.004792519
14	HTC single phase vapor	0.018832717	-0.017650497
15	HTC condensation with void < 1	-0.060127392	-0.020338983
16	Power after scram	-0.100973128	-0.054997078
17	Core form loss coefficients	-0.026367406	-0.026008182
18	Flow rate at LRVs - discharge coefficient (subcooled)	-0.074713677	-0.061309176
19	Flow rate at LRVs - discharge coefficient (two phase)	-0.137302519	-0.115488019

A sensitivity analysis was performed for the timing of the core disassembly phase of the accident (the start time of core disassembly and end time of core disassembly / core collapse), for each uncertain parameter, the obtained correlation coefficients are summarized in Table 21 for the start time of core disassembly and

Table 22 for core collapse time. Figure 50 represents the Pearson's and Spearman's correlation coefficients for the core disassembly start time and Fig. 51 shows the core collapse time.

TABLE 21. CALCULATED CORRELATION COEFFICIENTS FOR THE PARAMETERS INFLUENCING THE BEGINNING OF CORE DISASSEMBLY TIME

Uncertain parameter number	Parameter	Pearson's correlation Coefficient (ρ)	Spearman's correlation Coefficient (r_s)
1	UO2.CP.LE1800K	0.16557609	0.168040213
2	UO2.CP.GT1800K	-0.227025432	-0.242182477
3	UO2.TH.LE1800K	0.004916556	-0.005523409
4	UO2.TH.GT1800K	0.033216184	0.089748086
5	UO2.RH.LE1800K	0.140534296	0.108776339
6	UO2.RH.GT1800K	0.094002677	0.033871062
7	HTC single phase liquid	0.090399971	0.079870244
8	HTC subcooled nucleate boiling	-0.213500067	-0.174937168
9	HTC saturated nucleate boiling	0.046252676	0.009614963
10	HTC subcooled transition boiling	-0.107130204	-0.126746157
11	HTC saturated transition boiling	0.137836053	0.103541996
12	HTC subcooled film boiling	0.071632101	0.078058332
13	HTC saturated film boiling	-0.067283677	-0.015576597
14	HTC single phase vapor	0.025751484	-0.024490035
15	HTC condensation with void < 1	-0.074534582	-0.043690455
16	Power after scram	-0.097446683	-0.046817465
17	Core form loss coefficients	-0.020793051	-0.01946344
18	Flow rate at LRVs - discharge coefficient (subcooled)	-0.081310003	-0.064965808
19	Flow rate at LRVs - discharge coefficient (two phase)	-0.133090957	-0.109562219
20	Flow rate at calandria vessel rupture disk - discharge coefficient (subcooled)	-0.077102831	-0.041878544
21	Flow rate at calandria vessel rupture disk - discharge coefficient (two phase)	-0.24753759	-0.196712209
22	Pressure tube failure strain	-0.017781565	-0.024548483
23	Contact conductance for channel-to-channel contact heat transfer calculation	0.132204666	0.181191186
24	Contact angle for pressure-tube-to-calandria-tube sagging contact	0.048979734	0.098310831
25	Contact conductance for pressure-tube-to-calandria-tube sagging contact heat transfer calculation	0.380249086	0.295195512
26	Fuel channel rupture area	-0.369627436	-0.243526799

TABLE 22. CALCULATED CORRELATION COEFFICIENTS FOR THE PARAMETERS INFLUENCING THE CORE COLLAPSE TIME

Uncertain parameter number	Parameter	Pearson's correlation Coefficient (ρ)	Spearman's correlation Coefficient (r_s)
1	UO2.CP.LE1800K	0.145280397	0.157042665
2	UO2.CP.GT1800K	-0.195600359	-0.205260082
3	UO2.TH.LE1800K	0.016217432	-0.011805961
4	UO2.TH.GT1800K	0.071209188	0.102162478
5	UO2.RH.LE1800K	0.158407714	0.1317689

TABLE 22. CALCULATED CORRELATION COEFFICIENTS FOR THE PARAMETERS INFLUENCING THE CORE COLLAPSE TIME (Cont.)

Uncertain parameter number	Parameter	Pearson's correlation Coefficient (ρ)	Spearman's correlation Coefficient (r_s)
6	UO2.RH.GT1800K	0.100107396	0.043834015
7	HTC single phase liquid	0.080765336	0.083343074
8	HTC subcooled nucleate boiling	-0.224555162	-0.179602572
9	HTC saturated nucleate boiling	0.012836441	-0.021712766
10	HTC subcooled transition boiling	-0.104703753	-0.110344828
11	HTC saturated transition boiling	0.126880218	0.105318527
12	HTC subcooled film boiling	0.056396451	0.060724722
13	HTC saturated film boiling	-0.024829742	0.040911748
14	HTC single phase vapor	0.027107818	-0.000233781
15	HTC condensation with void < 1	-0.070757639	-0.014143776
16	Power after scram	-0.115929707	-0.060724722
17	Core form loss coefficients	-0.028765282	-0.030040912
18	Flow rate at LRVs - discharge coefficient (subcooled)	-0.06334752	-0.05295149
19	Flow rate at LRVs - discharge coefficient (two phase)	-0.138114544	-0.124839275
20	Flow rate at calandria vessel rupture disk - discharge coefficient (subcooled)	-0.087348732	-0.044944477
21	Flow rate at calandria vessel rupture disk - discharge coefficient (two phase)	-0.262407822	-0.215666506
22	Pressure tube failure strain	-0.032402713	-0.05371128
23	Contact conductance for channel-to-channel contact heat transfer calculation	0.137750531	0.18351841
24	Contact angle for pressure-tube-to-calandria-tube sagging contact	0.071810344	0.111922852
25	Contact conductance for pressure-tube-to-calandria-tube sagging contact heat transfer calculation	0.382966177	0.233489188
26	Fuel channel rupture area	-0.355553963	-0.223378141

For both selected FOMs (beginning of core disassembly and core collapse time), the 1st–22nd uncertain parameters' influence can be also considered through an equivalent uncertain parameter represented by the first fuel channel failure time (which varies along with these selected parameters), as depicted in Fig. 52. In Fig. 52 and Fig. 53, the correlation coefficients resulted from the sensitivity / parametric study being summarized in Table 23 for the beginning of core disassembly time and Table 24 for core collapse time, are shown. Based on these results, it can be concluded that the most influential parameters for both selected FOMs (beginning of core disassembly and core collapse time) are parameter 25 (contact conductance for channel-to-channel contact heat transfer calculation) and parameter 26 (the fuel channel rupture area).

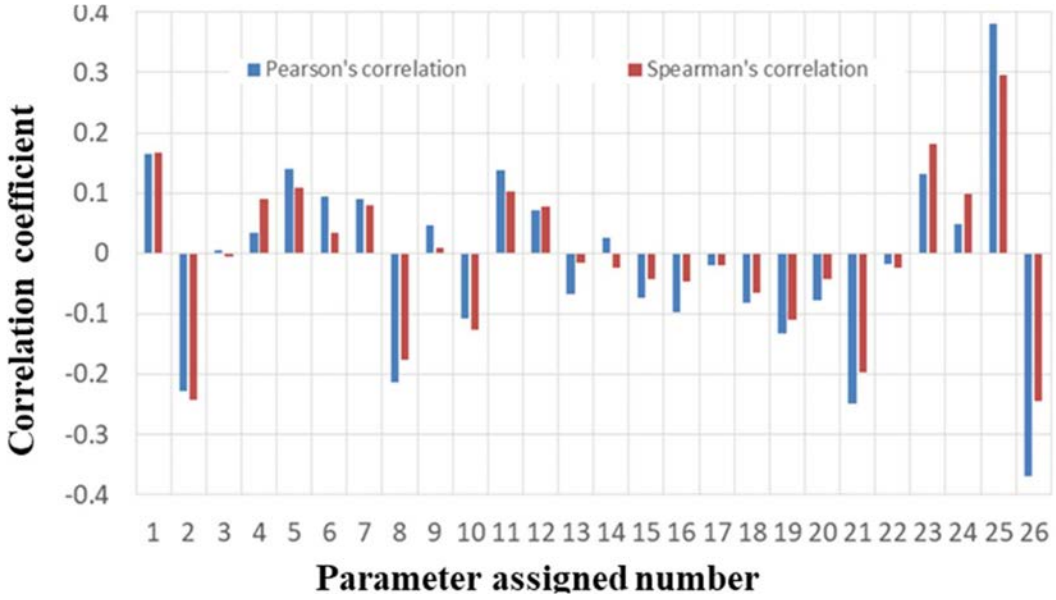

FIG. 50. Sensitivity analysis for the beginning of core disassembly time for 26 uncertainty parameters.

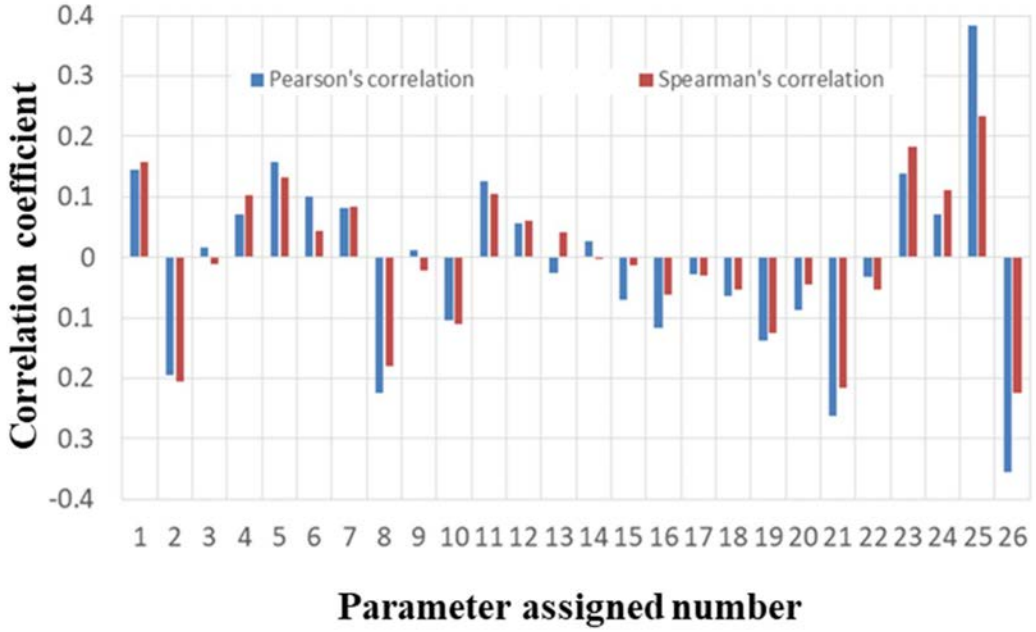

FIG. 51. Sensitivity analysis for the core collapse time for 26 uncertainty parameters.

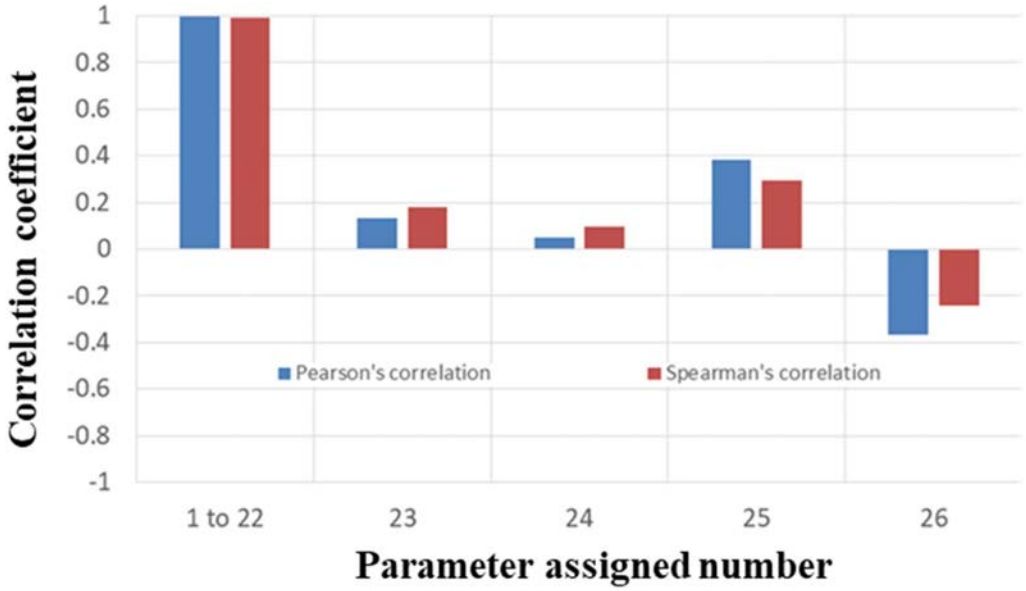

FIG. 52. Sensitivity analysis for the beginning of core disassembly time (based on the 1st fuel channel failure time).

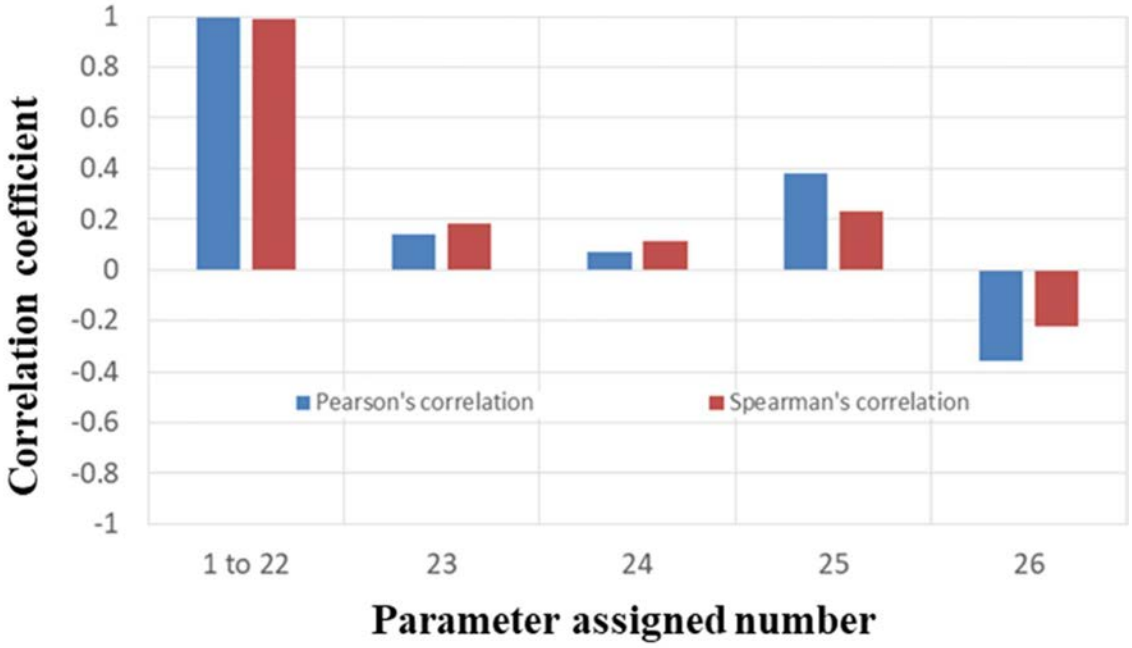

FIG. 53. Sensitivity analysis for core collapse time for six (6) uncertainty parameters.

TABLE 23. CALCULATED CORRELATION COEFFICIENTS FOR SIX (6) RELEVANT PARAMETERS INFLUENCING THE BEGINNING OF CORE DISASSEMBLY TIME

Uncertain parameter number	Parameter	Pearson's correlation Coefficient (ρ)	Spearman's correlation Coefficient (r_s)
1st to 22nd	First fuel channel failure time	0.997013	0.993804
23	Contact conductance for channel-to-channel contact heat transfer calculation	0.132205	0.181191
24	Contact angle for pressure-tube-to-calandria-tube sagging contact	0.04898	0.098311
25	Contact conductance for pressure-tube-to-calandria-tube sagging contact heat transfer calculation	0.380249	0.295196
26	Fuel channel rupture area	–0.36963	–0.24353

Selected uncertainty parameters #1–22 are considered together as being the equivalent uncertainty given by the first fuel channel failure time, which is directly impacting the results of the core disassembly and core collapse timings.

The sensitivity study was performed according to this assumption, and the 1st fuel channel failure time showed almost perfect correlation with the beginning of core disassembly time (Fig. 52) and core collapse estimated timing (Fig. 53).

TABLE 24. CALCULATED CORRELATION COEFFICIENTS FOR SIX (6) RELEVANT PARAMETERS INFLUENCING THE CORE COLLAPSE TIME

Uncertain parameter number	Parameter	Pearson's correlation Coefficient (ρ)	Spearman's correlation Coefficient (r_s)
1st to 22nd	First fuel channel failure time	0.993947	0.99135
23	Contact conductance for channel-to-channel contact heat transfer calculation	0.137751	0.183518
24	Contact angle for pressure-tube-to-calandria-tube sagging contact	0.07181	0.111923
25	Contact conductance for pressure-tube-to-calandria-tube sagging contact heat transfer calculation	0.382966	0.233489
26	Fuel channel rupture area	–0.35555	–0.22338

4.3. KOREA ATOMIC ENERGY RESEARCH INSTITUTE

The FOMs are hydrogen mass generation, fuel channel failure time, and calandria vessel failure time.

4.3.1. Steady state and reference case

The steady state simulation results obtained by the CAISER code are shown in Table 25. Based on the Wolsong unit 2 Final Safety Analysis Report [31], the steady state results were evaluated under 103% reactor power. All major parameters are in agreement with marginal deviation (see Table 25).

TABLE 25. STEADY STATE SIMULATION RESULTS WITH CAISER CODE

Parameter	Final Safety Analysis Report [32]	CAISER
RIH pressure (kPa)	11.42	11.83
ROH pressure (kPa)	10.00	9.81
RIH temperature (K)	541.15	541.15
ROH temperature (K)	583.15	583.50
ROH quality (%)	4.90	4.60
Suction pressure of PHTS pumps (MPa)	9.58	9.49
PZR level (m)	12.48	12.47
D_2O storage tank level (m)	1.40	1.42
Coolant flow rate per pass (kg/s)	1903.0	1899.6
Steam flow rate to turbine (kg/s)	1063.0	1064.0
Steam generator steam temperature (K)	533.15	533.98
Steam generator pressure (MPa)	4.7	4.7
Steam generator level NR (m)	2.5	2.5
Steam generator recirculation ratio (–)	5.1	4.6

In particular, the quality of ROH is about 4 % and this indicates that the void fraction can be as high as 30 % under normal operation pressure of CANDU 6 type reactor (~ 10 MPa) [32]. The SBO sequence reference case was run up to 500,000 s (139 h). The results (significant event timings observed during this simulation) for the SBO reference case calculated by the CAISER code are presented in Table 15.

4.3.2. Uncertainty analysis

The uncertainty analysis results for hydrogen mass generation in a vessel are displayed in Fig. 54 for 100 sample runs. The CDF of hydrogen mass generation is shown in Fig. 55.

The statistical analysis results for the hydrogen mass generation are provided in Table 26.

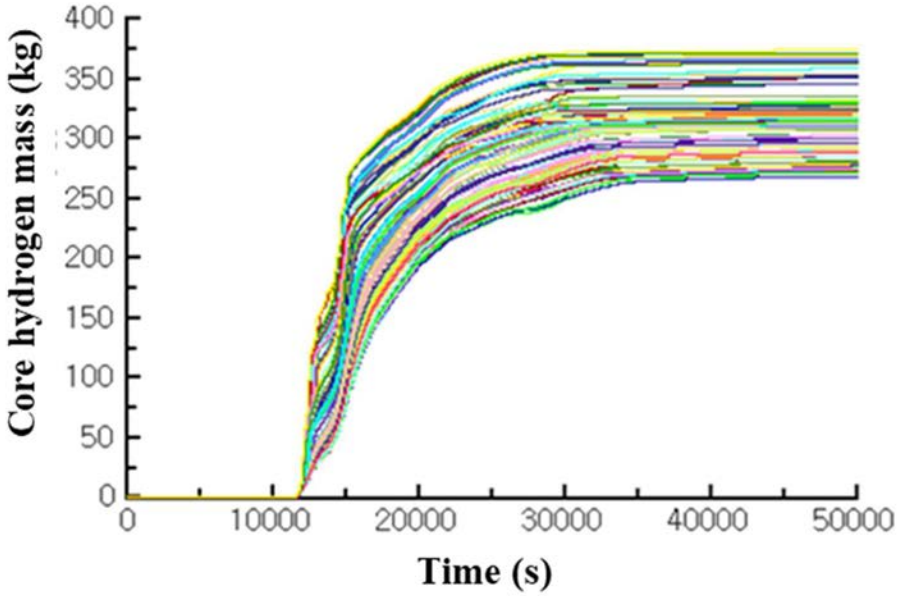

FIG. 54. Hydrogen mass generation history for 100 sample runs.

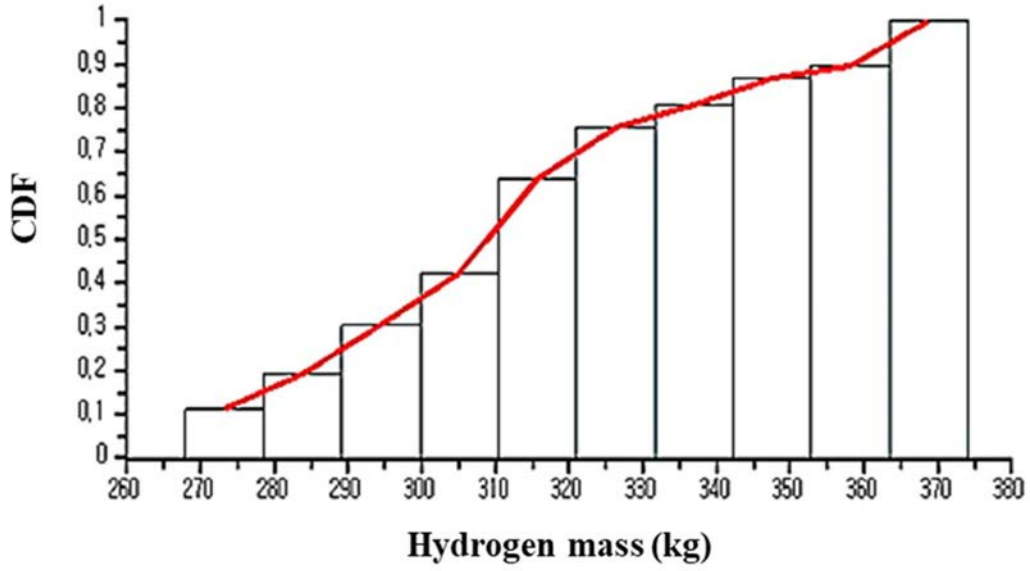

FIG. 55. CDF for a hydrogen mass generation.

TABLE 26. STATISTICAL ANALYSIS RESULTS FOR HYDROGEN MASS GENERATION

H_2 generation (in-vessel) [kg]	
5th percentile	273.3
Median	314.3
95th percentile	370.6
Standard deviation	28.3
Mean	315.8

The uncertainty analysis is developed as well for the fuel channel failure time. For the 100 sample runs, the fuel channel failure time is displayed in Figs. 56–59, which corresponds to four (4) nodes located in the vertical direction of the core, as shown in Fig. 60. It can be found that the bottom node of the core is largely affected by the change of parameter value, compared to the top node of the core.

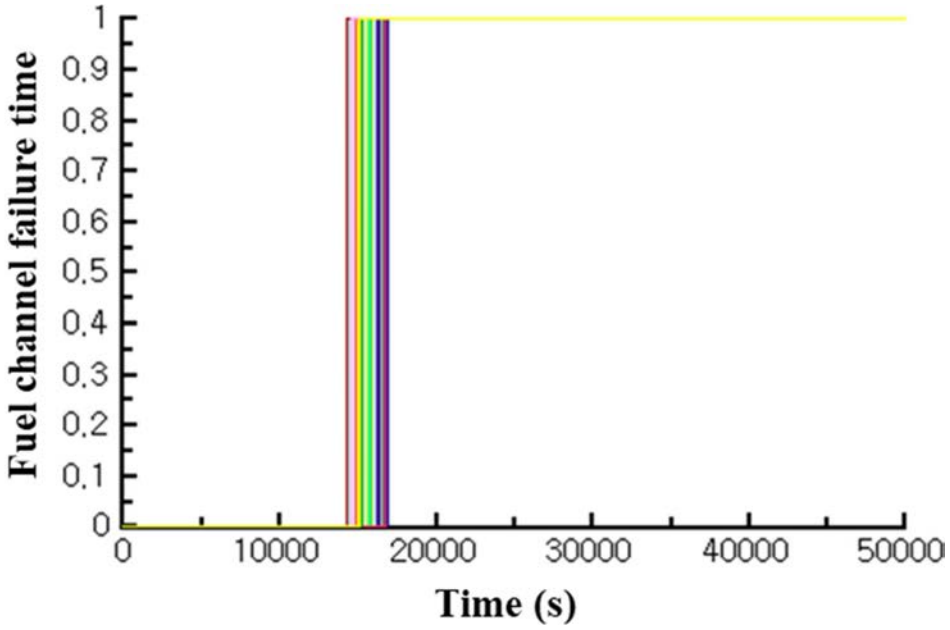

FIG. 56. Fuel channel failure time in the [1, 4] node for 100 sample runs.

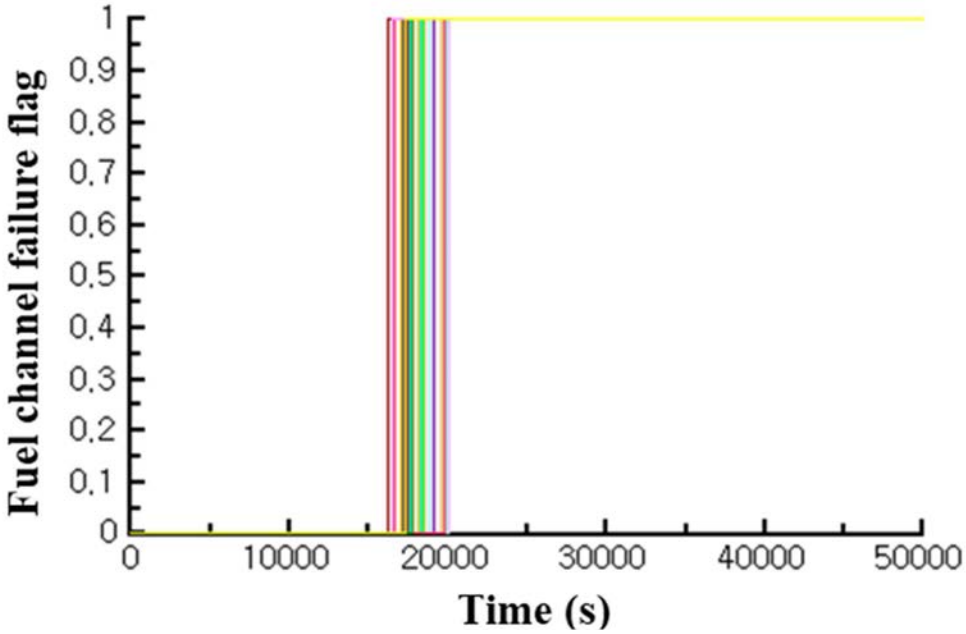

FIG. 57. Fuel channel failure time in the [1, 3] node for 100 sample runs.

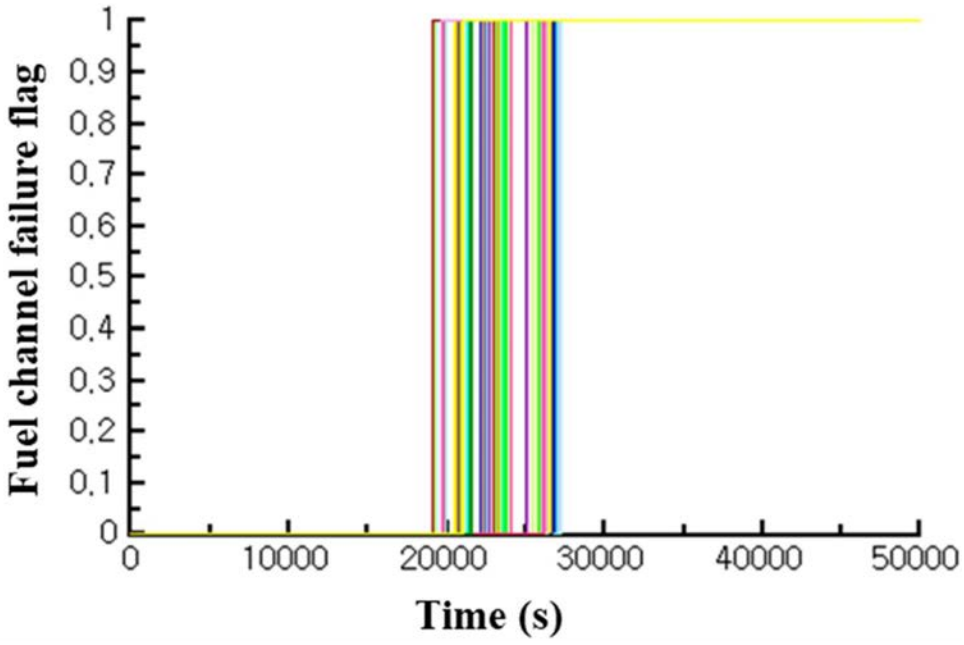

FIG. 58. Fuel channel failure time in the [1, 2] node for 100 sample runs.

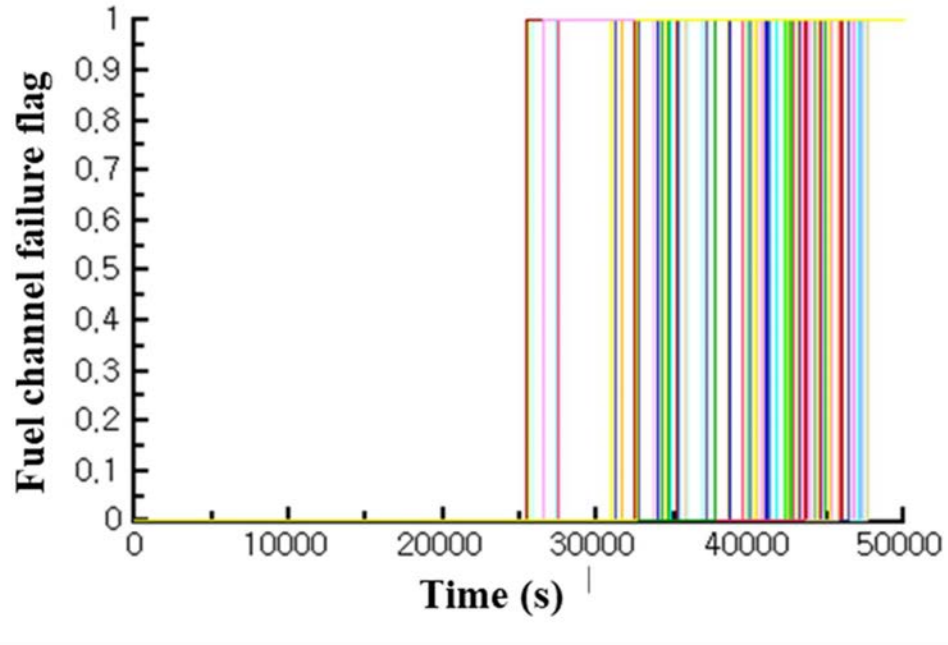

FIG. 59. Fuel channel failure time in the [1, 1] node for 100 sample runs.

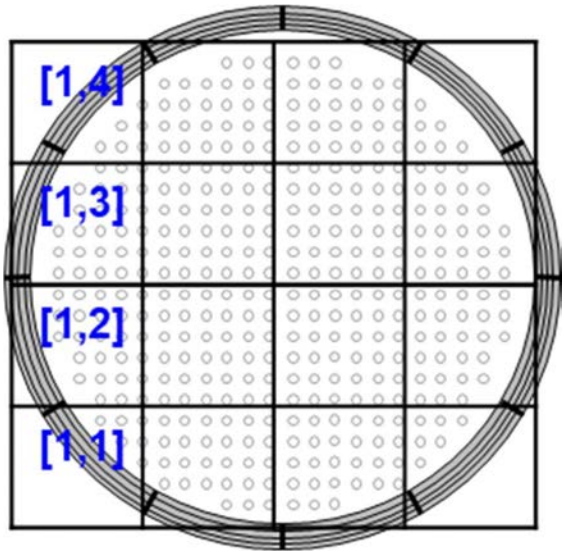

FIG. 60. Core nodal number in CAISER simulation.

The statistical analysis for the fuel channel failure time is shown in Table 27. The CDFs of fuel channel failure time are shown in Figs. 61–64 for the four (4) nodes in a vertical core direction (Fig. 60).

TABLE 27. STATISTICAL ANALYSIS RESULTS FOR A FUEL CHANNEL FAILURE TIME

Core Node	5% percentile	95% percentile	Median	Standard deviation	Mean
[1,4]	14821.5*	16665.5	15939.5	725.3	15988.6
[1,3]	16721.5	19848.5	18630.5	1087.8	18735.3
[1,2]	19962.5	26879.5	23862.5	2350.9	24105.6
[1,1]	27473.5	47061.5	41789.5	5662.7	40111.0

*Fuel failure time in seconds

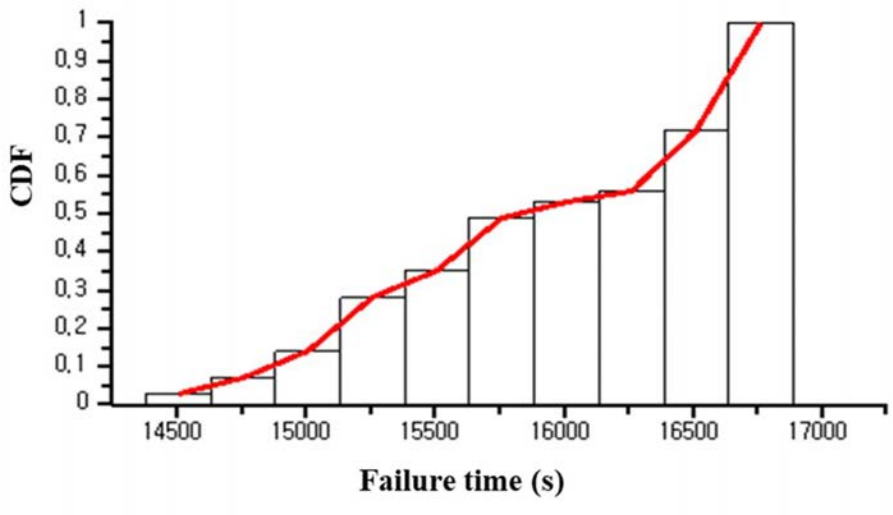

FIG. 61. CDF for fuel channel failure time in the [1, 4] node.

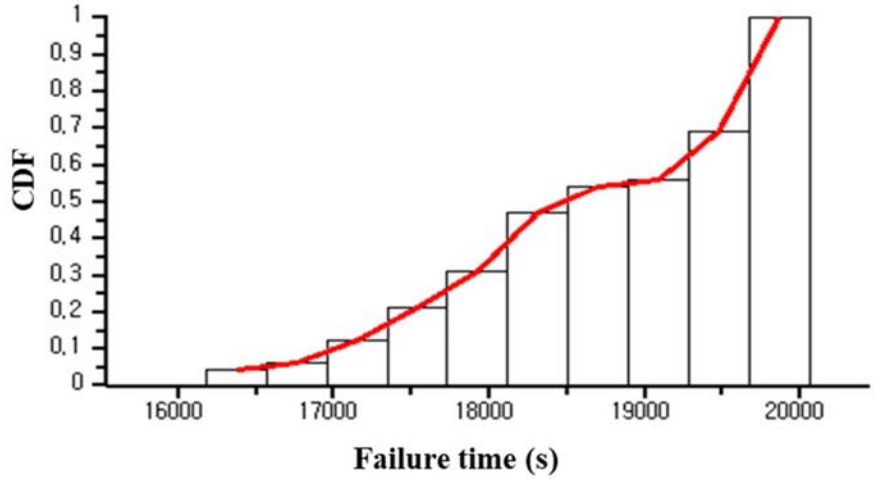

FIG. 62. CDF for fuel channel failure time in the [1, 3] node.

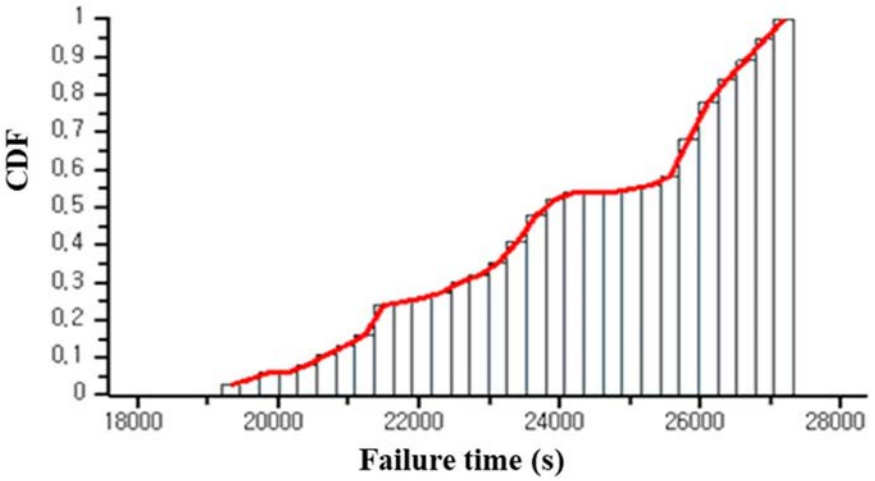

FIG. 63. CDF for fuel channel failure time in the [1, 2] node.

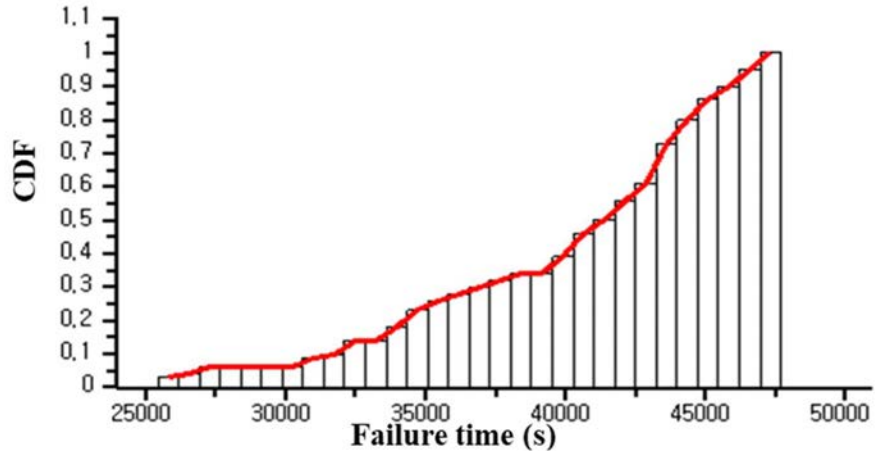

FIG. 64. CDF for fuel channel failure time in the [1, 1] node.

4.3.3. Sensitivity Analysis

Sensitivity analysis for hydrogen mass generation is performed by using a Pearson's correlation and a Spearman correlation, which are shown in Figs. 65–67. The Vfactor_PT, represents the view factor between the fuel rods and pressure tube; it has a high value of Pearson coefficient, reflecting that it has a high sensitivity on hydrogen mass generation in the core. For the hydrogen mass generation from a debris bed in a calandria vessel, the parameter db_porosity, meaning the porosity of a debris bed in a calandria vessel, has a high value of Pearson coefficient, reflecting that it has a high sensitivity on hydrogen mass generation from a debris bed.

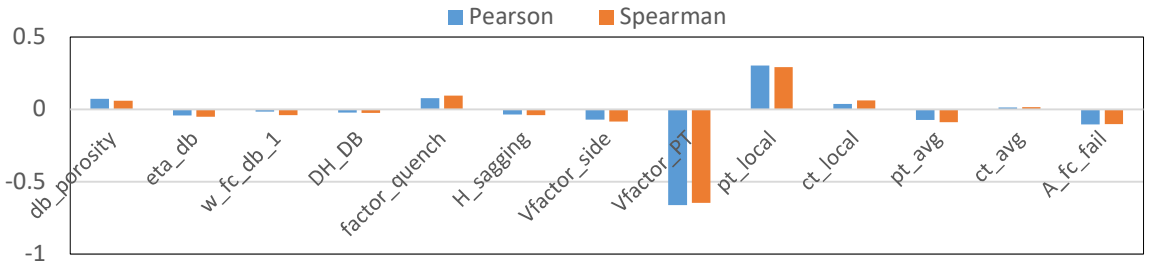

FIG. 65. Sensitivity analysis results for a hydrogen mass generation in the core.

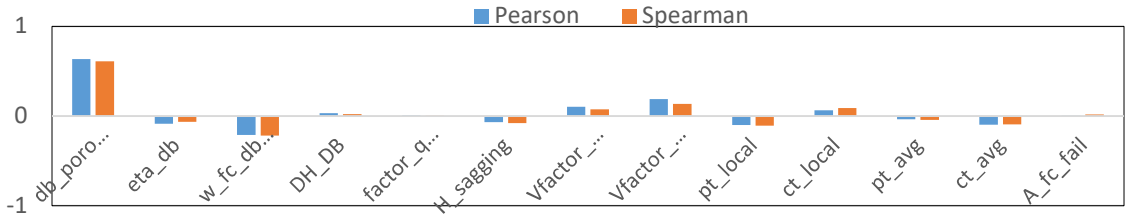

FIG. 66. Sensitivity analysis results for a hydrogen mass generation from a debris bed in the calandria vessel.

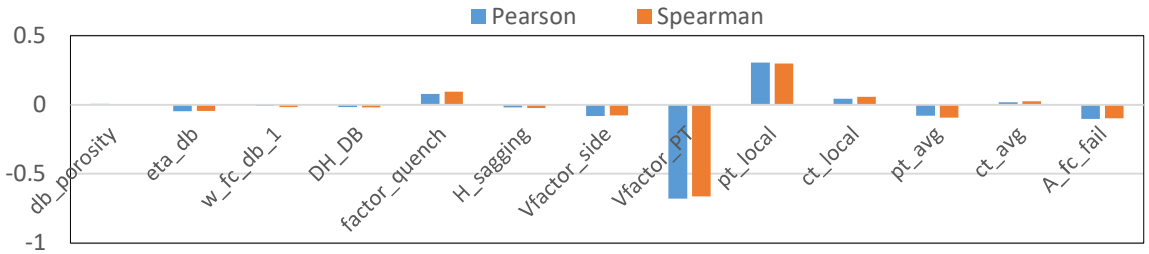

FIG. 67. Sensitivity analysis results for a hydrogen mass generation from fuel channels.

Sensitivity analysis for the fuel channel failure time has been performed by using a Pearson's correlation and a Spearman correlation analysis, which are shown in Figs. 68–71. For the case of Pearson correlation, the parameter Vfactor_PT, meaning the view factor between a fuel rods and a pressure tube, has a high value of Pearson coefficient, reflecting that it has a high sensitivity on a fuel channel failure time. While, for the case of Spearman correlation case, the parameter db_porosity has the highest value.

The sensitivity of fuel channel failure on these parameters is higher for a bottom node, compared with a top node in a core. For the case of fuel channel located at upper region in a calandria vessel, the fuel channel failure time is just determined by the thermal condition of corresponding fuel channel, while for the case of fuel channel located at lower region in a calandria vessel, the fuel channel failure time is largely affected by the mass of debris bed which is generated by the fuel channel failure located at upper region in a core. Hence, for the case of fuel channel located at lower region in a calandria vessel, the uncertainty of fuel channel failure time is accumulated as the fuel channel degradation progress, and it results to increase the uncertainty of fuel channel failure time at lower region in a calandria vessel.

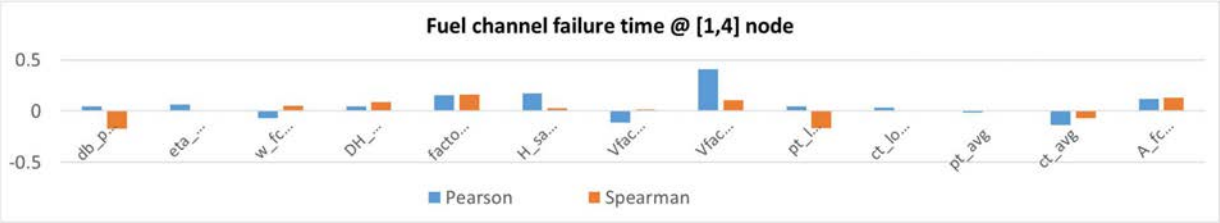

FIG. 68. Sensitivity analysis results for a fuel channel failure in the [1, 4] node.

FIG. 69. Sensitivity analysis results for a fuel channel failure in the [1, 3] node.

FIG. 70. Sensitivity analysis results for a fuel channel failure in the [1, 2] node.

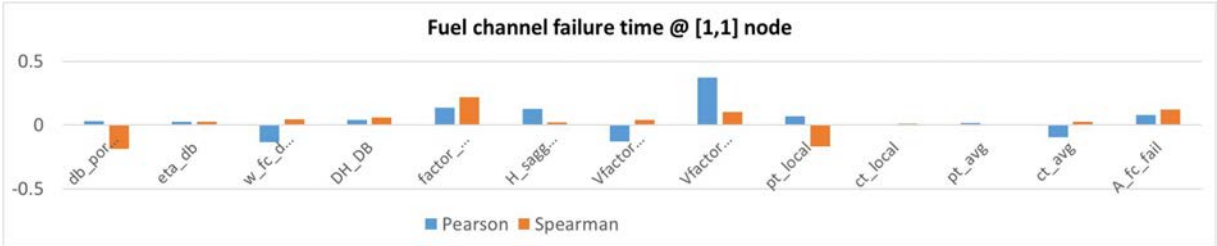

FIG. 71. Sensitivity analysis results for a fuel channel failure in the [1, 1] node.

5. SUMMARY AND LESSONS LEARNED

An unmitigated SBO severe accident scenario in a generic CANDU 6 plant was analysed by three participating organizations, CNL, UPB and KAERI, using their own analysis tools and various uncertainty and sensitivity analysis methods. It was found that the severe accident simulation results such as major events timing are relatively closely estimated by all three participating organizations. One output parameter predicted by various severe accident integrated codes represents one important FOM; it is hydrogen generation/releases in-vessel, i.e., inside the reactor (calandria) vessel.

The uncertain input parameters are selected based on used severe accident phenomenological models and engineering judgement by participating organizations. The actual number of these parameters is different per participating organization and it varies from 13 to 26. These selected uncertain input parameters are not identical among the participating organizations. The uncertain input parameters are, but are not limited to, the following severe accident related processes/phenomena: high temperature metal-water chemical reactions (oxidation), primary heat transport system and core voiding, fuel heat-up, debris formation, core collapse, and fission product releases, transport and deposition.

The tolerance limits predicted for the hydrogen mass generated in-vessel (due to high temperature metal-water reaction, or oxidation) by each participating organization are shown in Table 28. The parameters having the most significant sensitivity measures identified for the hydrogen mass generated in-vessel are provided in Table 29. It can be seen that there are noticeable differences among individual results, which are explained by the differences in phenomenology models employed in the used severe accident analysis codes.

TABLE 28. LOWER AND UPPER TOLERANCE LIMITS PREDICTED FOR HYDROGEN MASS GENERATED IN-VESSEL

Institution	Lower tolerance limit, kg	Upper tolerance limit, kg	Comments
CNL	15.0 (7.5 per PHTS loop)	269.4 (134.7 per PHTS loop)	Two-sided, 95%/95%
UPB	N/A	258.0	One-sided, 95%/95%
KAERI	273.3	370.6	Two-sided, 95%/95%

TABLE 29. MOST SIGNIFICANT SENSITIVITY MEASURES PREDICTED FOR HYDROGEN MASS GENERATED IN-VESSEL

Institution	Most significant parameter	2nd most significant parameter	Comments
CNL	MLOAD(1) Maximum allowable amount of suspended core debris in a loop	VFSEP Maximum PHTS void fraction where the primary coolant is modelled as a homogeneous two-phase mixture	Pearson
UPB	Contact conductance for channel-to-channel contact heat transfer calculation	Fuel channel rupture area	Pearson, Spearman
KAERI	Vfactor_PT View factor between a fuel rods and a pressure tube	pt_local Fuel channel failure temperature caused by a local melting of a pressure tube	Pearson, Spearman

It is advantageous that participating organizations implemented different uncertain parameters (pertinent to the modelling tools and processes being used). In their own individual analysis these uncertain input parameters cover diverse severe accident related phenomena or processes with their relevant PDFs. This allows the individual analyses to complement each other, provide a broad range of information, and help to refine and/or inform about the approaches and assessment outcomes. The following were lessons learned:

- Significant computational resources are often required to execute the simulations on computers/work stations as some integral severe accident codes need 24 hours (or more) per simulation run;
- It is typical to have multiple code simulation crashes, when a new set of input data (using new values of uncertain input parameters, and associated PDFs/bounds, generated for example by simple random sampling method), is implemented. Thus, the analyst has to assess the crashes, revise the input parameter values (such as allowable minimum or maximum values), and re-run the new 100 simulations (or similar);
- Defining the PDFs for some of the uncertain input parameters in a realistic fashion is not often a trivial task due to the complexity of the severe accident phenomena or processes under the assessment. However, internal evaluations show that the PDFs are very important for the final analysis results.

In summary, it was recognized that the selection of uncertain input parameters and their associated PDFs is very important for the uncertainty and sensitivity analysis outcomes.

6. CONCLUSIONS

Three organizations (CNL, UPB, and KAERI) developed analysis modelling SBO event in generic CANDU 6, with the goal to advance understanding and characterization of sources of uncertainty and investigate their effects on the key FOMs. The studies were carried out separately by each organization and included:

- CANDU 6 plant modelling and nodalization;
- Simulation of the reference case;
- Calculation of the uncertainty and sensitivity through coupling of the relevant severe accident codes with the corresponding quantification tools;
- Estimation of resultant FOMs' range,
- Sensitivity analysis of each input to the relevant FOMs.

The results of the uncertainty and sensitivity analyses were discussed for several FOMs:

- In-vessel hydrogen production (CNL, UPB and KAERI);
- First fuel channel failure time (UPB, KAERI);
- Core collapse time (UPB);
- Beginning of core disassembly time (UPB);
- Fission products (CsI) release to environment (CNL).

It was found that the major events timing for accident progression among participating organizations are rather close. However, there are differences in the uncertainty and sensitivity characterizations for the in-vessel hydrogen production FOM. These are explained by the significant differences in analysis approaches, and in phenomenological models implemented in the various severe accident analysis codes. Uncertainty and sensitivity analysis best practices and challenges were also discussed among the participants and the importance of input parameter selection (and definition of associated PDFs) was determined to be the most important aspect of the analysis.

The input parameters responsible for more significant uncertainties in in-vessel hydrogen production, first fuel channel failure time, core collapse time, beginning of core disassembly time and fission products (CsI) release to the environment were identified. This information is very important in future CANDU plant severe accident assessments and related phenomenological model refinements.

REFERENCES

[1] J. Kennedy, P. Maka, and M. Chai, MAAP5-CANDU Development, Proceedings of the 36th Annual Conference of the Canadian Nuclear Society and 40th Annual CNS/CNA Student Conference, Toronto, ON, Canada, 19–22 June 2016.

[2] INTERNATIONAL ATOMIC ENERGY AGENCY, 2013, Benchmarking Severe Accident Computer Codes for Heavy Water Reactor Applications, IAEA TECDOC 1727, IAEA, Vienna (2013).

[3] INTERNATIONAL ATOMIC ENERGY AGENCY, 2008, Analysis of Severe Accidents in Pressurized Heavy Water Reactors, IAEA-TECDOC-1594, IAEA, Vienna (2008).

[4] C. M. Allison, J. K. Hohorst, Role of RELAP/SCDAPSIM in Nuclear Safety, Science and Technology of Nuclear Installations **2010** (2010) DOI:10.1155/2010/425658

[5] F. Zhou, D. R. Novog, L. J. Siefken, C. M. Allison, Development and Benchmark of Mechanistic Channel Deformation Models in RELAP/SCDAPSIM/MOD3.6, Nuclear Science and Engineering **190** (2018) https://doi.org/10.1080/00295639.2018.1442060

[6] D. Dupleac D., M. Mladin M., I. Prisecaru, Generic CANDU 6 plant severe accident analysis employing SCAPSIM/RELAP5 code, Nuclear Engineering and Design, **239**, Issue 10 (2009) 2093–2103, ISSN: 0029–5493. https://doi.org/10.1016/j.nucengdes.2009.05.007

[7] M. Mladin, D. Dupleac, I. Prisecaru, Adapating and applying SCDAP/RELAP5 to CANDU in vessel retention studies, Annals of Nuclear Energy **37**, Issue 6, (2010) 845–852. https://doi.org/10.1016/j.anucene.2010.02.015

[8] MARS Code Manual Volume II: Input Requirements Thermal-Hydraulic Safety Research Department, KAERI/TR-2811/2004.

[9] K. S. Ha, S. I. Kim, H. S. Kang, and D. H. Kim, SIRIUS: A Code on Fission Product Behavior under Severe Accident, Transactions of the Korean Nuclear Society Spring Meeting Jeju, Korea, 18–19 May 2017

[10] D.C. Williams et al. Containment Loads Due to Direct Containment Heating and Associated Hydrogen Behavior: Analysis and Calculations with the CONTAIN Code, NUREG/CR–4896, SAND87–0633, Sandia National Laboratories (1987).

[11] J. H. Bae et al., Numerical simulation of CS28-1 experiment by using CANDU severe accident analysis code CAISER, Annals of Nuclear Energy **150**, 107820 (2021). DOI 10.1016/j.anucene.2020.107820

[12] Atomic Energy of Canada Ltd., CANDU 6 Technical Summary, Reactor Development Business Unit, AECL (2005).

[13] R. S. Shewfelt, D. P. Godin. Verification tests for GRAD, a computer program to predict nonuniform deformation and failure of Zr-wt2.5%Nb pressure tubes during a postulated Loss of Collant Accident. Atomic Energy of Canada Ltd (AECL) (1985) AECL-8384.

[14] The SCDAP/RELAP5 Development Team, SCDAP/RELAP5/MOD3.2 Code Manual. Volume II: Damage Progression Model Theory. NUREG/CR-6150 INEL–96/0422, Revision 1, 1996. NUREG/CR–6150 INEL–96/0422, Revision 1.

[15] F. Zhou, D. R. Novog, Mechanistic modelling of station blackout accidents for a generic 900 MW CANDU plant using the modified RELAP/SCDAPSIM/MOD3.6 code. Nuclear Engineering and Design **33**5 (2018). https://doi.org/10.1016/j.nucengdes.2018.05.009

[16] H. Glaeser, GRS Method for Uncertainty and Sensitivity Evaluation of Code Results and Applications. Science and Technology of Nuclear Installations **2008** (2008) Article ID 798901. https://doi.org/10.1155/2008/798901

[17] A. Wielenberg et al., “Recent improvements in the system code package AC2 2019 for the safety analysis of nuclear reactors”, Nuclear Engineering and Design **354** (2019). https://doi.org/10.1016/j.nucengdes.2019.110211

[18] S.S. Wilks, Determination of Sample Sizes for Setting Tolerance Limits. Ann. Math. Stat. 12, 91–96, 1941. I.M. Sobol, The Monte Carlo Method, Mir Publishing, Moscow, USSR (1975).

[19] I.M. Sobol, The Monte Carlo Method, Mir Publishing, Moscow, USSR (1975).

[20] M. Kloos, Main Features of the tool SUSA 4.0 for Uncertainty and Sensitivity Analyses, Proceedings of the 25th European Safety and Reliability Conference, ESREL 2015, Zürich, Switzerland, 7–10 September 2015.

[21] M. Perrez-Ferragut, Integration of a quantitative-based selection procedure in an uncertainty analysis methodology for NPP safety analysis (PhD. Thesis). 2012.

[22] Ho-Gon Lim, Sang-Hoon Han and Jae Jun Jeong, MOSAIQUE – A Network Based Software For Probabilistic Uncertainty Analysis Of Computerized Simulation Models, Nuclear Engineering and Design **241** (2011) 1776–1784. DOI:10.1016/j.nucengdes.2011.01.021

[23] K. Pearson, Notes on Regression and Inheritance in the Case of Two Parents. Proceedings of the Royal Society of London (1895).

[24] Laerd Statistics. https://statistics.laerd.com/statistical-guides/pearson-correlation-coefficient-statistical-guide.php.

[25] Jerome L. Myers, Arnold D. Well. Research Design and Statistical Analysis (2nd ed.) ISBN 978-0-8058–4037–7 (2003)

[26] R. M. Nistor-Vlad, D. Dupleac, I. Prisecaru, M. Perez, C.M. Allison, J. K. Hohorst, CANDU 6 Accident Analysis using RELAP/SCDAPSIM with the Integrated Uncertainty Package. Proceedings of the 2018 26th International Conference on Nuclear Engineering (ICONE26), London, UK (2018).

[27] Virgil E. Schrock, A Revised ANS Standard for Decay Heat from Fission Products, Nuclear Technology **46** (2017).

[28] C. D. Fletcher, R. M. Beaton. Evaluation of uncertainties in SCDAP/RELAP5 Station BlackOut simulations. US NRC (Draft prepared for the US NRC), JCN Number Y6198, RES ID: RES–C05–340 (2006).

[29] Quantification of Realistic Discharge Coefficient for the Critical Flow Model of RELAP5/MOD3/KAERI. T. S. Kwon, B. D. Chung, W. J. Lee, N. H. Lee, J. Y. Huh. Journal of the Korean Nuclear Society **27** (1995).

[30] R.S.W. Shewfelt, D.P. Godin, L.W. Lyall. Verification of High-Temperature Transverse Creep Model for Zr-2.5 wt.%Nb Pressure Tubes. Atomic Energy of Canada Ltd. (AECL) AECL–7813 (1984)

[31] KHNP Final Safety Analysis Report (Chap.15), Wolsong Unit II, Korea Hydro and Nuclear Power Co., Ltd. (KHNP), Korea (2016).

[32] , J.G. Collier, J.R. Thome, Convective boiling and condensation (3rd edition), pp.57, Clarendon press (1994).

LIST OF ABBREVIATIONS

ATHLET	Analysis of THermal-hydraulics of LEak and Transients
CAISER	Candu Advanced Integrated SevERe accident analysis code
CAREM	Central Argentina de Elementos Modulares (Argentine Modular Power Plant)
CDF	Core Damage Frequency (or Cumulative Distribution Function)
CNEA	National Atomic Energy Commission
CRP	Coordinated Research Project
CsI	Cesium Iodide
ECCS	Emergency Core Cooling System
FOM	Figure Of Merit
IAEA	International Atomic Energy Agency
KAERI	Korea Atomic Energy Research Institute
LOCA	Loss of Coolant Accident
LWR	Light Water Reactor
MAAP	Modular Accident Analysis Program
MELCOR	Methods of Estimation of Leakages and Consequences of Releases
PDF	Probability Density Function
PSA	Probabilistic Safety Assessment (or Parameter Space Analysis)
PWR	Pressurized Water Reactor
RELAP	Reactor Excursion and Leak Analysis Program
SAM	Severe Accident Management/Mitigation
SBO	Station Black Out
SCDAP	Severe Core Damage Analysis Package
SCDAPSIM	Severe Core Damage Analysis Package SIMulator
SCRAM	Safety Control Rod Axe Man

CONTRIBUTORS TO DRAFTING AND REVIEW

Ahn, Kwan-II	KAERI (Republic of Korea)
Dupleac, Daniel	UPB (Romania)
Gabrielli, Fabrizio	KIT (Germany)
Ho Bae, Jun	KAERI (Republic of Korea)
Jevremovic, Tatjana	International Atomic Energy Agency
Mascari, Fulvio	ENEA (Italy)
Morreale, C. Andrew	CNL (Canada)
Nistor-Vlad, Roxana	UPB (Romania)
Petoukhov, M. Sergei	CNL (Canada)

Research Coordination Meetings (RCMs)

1st RCM, EVT1803724, IAEA Headquarters, Vienna, Austria, 14–17 October, 2019.

2nd RCM, EVT1903891, IAEA Headquarters, Vienna, Austria, 20–22 October, 2020.

3rd RCM, EVT2004045, IAEA Headquarters, Vienna, Austria, 8–10 November, 2021.

4th RCM, EVT2103131, IAEA Headquarters, Vienna, Austria, 7–10 November, 2022.

IAEA
International Atomic Energy Agency

No. 27

ORDERING LOCALLY

IAEA priced publications may be purchased from the sources listed below or from major local booksellers.

Orders for unpriced publications should be made directly to the IAEA. The contact details are given at the end of this list.

NORTH AMERICA

Bernan / Rowman & Littlefield

15250 NBN Way, Blue Ridge Summit, PA 17214, USA
Telephone: +1 800 462 6420 • Fax: +1 800 338 4550
Email: orders@rowman.com • Web site: www.rowman.com/bernan

REST OF WORLD

Please contact your preferred local supplier, or our lead distributor:

Eurospan

1 Bedford Row
London
WC1R 4BU
United Kingdom

Trade Orders and Enquiries:

Tel: +44 (0)1235 465576
Email: trade.orders@marston.co.uk

Individual Customers:

Tel: +44 (0)1235 465577
Email: direct.orders@marston.co.uk
www.eurospanbookstore.com/iaea

For further information:

Tel. +44 (0) 207 240 0856
Email: info@eurospan.co.uk
www.eurospan.co.uk

Orders for both priced and unpriced publications may be addressed directly to:

Marketing and Sales Unit
International Atomic Energy Agency
Vienna International Centre, PO Box 100, 1400 Vienna, Austria
Telephone: +43 1 2600 22529 or 22530 • Fax: +43 1 26007 22529
Email: sales.publications@iaea.org • Web site: www.iaea.org/publications

24-02113E

International Atomic Energy Agency
Vienna